DEVELOPMENT OF A CONTROL FRAMEWORK FOR HYBRID RENEWABLE ENERGY SYSTEM IN MICROGRID

by

EDIN GOLUBOVIC

Submitted to the Graduate School of Engineering and Natural Sciences
in partial fulfillment of
the requirements for the degree of
Doctor of Philosophy

SABANCI UNIVERSITY
June 2014

DEVELOPMENT OF A CONTROL FRAMEWORK FOR HYBRID RENEWABLE ENERGY SYSTEM IN MICROGRID

Ecin Golubovic

APPROVED BY:

Prof. Dr. Asif SABANOVIC
(Dissertation Advisor)

Prof. Dr. Mustafa ÜNEL

Prof. Dr. Metin GÖKAŞAN

Assoc. Prof. Ali KOŞAR

Asst. Prof. A.Teoman NASKALİ

DATE OF APPROVAL: 23.05.2014

DEVELOPMENT OF A CONTROL FRAMEWORK FOR HYBRID RENEWABLE ENERGY SYSTEM IN MICROGRID

EDIN GOLUBOVIC

Mechatronics, PhD Thesis, 2014

Thesis Supervisor: Prof. Dr. Asif SABANOVIC

Keywords: microgrid, hybrid energy source, control of switching converters, sliding mode control, control in power electronics.

ABSTRACT

Electrical energy has an essential role in society as it ensures high quality of life and steady economic development. Demand for the electric energy has been steadily growing throughout the recent history and this demand is expected to grow further in the future. Most of electrical energy nowadays is generated by burning fossil fuels and there are serious concerns about the resulting emission. Renewable energy sources appeared as a viable alternative for environmentally hazardous sources. However, sources of renewable energy have considerably unpredictable and environmental conditions dependent power output and as such can't be directly incorporated into existing electrical grid. These sources are usually integrated to the electrical grid as part of microgrid or hybrid energy source that consists of two or more energy sources, converters and/or storage devices. In hybrid energy sources, generation and storage elements complement each other to provide high quality and more reliable power delivery.

This area of research is its infant stage and requires a lot of research and development effort to be done. Main objective of this thesis is to develop a framework for analysis and control of power electronics interfaces in microgrid connected hybrid energy source. The framework offers the generalized approach in treatment of control problem for hybrid energy sources. Development of the framework is done for the generalized hybrid source comprised of energy source(s), storage element(s), power electronic interfaces and control system.

The main contributions of this thesis are, generalization of control problem for power electronics interfaces in hybrid energy source, the development of switching algorithm for three phase switching converters based on the closed loop behavior of the converters and the development of a maximum power point tracking algorithm for the renewable energy sources.

MİKRO AĞDAKİ YENİLENEBİLİR HİBRİT ENERJİ KAYNAĞI İÇİN BİR DENETİM ÇERÇEVESİ GELİŞTİRİLMESİ

EDIN GOLUBOVIC

Mekatronik, Doktora Tezi, 2014

Tez Danışmanı: Prof. Dr. Asif SABANOVIC

Anahtar Kelimeler: mikro ağlar, hibrit enerji kaynağı, güç elektroniği çeviricinin denetlemesi, kayan kipli denetim, güç elektronikte denetim.

ÖZET

Elektrik enerjisi, yüksek yaşam kalitesi ve istikrarlı bir ekonomik gelişme sağladığı için toplumda önemli bir yere sahiptir. Elektrik enerjisine duyulan talep yakın tarihte düzenli bir şekilde artmış ve gelecekte daha da artması beklenmektedir. Günümüzde elektrik enerjisinin çoğu fosil yakıtların yakılmasıyla üretilmektedir ve ortaya çıkan emisyonla ilgili ciddi endişeler oluşmaktadır. Yenilenebilir enerji kaynakları çevreye zararlı kaynaklara göre daha uygun bir alternatif olarak ortaya çıkmıştır. Ancak yenilenebilir enerji kaynaklarının sağladığı güç önemli ölçüde çevre koşullarına bağlı ve tahmin edilemez durumdadır, ve bu nedenle direkt olarak mevcut elektrik ağına katılamaz. Bu kaynaklar genelde bir veya daha fazla enerji kaynakları, çeviriciler ve/veya depolama aygıtları içeren bir hibrit enerji kaynağı veya mikroağ çerçevesinde elektrik ağına entegre edilir. Hibrit enerji kaynaklarında üretim ve depolama elemanları birbirlerini tamamlayarak yüksek kalite ve daha tutarlı güç sağlar.

Bu araştırma alanı daha başlangıç aşamasındadır ve daha çok araştırma ve geliştirme çabası gerektirmektedir. Bu tezin ana amacı, mikroağa bağlı hibrit enerji kaynağındaki güç elektroniği arabirimlerinin analizi ve kontrolü için bir çerçeve geliştirmektir. Bu çerçeve hibrit enerji kaynaklarındaki kontrol problemine çözüm olacak genel bir tutum önerir. Bu çerçeve; enerji kaynakları, depolama elemanları, güç elektroniği arabirimleri ve kontrol sistemini kapsayan genelleştirilmiş bir hibrit kaynak için geliştirilmiştir.

Bu tezin sağlayacağı temel katkılar; hibrit enerji kaynağındaki güç elektroniği arabirimleri için kontrol probleminin genelleştirilmesi, çeviricilerin kapalı döngü dinamiğine dayalı üç faz çeviriciler için anahtarlama algoritmasının geliştirilmesi, ve yenilenebilir enerji kaynakları için maksimum güç noktası izleme algoritmasının geliştirilmesidir.

“To my beloved ones”

ACKNOWLEDGEMENTS

I would like to express my deep appreciation and gratitude to my advisor, Prof. Dr. Asif Šabanović for his patience, guidance, valuable suggestions and moral encouragement during my graduate studies.

I wish to thank my thesis jury members, Prof. Dr. Mustafa Ünel, Prof. Dr. Metin Gökaşan, Assoc. Prof. Ali Koşar And Asst. Prof. A.Teoman Naskali for showing interest in my work.

Special thanks go to Tarik Uzunovic, Ahmet Nergiz, Zhenishbek Zhakypov for a good company, sharing of ideas and their moral support during my PhD studies and Ali Turşucular, Gönenç Ülker and Emre Özsöy for their technical assistance in realization of this thesis.

Finally, I greatly appreciate my family and girlfriend for their love, encouragement and support during my PhD studies.

I acknowledge KONČAR Electrical Engineering Institute Inc. for providing the Graphical Programming Integrated Development Environment GRAP IDE software that was used for various testing and validation needs during the development of this thesis.

I acknowledge Yousef Jameel Scholarship Fund and The Scientific and Technological Research Council of Turkey BIDEB 2215 Scholarship Program for financial support.

TABLE OF CONTENTS

LIST OF FIGURES

LIST OF TABLES

1 INTRODUCTION

1.1 Motivation

Sustainable economic growth and stability of countries around the world is secured through abundant energy supply. Furthermore, amount of energy supply of a country, among other factors, defines standing of that country on global political scene. Looking beyond the economic and political reasoning, energy has become the most important player in the technological advancement of a modern society.

Energy consumption scales differently between different countries, however, consumption areas are similar including mainly heating/cooling, electricity supply and transportation/machinery fuel. Currently, majority of the consumed energy is harvested by non-renewable and non-environmentally friendly sources such as petroleum, coal and natural gas. Strong dependence on fossil fuels may lead to energy crisis in future and gradual or sudden increase in global fuel prices. Main problems related to the insecurity of energy supply are the fact that most of the fossil fuels come from politically unstable regions of the world; that those energy sources are nonrenewable; and that the fossil fuels have harmful environmental impact.

Remedy to the problems introduced by utilization of fossil fuels can be found in deployment of renewable energy sources (RESs), which can guaranty energy security of a country in the long run. World is currently is the transition phase where more and more RESs are being introduced as generators of energy mostly for electricity and heating/cooling needs. RESs cannot be direct replacement for existing electricity grid technology, because the grid is far too well established to abandon, while RES systems are not sufficiently developed to meet the total energy demand. Therefore RESs are gradually placed in the existing grids. RESs are mostly introduced to the existing grid system as distributed generation (DG) units, which generate electrical energy at the electricity distribution level.

When RESs are used as DG units they are accompanied with power electronic

based devices for power conversion and energy storage systems (ESS). In addition, number of DG units and ESSs at the low voltage side of utility grid may be interconnected together in a pattern that is different from the conventional power generation, grouped with the loads in a cluster that can generate and utilize electricity independently from grid or parallel to the grid. This kind of structure is known as the *microgrid*. The microgrid is particularly interesting as an electrical structure because it provides an opportunity to optimize the utilization of renewable energy sources with improved overall thermal and electrical efficiencies by properly locating different DG units while considering their geographical conditions and the nature of available loads. Such operating conditions require the microgrid systems to have wide range control systems in order to perform large number of tasks. For example, to guarantee the system security, optimal operation, emission reduction and a seamless transfer algorithm from grid-connected mode to islanded mode without violating system constraints and regulatory requirements are some of the main tasks.

Microgrid can be composed of many different energy sources; however, they are usually associated with RESs. Renewable energy sources have different dynamic characteristics when compared to the traditional generation sources. These dynamic characteristics present hurdles in control and integration. When connected to the grid renewable energy sources have to deliver power in controlled fashion and obey the grid standards which require specific frequency voltage generation, clean power delivery (low total harmonic distortion), high power factor and certain protection functions for safe and stable operation of the whole system. When RESs deliver power in stand-alone mode they have the requirement to generate voltages of certain amplitude and frequency and this fact imposes additional requirement on the control of these sources. Hence it is inevitable to develop rather effective control strategy in all levels of microgrid consisting of renewable energy sources to deal with mentioned issues.

Power generated by RESs depends on the environmental conditions. Their power output is highly stochastic and often RESs cannot offer necessary support to the operation of microgrid where stable active and reactive power is needed. Nevertheless, combination of different types of RESs, together with the energy storage can offer a viable solution and mitigate power reliability issues. In other words, when different types of RESs are combined into hybrid power generation system, these sources can complement each other in power delivery and a hybrid source based renewable energy system (with proper control) has great potential to provide high quality and reliable

power in microgrids. On the other hand, implementation of hybrid source is not so straightforward process due to the issues such as unavailable measurement, stochastic disturbances, nonlinearities and dynamics in each power component and the dynamic interactions between different sources. All of the mentioned issues make the control problem very challenging and worthy of considering.

Microgrid is a modern electrical architecture that incorporates renewable energy sources (RESs) and/or fossil fuel based conventional energy sources (CESs), energy storage systems (ESSs), loads and power electronic interfaces (PEIs) into self-contained portion of electrical distribution system where power is generated transmitted, consumed, monitored and managed on the local scale. Microgrids can operate in parallel to the utility grid where two-way power exchange is possible or they can operate as grid-independent power islands to supply local loads or remote areas. Connection and re-connection of microgrid with utility grid occurs at the point of common coupling (PCC), controlled by the microgrid control system. Typical microgrid structure is shown in the Figure 1-1 for demonstrative purposes.

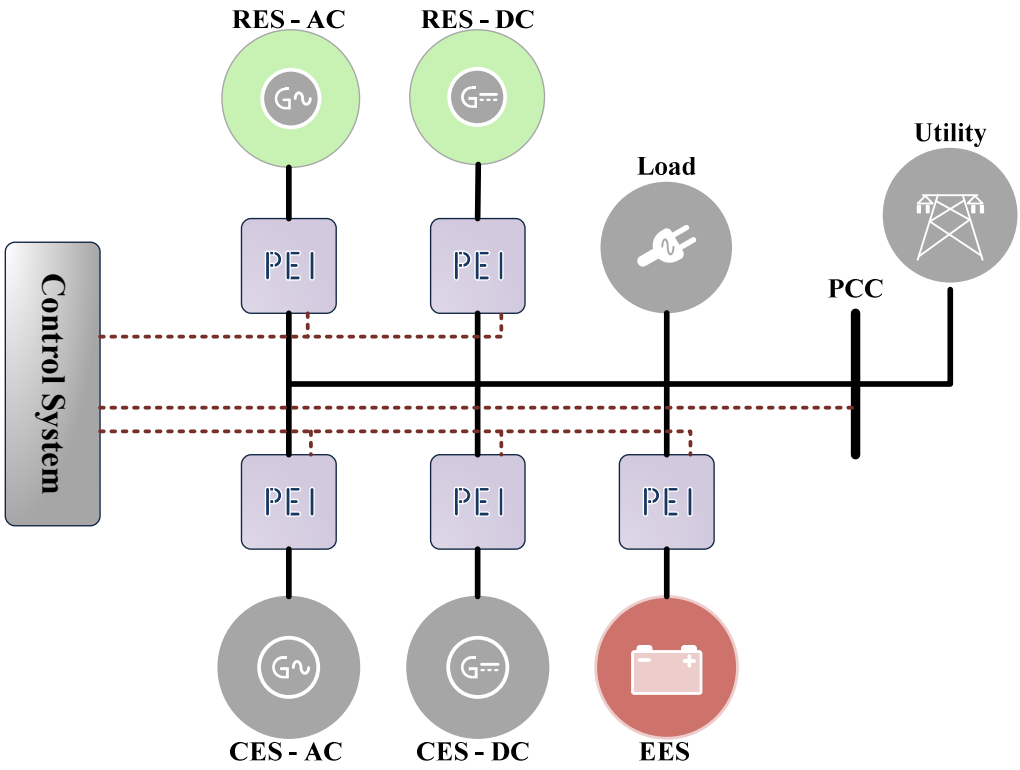

Figure 1-1 Typical microgrid

All of the components of microgrid have large individual impact on the design, operation and control of the overall system. Most of the challenges arise due to the combination of microgrid components with different dynamical responses. Additional challenges come from the operating nature of the sources inside microgrid, namely CESs are mostly dispatchable energy sources while the RESs are of non-dispatchable nature with difficult to predict energy output. To be able to deal with such challenges stringent requirements are put on the control system and power management of microgrid.

To implement control and power management in microgrids more effectively, multiple energy sources and energy storage units can be combined into hybrid energy source. Hybrid energy source can be considered as an energy node of a microgrid with bidirectional power flow capability and can deliver power according to the references generated by the microgrid controller and/or power management system. Microgrid architecture with hybrid energy source is shown demonstratively in Figure 1-2.

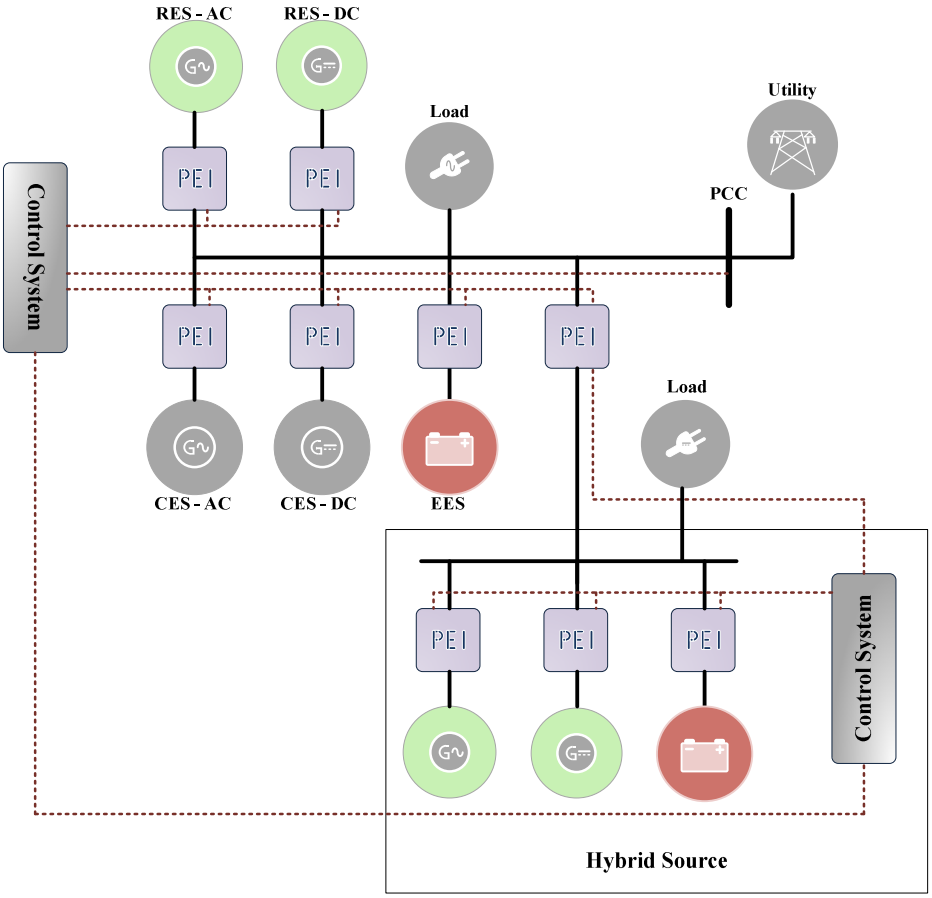

Figure 1-2 Microgrid with hybrid source

1.2 Objectives of the thesis

Hybrid energy source brings many advantages to the design and implementation of microgrid systems. Namely, microgrid with hybrid energy sources becomes a structure where all of the sources have similar or same dynamic response. Even though hybrid source may be composed of non-dispatchable sources, as a whole, together with energy storage elements, proper power electronic interfaces and control system, this source could be turned into dispatchable source. In the same time, implementation of hybrid energy source increases reliability of the microgrid system, allows for easier realization of plug and play feature and upgradability of the whole system is increased. Additionally overall system complexity is decreased since many control tasks are handled by the hybrid energy source controller.

Main objective of this thesis is to develop a framework for analysis and control of power electronics interfaces in microgrid connected hybrid energy source. Development of the framework will be done for generalized hybrid source comprised of energy source(s), storage element(s), power electronic interfaces and control system. Main justification of the stated objective lies in the advantages that unified approach to control of power electronics interfaces would bring to the design and control of hybrid source as an element of a microgrid. Basically, most important advantages that standardized control scheme would bring to the design of the hybrid source are; decreased cost of design; decreased design time; decreased design complexity; increased design flexibility; and scalability of the design.

In the attempt to accomplish the main objective, other objectives of this thesis are identified as follows;

- Modeling and analysis of sources and storage units as the elements of hybrid energy source in microgrid.
- Definition of operational requirements of power electronics for interface of sources and storage elements.
- Analysis of control system requirements for sources and storage elements.
- Definition of power electronic interface and control system for hybrid source in microgrid.
- Development of unified approach to the power electronics interface analysis and control.

- Identification of requirements for interconnection of hybrid source and microgrid.

While achieving the main objective and other objectives listed above, primary focus will be put on the hybrid source including renewable energy sources, namely, wind energy source, solar energy source, hydrogen fuel cell, and battery storage element as shown in the Figure 1-3. Nevertheless, the developed framework will permit selection of different sources and storage units as the hybrid source elements.

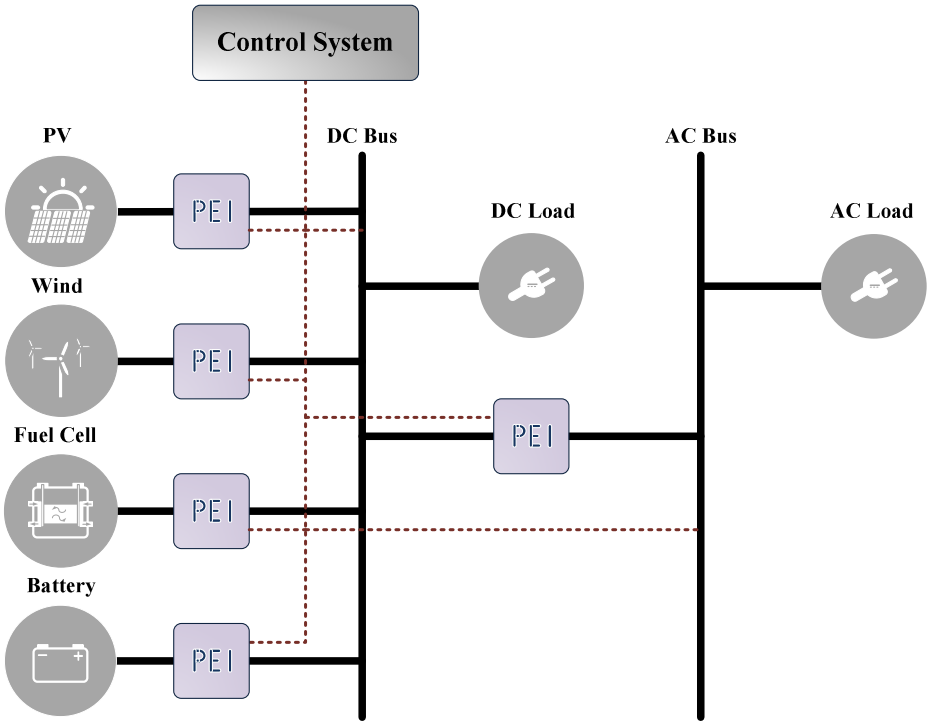

Figure 1-3 Targeted hybrid source structure

1.3 Thesis Outline

The rest of this thesis is outlined mostly in accordance to the specified objectives from the previous section.

Chapter 2 contains the literature review about distributed generation in microgrid, microgrid architectures, microgrid components and hybrid source in microgrid.

Chapter 3 covers the sources considered for implementation of hybrid energy source. Sources under consideration are renewable energy sources, namely, solar, wind, fuel cell and battery storage system. Each of these sources is modeled, analyzed and

main power electronic requirements and control system requirements are identified and presented at the end of each section. At the end of the chapter, power electronic interface and control system requirements are defined for hybrid source under consideration.

Chapter 4 is concerned with the development of a framework for analysis and control of power electronics interfaces needed for the realization of a hybrid energy source. Basically this chapter considers the unified analysis and control of power electronics converters needed in interfacing the DC and AC sources and storage units.

Chapter 5 deals with the issues associated with the interconnection of hybrid source with microgrid. In this chapter three main topics are discussed, MPPT algorithm based on sliding mode self optimization, power distribution in hybrid source and hybrid source output converter control.

Chapter 6 includes the simulation and experimental results and;

Chapter 7 is conclusion chapter where summary, main contributions and future work are given.

2 LITERATURE REVIEW OF MICROGRID TECHNOLOGY

In this chapter, literature review of microgrid systems with distributed renewable energy sources and hybrid energy source is given in detail. Firstly, microgrid concept is introduced and general information about microgrids is given. Next, types of microgrids are discussed and microgrid operation modes are explained. Many different types of energy sources and storage systems can be incorporated in microgrid structure. Details about sources and storage systems are provided together with their relevant literature references. Power electronics technology is crucial for successful operation of microgrid. This technology is reviewed and associated literature review is given. Control strategy and methods used in microgrid systems are explained as well. At the end of this chapter, hybrid source related literature is reviewed.

2.1 Distributed Generation and Microgrid Systems

In current electrical energy grid systems, energy is delivered from the point of generation to the consumers (loads). Grid system can be divided in three subsystems; namely generation subsystem, transmission subsystem and distribution subsystem. *Generation subsystem* is composed of electrical energy generation plants with high production capacity. Electrical energy generated by these plants is delivered to the distribution stations via *transmission subsystem*. On the other hand *distribution system* delivers power from distribution stations to the consumers (loads). Although, current centralized electrical energy grid system is well established, it has certain disadvantages that need to be addressed in the future. First of all, most of the generation comes from fossil fuel based plants. Besides the fact that these fuels are nonrenewable source of energy, it must be added that at least 50 - 70% of fuels energy content is lost as waste heat in the atmosphere. Nuclear power generating plants are indeed more efficient on generation level, however they also have nonrenewable nature and their environmental

effects can be disastrous. Another disadvantage of current electrical energy system lays in its centralized nature; it is often the case that the load centers are located relatively far from the generation plants. This fact makes it difficult for power system operators to monitor and act on disturbances occurring at load centers. This disadvantage has great importance for critical loads that need to receive power with higher quality that the rest of the loads. Also, in current system, due to the long transmission lines, transmission losses are high as well. Combined transmission and distribution losses are ranging from 6%-8% of generated power. Another disadvantage worth of mentioning is that system has aging equipment and complex infrastructure, which makes this system prone to often black-outs. Finally, construction of new generation stations, transmission system and distribution system to supply a geographical region with electrical energy is a process that needs strong economical justification. In other words, rural and remote areas often don't get "energized" because it is not profitable for utility providers.

All of these disadvantages have been motivation for seeking out solutions that would remedy and improve existing system. Certain number of these disadvantages has been addressed by an introduction of distribution generation (DG) units. DGs are small in size and have low power generation capacity compared to centralized generation plants. DGs are modular and can be located on-site, near the load center. They are used in parallel with utility gird or as autonomous generators to secure less or no down time (UPS) for loads, to "energize" the remote areas, to increase power quality for sensitive loads and to increase the overall efficiency of the electrical energy system. DG units that gained special popularity are those that generate energy from renewable sources such as wind, sun, geothermal, tidal, biomass and hydrogen. An interesting fact, coming from future energy demand and supply prediction studies, says that increased penetration of DG units is expected in near future [1, 2]. The increased penetration of DGs, diversity of their ownership and independent operation might create different operating conditions within electrical grid, namely, reverse power flow, excessive voltage rise, increased fault levels, harmonic distortion and stability problem. High degree of penetration of DG, their geographical distribution and sizing will have considerable impact on operation, control, protection and reliability of existing power utility [3]. In other words, increased deployment of DG units in electricity distribution networks is changing the nature of these networks from passive to active. Main issue is that distribution networks were not initially designed for such operation and above mentioned problems become emphasized in such systems.

From the above reasoning it can be concluded that, introduction of DG units in electrical distribution network solves certain problems while with the increased deployment of such units some other problems are created. When dealing with this problem, actual solution can be brought down to two possible options; first is, to redesign the network architecture completely and second is, to introduce some kind of electrical system architecture that will be able to operate as part of the existing network while allowing the deployment of DG units without mentioned drawbacks. First option is of course expensive to realize. Second solution is introduced through concept of microgrid. There exist no official, widely recognized definition of microgrid concept; however its characteristics and features are discussed in literature [4 – 6]. Microgrid is a modern electrical architecture that incorporates DG units, energy storage systems (ESSs) and loads into self-contained portion of electrical distribution system where power is generated transmitted, consumed, monitored and managed on local scale. Microgrids can operate in parallel to the utility grid where two-way power exchange is possible and they can operate as grid-independent power islands to supply local loads or remote areas. Microgrids basically benefit both utility and costumers, to the utility they can provide power or additional services (e.g. frequency and voltage support) and to the costumers they provide reliable and high quality power.

In more futuristic manner, according to [6 – 8], the architecture of future electrical energy systems will look very different from that of conventional energy system along with the microgrids expected to be the main building blocks. The smart grid concept is also introduced in these works as structure having high energy efficiency, sustainability, and renewable energy sources as generators, reliability, security, advanced sensing, measurements, advanced control methods, load usage awareness, advanced load components (e.g. electric vehicles), and integrated information and communication infrastructures.

Construction of microgrids offer opportunity for optimized utilization of renewable energy sources (RESs) and energy storage systems. Since microgrid is deployed on specific geographic location RESs whose operation is optimal for that region can be chosen as DG units. Moreover ESSs can be incorporated in the microgrid system according to the load characteristics and power specifications. Next to the electricity generation, heat generation is also concept often associated with microgrids. It is expected that microgrid incorporates both electricity and heat loads and generators in the future. This scenario is known as combined heat power generation (CHP) [9, 10].

Potential applications of CHP in microgrids are domestic water and space heating, generation of heat for industrial processes and water and space cooling and refrigeration. Microgrids that incorporate CHP are expected to have increased overall energy utilization efficiency. As simple example, generation of heat using solar energy or generation of heat from conversion of conventional fuel into electrical power process can be locally used for wide range of applications such as residential heating, sterilization chambers in hospitals or heating for industrial process.

In conclusion, microgrid that incorporates RESs and ESSs is modern concept that can offer viable solution to the problems of scarcity of fossil fuel in future, environmentally friendly electricity generation, electricity supply to remote areas and power supply to critical loads that need uninterrupted power supply.

2.2 Microgrid Architecture

Microgrid is power architecture located at the distribution level of utility power system. Plainly speaking microgrid includes variety of distributed generation sources, energy storage systems and loads in its structure. Next to these three, microgrids include power electronic interfaces, control system and communication system. Power electronics interface are needed to ensure high quality, reliable and efficient power transfer from generation and storage units to loads/grid and from grid to loads/storage devices. Power electronic equipment also has protection function to deal with emergency/faulty conditions. Control system is used to control power transfer in microgrid and to manage the whole system. Since parts of the microgrid often operate as independent entities, communication system is included to provide means for information transfer between these entities or central controller, if one exists in the system. Microgrid contains one more important component in its architecture being the point of common coupling (PCC). PCC is a controlled switch placed between the utility grid and microgrid which allows microgrid to be disconnected or reconnected to the utility grid according to the operating conditions. Typical structure of microgrid is shown in Figure 1-1 in previous chapter.

Distributed generation sources are used in microgrids to generate energy out of available energy resources. According to the nature of resources they use, DG sources can be classified into renewable energy sources and nonrenewable energy sources.

Renewable energy sources are sustainable and environment friendly sources that include generation technology such as wind turbines, photovoltaic cells, fuel cells, mini hydro turbines, wave/tidal turbines, geothermal turbines and biomass turbines. Nonrenewable energy sources include generation technology such as induction and synchronous generators driven by internal combustion engines operating using natural gas, propane or fuel oil. Some of these technologies are discussed in the next subsection, more information can be found in literature [11, 12].

Energy storage systems are used to store excess energy in microgrid when load demand is lower than momentarily capacity of generators and in the same time these systems are responsible for compensation of lack of energy when momentarily capacity of generators is lower that the load demand. Storage systems are critical components of microgrid that ensure power balance despite the load fluctuations and transients, in other words ESSs can be thought of as energy buffers that balance energy between supply and demand. Most commonly used ESSs are batteries, flywheels, supercapacitors and superconducting magnetic energy storage systems (SMES) as discussed in [13, 14].

Microgrids may include many different kinds of loads. These loads can be generally classified into two groups, sensitive and non-sensitive. Sensitive loads need to be supplied by high quality power and more importantly need to be supplied constantly (uninterrupted power supply). Non-sensitive loads have more flexible power quality specifications and can be shaded (turned off) when necessary. According to authors in [15, 16] classification of loads in microgrid is important; to be able to meet net import/export power in grid-tie mode; to stabilize voltage and frequency in island mode; to reduce the peak load to optimize operation of DG sources; and to improve power quality and reliability of sensitive loads. Microgrid can have both AC and DC type loads.

Power electronics technology allows interconnection of generators, storage elements and loads in microgrid. These interfaces guaranty compatibility of different elements in microgrid while providing efficient and flexible energy exchange. Power electronics interfaces allow microgrid systems to operate in either islanded or grid-tie mode. In general sense power electronics interfaces are expected; to provide fixed power and local voltage generation; to facilitate the DG unit to satisfy load demand using energy storage systems; to incorporate control methods for load sharing between DG units; and to integrate various key technologies for future power systems [17 - 19].

Another element in microgrid closely related to power electronics is control system. Main tasks of control system can be defined as; control of export/import of energy from and to utility grid; control of active and reactive power flow in the system; control of DG sources and their characteristics; and control of system frequency and voltage within set limits. Control in microgrid systems has important place in research of microgrids and covers many different topics.

Communication system is component of microgrid that realizes exchange of important information between different parts of microgrid. For the sake of better match between demand and supply of energy inside the microgrid, coordination between controllers of DG units, ESSs, loads and grid is done using communication system. This system in overall provides increased energy utilization efficiency and increased economic benefit for the microgrid operator. There exists no standard communication protocol used in microgrid yet, however general ways of dealing with this problem are discussed in literature and will be presented in following subsections.

2.3 Microgrid Classification

Classification of microgrid architectures can be done in few ways. In [16] this classification is done based on microgrid applications as; utility microgrids; industrial and commercial microgrids; and remote microgrids. On the other hand, more common classification is done based on the way power is distributed and transmitted inside microgrid, namely, DC microgrids, high frequency AC microgrids, line frequency microgrids and hybrid DC and AC microgrids. Each of these architectures has certain advantages and disadvantages that depend on the nature of components found inside specific microgrid. Hence during the microgrid design process these advantages and disadvantages should be considered and feasibility and economic studies should be performed to properly decide on suitable architecture for that specific microgrid.

2.3.1 DC Microgrids

Most of the modern loads found in residential buildings, office buildings and commercial facilities are of DC nature (PCs, printers/scanners, TVs, various home

appliances, etc). Number of pure AC loads is significantly decreased in modern systems due to the advances in power electronics and control theory areas. Even the conventional loads driven by AC motors (washing machines, refrigerators, air conditions, etc.) are being replaced by AC motors with inverters, supplied by DC power, that can control the motor speed and decrease overall energy consumption. Even though there are so many DC loads in usage, due to the AC power distribution system convention they are being driven by AC power. To accommodate the difference in power characteristics, AC/DC converters are being placed at their power inputs. These converters are usually designed using bulky line transformers and passive electronic components resulting in inefficient power conversion and introducing undesirable dynamics to the power system. As solution to these issues an introduction of DC power distribution system has been proposed and applied to many different systems such as telecommunication systems [20], ship power systems [21] and electrical vehicles [22], where they proved to be more efficient and cost effective than AC distribution systems. DC distribution systems are suitable for application to microgrids that contain DC loads, DC sources and DC storage units.

Low voltage DC (LVDC) distribution network has been proposed in [23] to tackle the above mentioned problems and to realize future power systems based on DC microgrids. In [24] authors show that LVDC distribution network can improve efficiency of power delivery, ensures higher power quality than present distribution network (conventional AC) and can facilitate DG units connection. Opportunities and challenges in research of DC distribution system for industrial power system are discussed in [25]. Authors point out the interaction between power converters and issues related to the grounding of DC power distribution systems. Feasibility of a DC distribution network is analyzed systematically in [26] Application of DC microgrid to small scale, residential buildings is presented in [27, 28]. In overall it can be concluded that microgrids based on the DC distribution network have advantageous features including simple structure, low system cost and overall improved efficiency (decreased number of converters) compared to the AC microgrids [23, 24, 29].

Figure 2-1 depicts a typical structure of DC microgrid. In this configuration DC generation and storage units are interfaced to DC link through DC/DC converter, AC generation units are interfaced to DC link through AC/DC converters, local DC loads are fed from DC link directly or through additional DC/DC converter and pure AC loads are interfaced through DC/AC converter. Connection of DC microgrid to utility

grid is done through central DC/AC converter. On the DC distribution level synchronization of source and storage outputs is not required. This advantage of the system decreases the complexity of control system. Different variations of DC microgrids are discussed in [30] where three DC link configurations are identified as monopolar DC link, bipolar DC link and homopolar DC link.

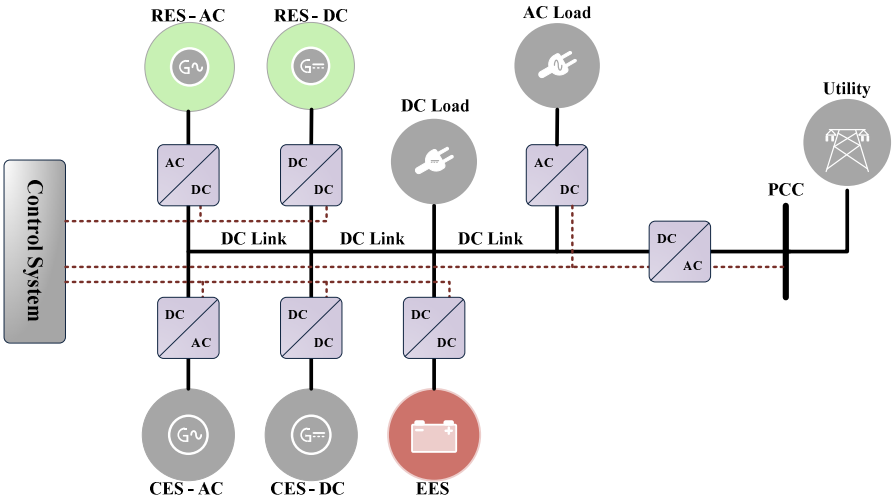

Figure 2-1 Typical structure of DC microgrid

2.3.2 High Frequency AC Microgrids (HFAC)

In high frequency AC microgrids power is distributed at frequency higher than line frequency (50Hz/60Hz). Power electronics in these systems incorporate high frequency transformers and suitable converters. Typical HFAC microgrid is shown in Figure 2-2. Usually these systems operate at multi-kHz frequencies, nevertheless some microgrid systems can be developed to operate at 500Hz [31]. In general, high frequency power transfer offers certain advantages over and line frequency AC and DC microgrids, namely, power quality is easier to improve at higher frequencies, acoustic noise can be minimized with frequencies above 20 kHz, soft switching can be explored to reduce power losses and power transformers and passive filter elements can be made smaller in value and size [32]. On the other hand main disadvantage of HFAC is that they are limited to local areas since the losses are dramatically increasing with the distance.

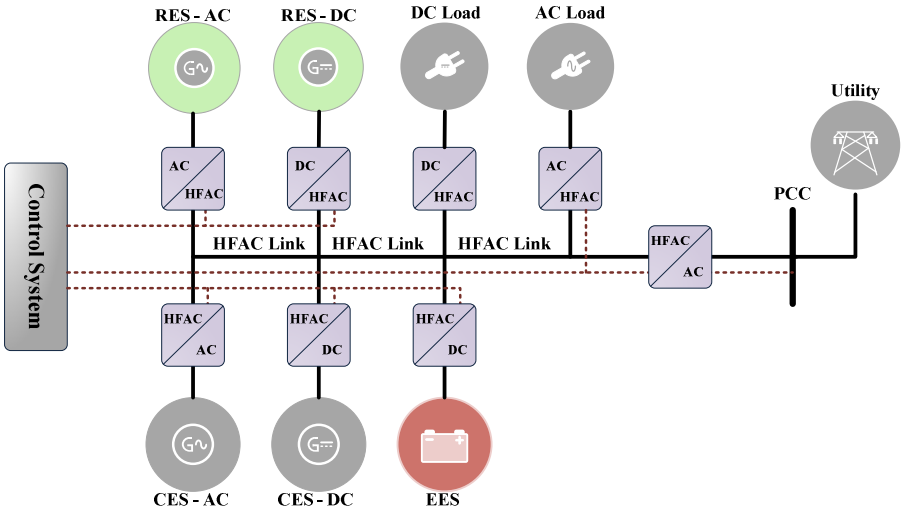

Figure 2-2 Typical structure of HFAC microgrid

2.3.3 Line Frequency AC Microgrids (LFAC)

Typical line frequency AC microgrid is depicted in Figure 2-3. DG units that generate grid compatible AC power can be connected to the AC distribution network directly, while DG units that generate variable AC power have to be connected to the distribution network through additional AC/DC/AC or AC/AC converter. DG units that generate DC power are interfaced using DC/AC converters and storage units are interfaced using bi-directional DC/AC-AC/DC converter. AC loads are fed directly from distribution network and DC loads require AC/DC converter for operation.

Control, protection, configuration and operation of LFAC microgrids with renewable and non-renewable based DG units have been investigated thoroughly in literature. Explicit literature review will not be given in this section for the sake of consistency. Literature review covering these concepts will be given in later sections when they are discussed in detail, additional review of LFAC can be found in [33].

Advantages of AC microgrid lay in its convenience due to the popularity of AC distribution network. Most of the operational loads on the market are designed to work with AC power. Compared to the DC microgrid, AC microgrids don't need require central inverter which makes this configuration more modular and in the same time more failure resistant. When compared to DC microgrid, AC microgrids are less efficient and have synchronization requirements which increase the complexity of the overall system.

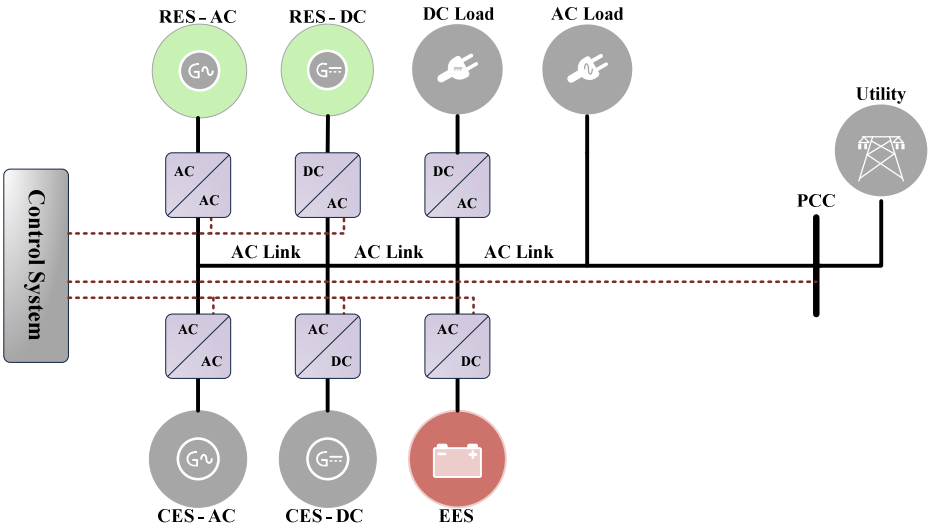

Figure 2-3 Typical structure of LFAC microgrid

2.3.4 Hybrid DC/AC Microgrids

Hybrid AC/DC microgrid architecture naturally appeared out of need to combine advantages of both AC and DC microgrids. In hybrid microgrids, DC sources are combined with DC loads and energy storage units while AC sources are combined with AC loads. Hybrid architecture presents effective way of integration of variety of DG units into existing utility grid [34, 35]. In these systems power converters are used to decouple AC and DC parts of microgrid electrically and in the terms of control and management. In hybrid microgrid DG units that generate AC power are placed on the AC side of microgrid together with AC loads and DG units that generate DC power are found on the DC side of microgrid together with storage and DC loads.

Main advantages of hybrid microgrid can be summarized as follows [36]; elimination of unnecessary multi-conversion processes which implies reduction of total power loss; simplification of equipment and cost reduction by elimination of embedded AC/DC converters for DC loads; the connection of all DC loads to the DC side of hybrid microgrid make it easy to control harmonic injections into the AC side through the central DC/AC converter, thus guarantying high-quality AC power in the utility grid; and DC grid is capable of solving negative and zero sequence currents problems caused by unbalanced loads in AC distribution network thus eliminating the need for neutral wire in transmission which results in reduction of related transmission losses.

2.4 Microgrid Operation Modes

Microgrids can be seen as controllable entities that operate as generator or load depending on the given conditions. Microgrids can be connected to utility grid or operate isolated from it, i.e. microgrids have two operating modes; grid-tie and island. In each of these modes microgrids operate on certain set of technical conditions that define control, communication and protection functions of the overall system. Microgrid is an electrical structure that can be isolated from the utility grid intentionally, or when utility grid fails (fault condition) or blacks out. The action of disconnection and reconnection from and to utility grid is controlled by microgrid control system and main switch is positioned at point of common coupling PCC.

2.4.1 Grid-Tie Mode

In this mode microgrid is electrically tied to the utility grid. It can be connected to the medium voltage (e.g. 11-65 kV) or low voltage (e.g. 110-690 V) networks depending on its location in the distribution network and the generating capacity [37]. In this mode microgrid either receives power from utility grid or injects power to the utility grid depending on the current economical or technical operating conditions. Technical operating conditions can imply that the power demand in microgrid is higher than the current generation capacity so deficit power must be received from grid or the power demand is lower than the current generating capacity so excess power is injected to the utility grid. Economical conditions on the other hand would consider the current cost of power import from and export to utility grid.

In grid-tie mode, inverter interfacing microgrid with utility operates on voltage reference present at the utility grid. Voltage amplitude, frequency and phase angle references are obtained from grid voltage and inverter voltage is synchronized to it. After synchronization is achieved, inverters' active and reactive powers are controlled according to the references commanded by microgrid operating manager [38, 39]. In this mode inverter operates as controlled current source.

2.4.2 Island Mode

In island or standalone mode microgrid is disconnected from utility grid and operates as electrical island. All loads are supplied from available power generated by DG units or stored in ESSs. If generated power is higher than the demand power, excess power is stored to ESS and if the demand power is higher than the generated power, loads are supplied from ESS. Additionally non-sensitive loads can be shed if power capacity of microgrid is insufficient to support all of its loads [40, 41].

In island mode, inverter interfacing microgrid with utility grid operates as controlled voltage source. Reference voltage amplitude, frequency and phase angle are generated internally by microgrid operating manager and no synchronization with grid voltage is required. System voltage is regulated by balancing generation power and load demands [15].

Transition from grid-tie to island mode and vice versa is important topic to consider from the system stability point of view. Control method implemented in microgrid has to consider smooth transition between these two modes as one of the important requirements.

2.5 Distributed Energy Sources in Microgrid Systems

Energy sources in microgrid are mainly distributed energy sources, in literature also called distributed generation (DG) units or microsources. DG units that are of special interest for microgrid are small (<100 kW) energy sources with power electronic interfaces. DG technologies applicable for microgrid may include emerging technologies such as wind turbine, solar PV, micro-hydropower turbine, diesel powered generators, hydrogen fuel cells, small gas turbines and some well-established technologies like single-phase and three-phase induction generators and synchronous generators driven by IC engines [42]. Additionally combined heat power (CHP) systems are also very often used in microgrids. Different kinds of sources are being used in CHP systems such as microturbines driven by natural gas, hydrogen, or biogas, Stirling engines, and IC engines [43]. Microgrids may include two or more of these DG units. Choice of type of DG unit depends on many factors such as the climate and topology of the region, fuel availability and economic considerations. More information about DG

sources can be found in [11, 12].

DG units inside microgrid can be distinguished by their interface characteristics as conventional rotary DG units and electronically-coupled DG units. Example of conventional DG unit could be synchronous generator driven by a reciprocating engine or an induction generator driven by a fixed-speed wind turbine. Examples of electronically coupled DG units are fuel cells, PV systems and variable speed wind turbines. In terms of power flow control, a DG unit is either a dispatchable or a nondispatchable unit. The output power of dispatchable DG unit can be controlled through set points provided by control system. On the other hand the output power of a nondispatchable DG unit is controlled based on the optimal operating condition of its energy source. For example, a nondispatchable wind or solar unit is operated based on the maximum power tracking concept to extract the maximum possible power coming from wind turbine and solar panel, respectively.

2.6 Control of Microgrid Systems

Control of microgrids can be discussed from many different perspectives because indeed it is a research that covers many topics. This literature review deals with several aspects of control in microgrids.

Power electronics interfaces in microgrids are used to interface various components of microgrid and allow reliable and high quality power exchange between sources/storage units and grid/loads. Such power electronics intense structure requires proper control strategies to be implemented [44]. Since microgrid design can vary in terms of services it provides (power back-up, grid support, main source of power), components it incorporates (sources, storage units, loads) and architecturally (AC, DC, hybrid), generalized control tasks are difficult to formulate. This problem can be looked at from different perspective, namely, definition of control tasks through the requirements of the standards for integration of microgrids into utility grid, for example IEEE Std. 1547.4 – 2011 [45],

Based on Std.1547.4-2011 four modes of operation of microgrid have been identified as grid-tie mode, island mode, transition-to-island mode and reconnection mode. Grid-tie and island mode have been discussed previously in this text, as main modes of operation while other two modes can be seen as transitional modes. Properly

designed microgrid control system has to allow the operation of microgrid in all modes while satisfying its various technical requirements.

In grid tie mode, control system needs information about protection devices status, current generation level, local loads and system voltage levels so the transition from grid-tie to island mode can be planned in advance [45]. Both AC and DC microgrids are based on the inverter for interface with utility grid and power transfer, so proper control of these devices is crucial for successful operation of the whole system. During grid-tie mode inverters are operating in current mode. In current mode inverter is given active and reactive power references to be controlled. Grid voltage is used as reference to obtain the voltage signal with correct frequency, amplitude and phase angle needed for current reference computation and power factor correction [46 – 48]. This control scenario in grid-tie mode implies that all sources and storage units can be viewed as current sources whose power flow can be controlled by controlling their output currents. Overall system stability is maintained by utility grid [49], as utility grid is expected to support difference in active/reactive power requirements and maintain voltage amplitude and frequency [50].

In island mode microgrid is disconnected from the utility grid so voltage reference, normally present in grid-tie mode, is lost and control system is responsible for its generation internally. The main task of control system in this mode is to ensure generation of adequate amount of power for local loads, which implies that the microgrid voltage amplitude, frequency and phase angle has to be maintained at the levels required by the connected loads. In island mode system inverters operate in voltage mode and together with sources and storage units they can be seen as synchronous generators with fixed frequency reference and fast voltage regulation control, so all the control techniques developed for these systems can be directly applied here as well. In general it can be said that sources and storage units in this mode are controlled voltage sources whose outputs share the load demand in proportion to their power ratings [51] not to overstress any individual unit [52 - 54]. Reason for such share of power resources is that there usually doesn't exist a single dominant energy sources to supply overall power demand [55 - 57]. Each inverter in the system supports the power demand by adjusting its terminal voltage characteristics and consequently its output power. IEEE Std. 1547.4 – 2011 suggests that, in island mode there should always be power reserve margin as a function of load factor, magnitude of load and the load shape, reliability requirements of the load and the availability of DG units. To

maintain power reserve margin control system should implement techniques such as load following, load management and load shedding. This standard further puts requirements on the system stability that should be maintained for load steps, DG unit power outage and various faults. Control system should be flexible in order to meet these requirements.

In transitional modes, transition-to-island and reconnection mode, control tasks are defined in the terms of safe, stable and seamless transition from one mode to other. In transition-to-island mode DG unit generating capability has to be available in the system to support voltage amplitude and frequency for the time necessary for transition to occur. In reconnection of microgrid to utility grid both systems have to be synchronized in voltage. In other words, microgrid voltage has to be controlled to follow utility grid voltage.

Following the IEEE std.1547.4-2011 tasks of the microgrid controllers are defined as above. In [58] summary of microgrid controller responsibilities is given. According to the authors microgrid controller has to ensure that: (i) DG units work properly with predefined operating point (e.g. maximum power point tracking); (ii) active and reactive powers are transferred according to the necessity of microgrid and/or distribution system; (iii) disconnection and reconnection processes are conducted seamlessly; (iv) production of local DG units and power exchange with utility is optimized; (v) heat utilization for local installation is optimized; (vi) sensitive loads are supplied uninterruptedly; (vii) in the case of general failure the microgrid is able to operate through black-start; and (viii) energy storage systems can support the microgrid and increase system reliability and efficiency.

Based on the controller tasks and coordination, different controller architectures are proposed in literature. Among classifications the most common is classification of microgrid controller into; autonomous (local) controller and hierarchical controller which is further divided into centralized and decentralized type. Each of these architectures has their comparative own advantages and disadvantages regarding cost, operation and reliability which have to be analyzed in the design process of microgrid. Due to this reason, for a given microgrid, the most suitable architecture has to be decided.

Autonomous (local) controllers are mainly used to control DG sources. This type of controller aims to keep DG sources at their optimal operating point and control their power electronic interfaces. Measured data used by local controllers are local currents

and voltages [58] and they usually don't require communication interface with the rest of system which results in design simplicity and low cost. These controllers must ensure easy addition of new sources to microgrid system, sometimes called "plug-and-play" characteristic.

It is difficult to specifically define the local controller because the details of their implementation would depend on whether they are operating in DC, AC or hybrid microgrid. Nevertheless, authors in [53] put effort towards this task by defining a general model of DG source connected to a microgrid. This model contains three basic elements, prime mover (source), DC interface with storage and voltage source inverter (power electronic interface). In this model, inverter is responsible for regulation of magnitude and phase of output voltage in order to control active and reactive power. Most common methods to regulate power is droop-based active and reactive power control, namely voltage-reactive power and frequency-active power droop control [59, 60].

Hierarchical control system can be of centralized nature or decentralized nature. Centralized controllers are best used for microgrids that include DG sources, storage units and loads that have single owner or multiple owners with the same goal. Centralized controllers are also suitable for small scale microgrid that can be controlled with a presence of an operator [61]. On the other hand, decentralized controllers are the most suitable for microgrids that include DG sources, storage units and loads that have different owners with different goals so certain decisions should be taken locally. In decentralized control systems action of controller of each unit usually should have certain degree of intelligence [61] and be able to send and receive information through communication channels.

Authors in [15] have identified three control levels in hierarchical controller structure, namely, *grid level, management level and field level*. Functions of *grid level* are to manage the operation of the medium voltage and LV areas with several microgrids. Distribution network operator (DNO) and a market operator (MO) are found on this level. DNO is interfaced with several microgrid central controllers (MGCC) found at the *management level*. At *management level* MGCC has tasks of; restoration control which improves voltage and frequency of the system; synchronization between microgrid and utility grid; managing the load serving or shading; and optimization of the production using some predefined cost function. At the *field level,* local controllers (LC) are found that are responsible for inner control of DG

units and storages in order to meet the voltage and frequency references. Local controllers can be also identified as load controllers for the case of controllable loads. These controllers are capable of working both when connected and disconnected to and from the main grid while guaranteeing the satisfactory performance of the system.

DNO and MO operate and manage the microgrid and their main connection to microgrid is through MGCC. The MGCC has function of production maximization and coordination of LCs. On the other hand many microgrids can be interconnected, forming a network. In this case, an intermediate management control structure is added to carry out some management tasks [62].

2.7 Energy Management System and Communication in Microgrids

Energy Management System (EMS) is a control layer of microgrid that is responsible for optimal allocation of power among DG units, supplying loads economically, synchronization and resynchronization of microgrid to utility grid and managing system status. Microgrid EMS has to ensure that given microgrid provides high-quality power in reliable, sustainable, environment friendly and cost-effective way. EMS should coordinate variety of DG units, storage units and loads. Microgrid EMS operates by receiving load and energy load and energy resource forecasting data, customer information/preference, policy, and electricity market information to determine the best available controls on power flow, utility power purchases, load dispatch, and DG / storage unit scheduling [63].

Energy management problem in microgrids lays in finding optimal dispatch of DG and storage units (in power system literature also called unit commitment). In grid tie mode EMS objective is to maximize profit [64] and in island mode EMS objective is to economically supply the local load [65]. Usually additional objectives can be considered such as minimization of greenhouse gas emission [65, 66] using multi-objective optimization techniques.

There are two approaches to the design of microgrid EMS, namely centralized and decentralized [63, 67] which are very closely related to the control architecture implemented in the given microgrid.

Centralized EMS consists of a central controller that is provided with the relevant information of every DG unit in microgrid and microgrid itself such as cost functions,

technical limitations, network parameters and mode operation as well as information from forecasting systems (e.g., local load, wind speed, solar radiation). General framework for the development of centralized EMS is proposed in [68]. In [69] authors utilize dynamic linear programming in centralized EMS for a microgrid composed of hydrogen storage and wind. In [70] linear programming with heuristics is proposed in implementation of centralized EMS for a PV-storage microgrid. Different evaluative algorithms for optimization are also applied to the centralized EMS problem in [71] and [72]. In centralized architecture, computationally powerful central controller is necessary to process large amount of real time data coming from DG units, storage units and loads in a timely manner. This structure also requires the implementation of a reliable two-way communication infrastructure. Centralized EMS is easy to implement, has standardized procedure but high expansion cost and high communication network capacity.

In decentralized microgrid EMS each microgrid component is controlled by local controller rather than by a central controller. Each of the local controllers communicates with other local controllers through communication network. Local controllers can make their own operational decisions independent of central controller. Decentralized EMS is usually constructed using Multi-Agent Systems (MAS). A decentralized EMS based on MAS for microgrids was first proposed in [73] as an alternative for coordinated operation of microgrids in a competitive market environment and with multiple generator owners. In these systems consumers, generators, energy units and the main grid participate in the market by sending buying and selling bids to the central controller based on their particular needs, availability, cost functions, technical limitations, expectations and forecasts. A similar MAS approach is also proposed in [74]. Additional agents assigned to different tasks such as load shifting and load curtailment to allow demand side management are proposed in [75] as well. There is no need for manipulation of large amounts of data which reduces computation time. Another important advantage of decentralized EMS is its flexibility, as it provides the plug-and-play feature. Disadvantages of this type of the EMS come into play when it is applied to microgrids that require strong cooperation between the different DG units in order to operate the system in a secure and reliable way.

From the discussion above it can be seen that for a microgrid that is controlled in centralized or decentralized manner communication system is important component of the overall system. Since there is no standard way of communication system design

many different communication configurations and protocols are possible. In a conventional power utility system, the standards related to the communication system has been provided to ensure the exchange of critical information, e.g., control commands, status information, and measurement data, efficiently. Among the standards are Distributed Network Protocol (DNP), UCA 3.0, Modbus, and PROFIBUS, as well as other protocols with custom communication links. In [76, 77] authors provide a contemporary look at the current state of the art in communication systems of modern power grid.

2.8 Protection of Microgrid Systems

Microgrid protection system has a role of electrical protection of all equipment in microgrid. Microgrid protection system differs from the conventional utility grid system in type of protection devices used and in methods involved for detection of abnormal conditions in electrical network [78]. One of the major challenges in protection of microgrid is the design of protection system that can adequately operate in both grid-tie and island mode. This challenge mainly exists because fault currents have different characteristics in these two modes [79, 80].

In a properly protected microgrid, when fault occurs on utility grid microgrid is disconnected from faulty utility grid (islanding action), on the other hand if fault occurs in the certain section of microgrid that section alone is disconnected from the rest of microgrid and reconnected once the fault is cleared. This scenario gives out important properties of microgrid protection system. Firstly, the fault nature varies so protection has to be able to deal with various fault conditions, and secondly, protection equipment has to be placed strategically so fault can be localized with least possible influence to the rest of the system. In general, proper coordination between DG units, storage units, loads and protective equipment is crucial for safe operation of microgrid. Additionally, settings of the protective equipment should be always updated according to the mode of operation of microgrid (island or grid tie) [81 – 83]

Microgrids generally incorporate both AC and DC type of equipment, so protection system has to be designed to protect both. Several protection methods for AC microgrid are reviewed in [84]. These methods resemble those used for protection of conventional utility grid. The issues of protection of microgrid and requirements for

protection of modern microgrids and smart grids are discussed in [79]. DC microgrid protection guidelines can be found in electrical safety standards for DC networks such as Finnish standard SFS 6000 or German standard VDE AR-N-4105.

Widely used devices for protection devices are over-current relays, re-closers, sectionalized circuit breakers and fuses for AC equipment and fuses, molded-case circuit breakers, power circuit breakers, fast static switches and isolated case circuit breakers for DC equipment [30].

When microgrid is looked at as whole, regardless of working mode or the type of equipment protection categories can be classified to: (i) utility protection; (ii) power electronic converter protection; (iii) DG unit protection; (iv) feeder protection; and (v) bus bar protection [30].

2.9 Hybrid Energy Source in Microgrid

Utilization of hybrid energy sources in microgrid is one of the most efficient ways to overcome the reliability and control of power delivery. These sources can consist of many different, both renewable and nonrenewable, energy sources. In literature authors mostly cover specific solutions. Most of the hybrid sources described in the literature are based on the wind turbine and photovoltaic (PV) modules as sources and battery units as storage elements [85 - 87]. Addition of fuel cell to wind turbine, PV module and battery is analyzed in [88 - 90]. This solution is very attractive from the energy reliability point of view since these sources can controlled to complement each other in operation effectively. Additionally, this combination is possibly the most pollution free combination of sources. A hybrid source alternative with diesel generator in combination with other renewable energy sources is analyzed in literature. Diesel generator and fuel cell are presented in [91, 92], diesel generator and wind turbine in [93] and diesel generator, wind turbine and PV module in [94].

Similar to the microgrid systems, system configurations for hybrid energy sources are DC coupled hybrid source, AC coupled hybrid source and combined AC/DC hybrid source [95, 96]. In DC coupled hybrid source system all of the sources and storage units are coupled to the common DC bus through appropriate power electronic interface and DC bus is interfaced to AC bus through an inverter. Such configuration is mostly used for low power hybrid sources [95]. In AC coupled hybrid energy surce different sources

and storage elements are connected to a common AC bus through appropriate power electronic interfaces. Third configuration is mixture of DC coupled and AC coupled hybrid energy source [96].

Considering the available literature in this field, most evident technical problems related to the utilization of hybrid energy source in microgrids are related to the selection of overall system configuration type, reduction of the system cost, design of appropriate control strategies, identification of control system requirements and specifications, optimal sizing of components, and selection of suitable energy storage technologies [97].

2.10 Conclusion

In this chapter microgrid technology has been reviewed. From the presented literature review it can be concluded that currently a lot of research is being undertaken on the topic of design and control of microgrids and hybrid energy sources. In general, elements of the microgrid and hybrid energy source are looked upon individually and their control strategies are proposed. However, when several DG sources and energy storage units are connected together in microgrid or hybrid energy source, problems arise in uniqueness of the approach to the control of such system. Lack of electrical standards for development of such systems adds up to that problem.

Microgrid control problem can be considered in different levels. Upper levels of control system are mostly dealing with monitoring, management and global operation strategies while lower levels of control system are mostly concerned with the control of power electronics interface control and local power control. It is evident from literature review that there has been no attempt in literature to generalize the control problem, such that certain or mixture of control approaches could be applied, directly or with little change, to the control of elements in modern microgrids consisting of renewable energy sources and hybrid energy sources in general.

Renewable energy distributed generation penetration in utility grid has been identified as viable solution to the scarcity of fossil fuels and increasing environmental pollution problems, however the increased penetration of these sources causes stability and other operational problems. As a remedy, microgrid system has been presented and the way that this technology solves issues involved with integration of distributed generation has

been analyzed. There exist several possible microgrid architectures, DC, LFAC, HFAC and hybrid AC/DC. Advantages and disadvantages of these architectures are given together with their explanation. Further, operation modes of microgrid have been identified as grid-tie and island. Nature of both modes and their operational requirements are given. Implications of these modes on the control of microgrid systems have been listed and architectures of overall microgrid controllers are analyzed. Additionally protection, energy management and communication in microgrid systems have been reviewed. Hybrid energy source place in literature and important research challenges have been identified.

3 HYBRID SOURCE IN MICROGRID SYSTEM

This chapter is organized to present work done towards accomplishing part of the objectives identified in Chapter 0. Through the work in this chapter following objectives were realized;

- Modeling and analysis of sources and storage units as the elements of hybrid energy source in microgrid;
- Definition of operational requirements of power electronics for interface of sources and storage elements into hybrid energy source;
- Analysis of control system requirements for sources and storage elements;
- Definition of power electronic interface and control system for hybrid source in microgrid.

Modeling and analysis of PV system, wind energy conversion system, fuel cell system and battery storage system were done considering elements of these systems that are the most important for the definition of their power electronic interfaces and control systems. In all of the mentioned systems, energy sources (PV module, wind turbine, fuel cell and battery storage unit) were modeled considering physical phenomena that are affecting or defining their electrical characteristics. Furthermore, based on the electrical characteristics of the modeled sources set of the power electronic interface and control system requirements are given. As the final section of this chapter the proposed hybrid source and it's power electronic interface and control requirements are identified based on the previous analysis for individual energy sources.

3.1 Solar Photovoltaic (PV) System

Sun energy is converted to electrical energy by means of solid-state electrical device called photovoltaic (PV) cell or simply solar cell. PV cell converts light into direct current electricity and has current-voltage characteristics that are function of the

characteristics of the light source, construction material and the device design. PV cells are made out of various semiconductor materials including silicon, cadmium sulfide, cadmium telluride and gallium arsenide. These semiconductors are usually employed for construction of PV cell in single crystalline, multi-crystalline, or amorphous forms.

PV cells are usually low power devices with power range between 1W and 4W. Considering the voltage and current characteristics of a single PV cell it can be noted that these devices usually have low output voltage and high current output. For these reasons, PV cells are often combined into PV modules (solar panels) to achieve higher voltage outputs while current characteristics remain unchanged. PV modules can be constructed to produce outputs at various power levels. Currently, these modules are produced to generate up to 300W of DC power. Lower limit of generation power varies depending on the application of PV module, e.g. educational modules can be found with generation capacity of few watts.

PV module integration into hybrid source should be done using particular configuration of PV modules, proper power electronics interface and control system. In order to define these elements of integration, PV cell and consequently PV module as series combination of PV cells should be modeled and analyzed. Furthermore, model should reveal electrical behavior and important characteristics of a PV module that will allow for definition of power electronics interface and control system design requirements.

3.1.1 PV Module Modeling and Analysis

When the light is incident on the PV cell charge is generated that causes electric current to flow once the cell terminals are loaded or short circuited. Generation of charge happens when the energy of the incident photon is sufficient to detach the covalent electrons of the semiconductor. Most basic explanation of electricity generation by PV cell can be described as the absorption of solar radiation, the generation and transport of free carriers at the p–n junction, and the collection of these electric charges at the terminals of the PV cell. The amount of current is dictated by the irradiance of the incident light, PV cell temperature and some other factors. Physics of the PV cell is relatively complex and its consideration is outside of the scope of this thesis. PV cell be analyzed based on electrical characteristics which is important for the

study of power electronics interfaces and PV systems integration into considered hybrid source and microgrid in general.

Modeling of PV cell is relatively well explored topic in literature. PV cell is generally modeled as the current source in parallel with diode. Simplest model considers the current source and diode as ideal and model doesn't consider any loss elements. More complicated model is considering the series resistance at the output of the cell to model the ohmic losses. On the other hand, model used in this thesis is considering current source to represent current generated by the irradiated light, a diode in parallel to it to represent cell polarization process and resistor in series and parallel (shunt) to model the ohmic losses of PV cell. Model under consideration is depicted in Figure 3-1. Such model is often called "one diode model" and it is used by PV cell manufacturers to determine the technical characteristics of their solar cells (data sheets).

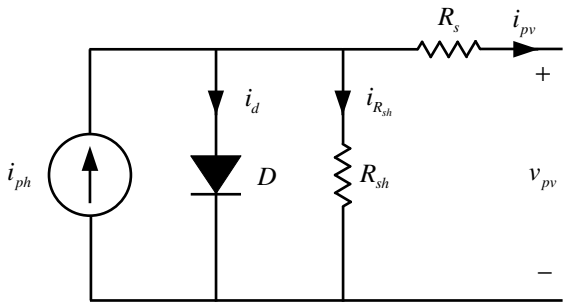

Figure 3-1 PV cell electrical model

Considering the circuit in Figure 3-1, electrical characteristics of PV cell can be modeled by expressing the terminal voltage v_{pv} in the terms of terminal current i_{pv} or by expressing the terminal current i_{pv} in the terms of terminal voltage v_{pv}. Either way the governing electrical equations are obtained using Kirchhoff's current and voltage laws. From Kirchhoff's current law following relation can be obtained,

$$i_{ph} - i_d - i_{R_{sh}} - i_{pv} = 0, \tag{3.1}$$

with diode current expressed as,

$$i_d = i_0 \left(e^{\frac{V_d}{V_t}} - 1 \right), \tag{3.2}$$

where

$$V_t = \frac{AkT_n}{q}. \tag{3.3}$$

From Kirchhoff's voltage law following relation can be obtained,

$$v_{pv} + R_s i_{pv} - V_d = 0. \tag{3.4}$$

Finally, PV cell current can be expressed as,

$$i_{pv} = i_{ph} - i_0 \left(e^{\frac{v_{pv} + i_{pv} R_s}{n_s V_t}} - 1 \right) - \frac{v_{pv} + i_{pv} R_s}{R_{sh}}. \tag{3.5}$$

In the above equations i_{ph} is the photo-generated current at standard testing condition (STC), i_0 is the diode saturation current at STC, R_s is the series resistance, R_{sh} is the shunt resistance, A is the diode quality factor, k is Boltzmann's constant, q is the charge of the electron, T_n is the temperature at STC and n_s is the number of cells connected in series (for single cell n_s this coefficient is 1).

Model parameters can be extracted from the PV cell manufacturers' datasheet. All the values given in datasheet are given under STC, the testing conditions used to measure PV cell nominal power. Parameters not found in datasheet can be determined using method in [98].

Photo-generated current i_{ph} depends on the sun irradiance and temperature of the PV cell or PV module. Above given model only considers dependence of this current on the irradiance, temperature is considered constant (specified during STC). Temperature dependency is omitted because it does not provide any crucial information when considering the power electronics or control of PV system.

To justify the model from (3.5), simulation of electrical characteristics of commercial 300W PV module is done and results are shown in Figure 3-2. In this figure dependence of the electrical characteristics on the irradiance is indicated by multiple *i-v* responses for different irradiance values. It is clearly seen from this figure that photo-generated current values increase with the increase of the irradiance. It is often the case that there exist a linear relationship between irradiance and photo-generated current.

Additionally, Figure 3-3 shows the power change of module with respect to its terminal current. There is one maximum power point (MPP) for every test irradiance (global maximum). MPP is clearly shown with dot on the graph.

Simulated PV panel electrical data are given in the Table 3-1.

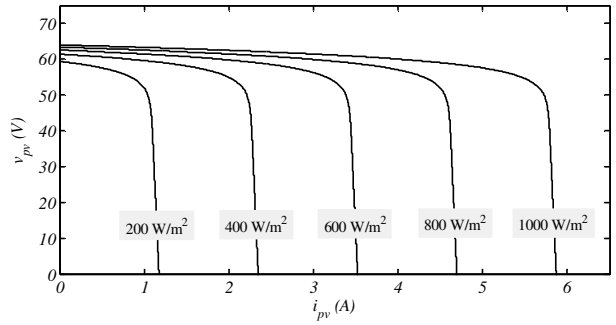

Figure 3-2 i-v characteristics of solar module

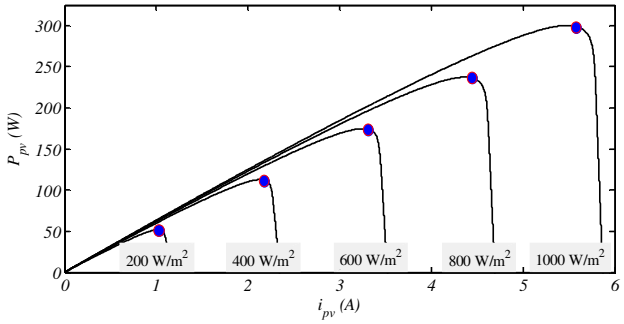

Figure 3-3 PV module power curves

Electrical data SUNPOWER SPR-300NE-BLK-D PV module (Measured at Standard Test Conditions (STC): Irradiance 1000W/m², AM 1.5, and cell temperature 25° C)	
Nominal Power	300 W
Panel Efficiency	18.4%
Rated Voltage (Voltage MPP)	54.7 V
Rated Current (Voltage MPP)	5.49 A
Open-Circuit Voltage	64 V
Short-Circuit Current	5.87 A

Table 3-1 Simulated PV panel electrical Data

3.1.2 Common PV System Configurations

Available PV systems reveal several possible system configurations. These configurations are as follows;

- centralized configuration (Figure 3-4),
- string configuration (Figure 3-5),
- multi-string configuration (Figure 3-6), and
- modular configuration (Figure 3-7).

In centralized configuration solar panels are connected in a string composed of PV panels connected in series to reach high value of DC voltage in order to avoid further voltage amplifications. Multiple strings are then connected in parallel through sting diodes to reach high power levels. In grid connected centralized PV systems, PV panels are interfaced to the AC bus through centralized inverter. A centralized configuration is nonflexible and inefficient due to power losses coming from centralized MPP tracking, PV panel mismatch and losses in the string diodes. This configuration of PV system is not preferred for microgrid integration.

A string configuration of PV system is modification of centralized configuration where each string of PV panels in series is connected to separate inverter for AC bus integration. This configuration still achieves high input voltage so voltage amplification may be avoided. If voltage amplification is necessary additional DC-DC converter can be added before the inverter. Overall efficiency improvements are obvious because of the lack of string diodes and improved MPP tracking performance for a string.

A multi-string configuration is modified version of string configuration. In a multi-string configuration several strings are interfaced with separate DC-DC converter to a common inverter. Each string can be controlled separately and power decoupling is achieved between strings and AC bus. This configuration of PV system is flexible, easily expandable and efficient comparing to central configuration. This configuration is suitable for microgrid implementation.

In a modular configuration of PV system, each PV panel is interfaced with an inverter. This configuration gives an opportunity to individually design MPP tracking for each panel which in turn increases efficiency of the system. This kind of system is easily expandable and has plug-and-play feature. Main drawback is in design complexity because of necessity for high voltage amplification. This configuration is ideal for microgrid implementation.

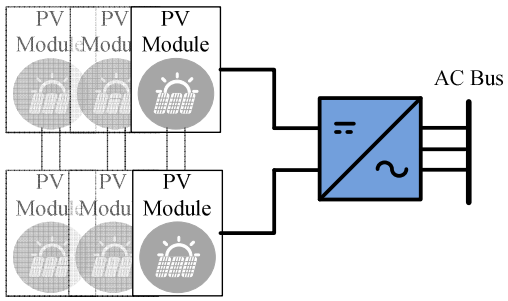

Figure 3-4 Centralized configuration of PV modules

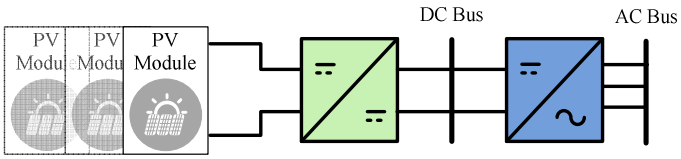

Figure 3-5 String configuration of PV modules

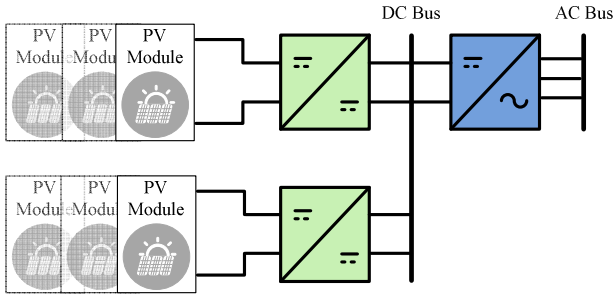

Figure 3-6 Multi-string configuration of PV modules

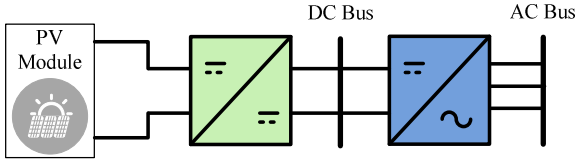

Figure 3-7 Modular configuration for PV modules

3.1.3 Power electronics interface and control system requirements for PV systems

Most important characteristic of PV module is that output power is determined by terminal voltage and current which are results of output loading. This characteristic of PV system partly reveals design requirements for power electronic interface. Other design requirement of power electronic interface comes from the microgrid interface requirements. Power electronics interface for PV system has two main tasks, namely, one is to convert the generated DC current into a current suitable for interfacing to a microgrid, and other is to control the terminal conditions of the PV panel such that energy capture is maximized and panel is operated at maximum power point (MPP).

Based on the PV system configurations discussed in the previous section, power electronics interfaces for these systems can be identified as a single stage power electronics interface and a multi-stage power electronics interface. Single stage power electronics interface includes DC-AC inverter as shown in Figure 3-4. This inverter is responsible for both MPP tracking and supplying grid current. On the other hand, a multi-stage power electronics interface, shown in Figure 3-5 -Figure 3-7, consists of a

DC-DC converter and a DC-AC inverter. A DC-DC inverter is responsible for MPP tracking, while a DC-AC inverter is responsible for grid current injection.

The DC-DC inverters in multi-stage configuration and the DC-AC inverters in both single stage and multi-stage configurations can be constructed based on variety of power electronics topologies. The selection of topology is based on factors such as cost, efficiency, isolation and reliability. Cost of the power electronics interface can be reduced by using less number of components which in turn increases the reliability as well. Technically speaking, efficiency is the most important factor for the selection of power electronics topology. The efficiency of power electronics interface depends on conduction and switching losses. The conduction losses can be effectively reduced by reducing the usage of components and their operating ranges and switching losses can be reduced by soft switching techniques either by zero voltage crossing or zero current crossing techniques. The major advantages of soft switching technique over hard switching conditions are to reduce the losses over the device by about 20–30%.

Most suitable power electronics interface configuration of PV source for integration into hybrid source is the multi-stage configuration. Requirement of the hybrid source is to have all of it energy sources connected to a common DC bus through a power electronic converter. In the case of PV source, since it is a DC source, this converter must be DC-DC. Control requirements for this converter are, as stated previously, controlled transfer of power from source to DC bus through the implementation of maximum power point tracking algorithm; source, converter and DC bus protection; and source health monitoring.

3.2 Wind Energy Conversion System (WECS)

General structure of WEC system is shown in Figure 3-8. Wind energy conversion systems convert the kinetic energy of the wind into mechanical energy using wind turbine. Wind turbine comes in many different configurations, horizontal wind turbine with three blades being the most commonly used. Despite different mechanical configurations, wind turbine, used for electricity generation purpose, is always coupled to an electrical generator. Type of generator is usually choice of the designer with the trade offs of efficiency, integration complexity and cost. Mechanical drive train is placed between turbine and generator and serves the purpose of transmission of motion.

Depending on the type of generator used, mechanical drive train complexity varies. Variable speed turbines include a blade pitch angle control for controlling the amount of power to be transferred. Power electronic interface in these systems has function of delivering power from output of the generator to the AC bus or storing it through implementation of storage elements in the system. Control system has function of controlling blade pitch system, supplying necessary control signals to power electronic interface, measuring variables of interest and making high level and low level decisions when necessary.

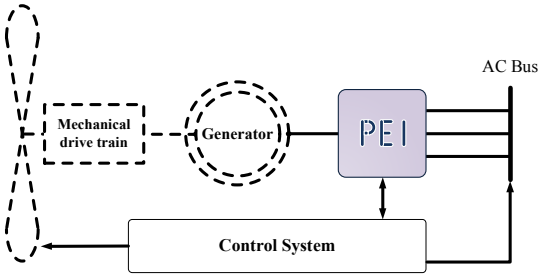

Figure 3-8 General structure of WEC system

Wind turbines currently in use are ranging from few kW up to 2 MW in capacity and even larger ones are being built. A lot of different concepts for construction of turbines have been developed and tested [99]. One important modification in newer wind turbines is the introduction of pitch controllable blades, where it is possible to control the wind power input of the generator. These systems are called variable speed wind turbine systems in general classification. There exist also constant speed wind turbine systems; however these systems are less popular due to their low efficiency and control inflexibility.

3.2.1 WEC System Configurations

Most of the modern WEC systems are constructed using variable speed wind turbines. Variable speed wind turbines have many advantages over constant speed wind turbines such as increased power production, delivery of power with reduced fluctuation and ability to increase or decrease their speed if the wind speed or torque vary, which imposes less wear and tear on the shaft, gearbox, and other components in the drive train [100]. Variable speed wind turbines can incorporate few different types of

generators in their structure, namely, permanent magnet synchronous generators (PMSG), electrically excited synchronous generators (EESG), induction generators (IG), and doubly fed induction generators (DFIG), which are electronically coupled to microgrid through power electronics converters.

In the case of synchronous generators and induction generators without rotor windings, a full power rated converter is connected between stator and microgrid. Total power produced from these generators must flow through power converters, hence the name *full power rated electronic converter*. On the other hand, for induction generators with rotor windings, stator is directly connected to the microgrid and their rotor is connected to *partial power rated electronic converter* and slip rings. Rotor connected converter supplies only portion of the power to the system and can be rated at power lower than the maximum generator power.

Induction and synchronous generators are usually interfaced to microgrid through back-to-back full power rated electronic converters. Back-to-back converter consists of two voltage source converters (VSC) with shared DC link. Back-to-back converter gives good technical performance since full control of active and reactive power is achievable. When using such power electronics interface for generators, they are being decoupled from microgrid and can operate at wide range of speeds, necessary for optimal generation. Power extracted from the generator is sent to microgrid through the power converter which can control active and reactive powers independently.

Four possible configurations of generators with full power rated power electronic converter are shown in Figure 3-9 - Figure 3-12 [100]. Depicted solutions have almost same controllable characteristics, where generators are decoupled from microgrid by a DC link and decoupled control of active and reactive powers. In the case of wind turbines including induction generator, the turbine blades are mounted to the generator through gearbox. Generator is further interfaced to microgrid through back-to-back full power rated converter. Power electronics interface for induction generator is shown in Figure 3-9. In wind turbines including synchronous generator, turbine blades can be coupled to the generator through gearbox, Figure 3-10 or in the case of multi-pole synchronous generators without it, Figure 3-11. Power electronics interface for both of these generator types is the same, full power rated back-to-back converter. It is important to notice the additional AC-DC converter used for field excitation of synchronous generators. Use of this additional converter is avoided by using PMSG as shown in Figure 3-12.

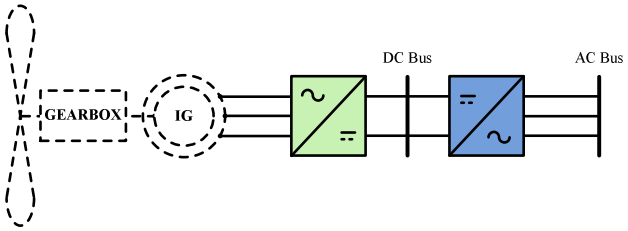

Figure 3-9 Power electronics interface for induction generator

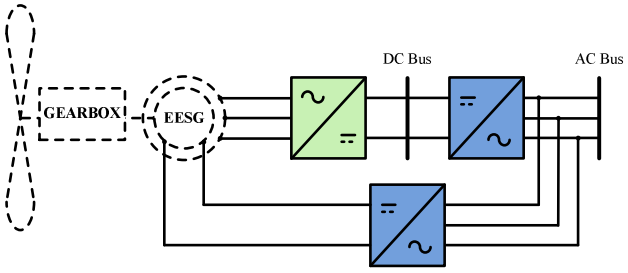

Figure 3-10 Power electronics interface for synchronous generator with gearbox

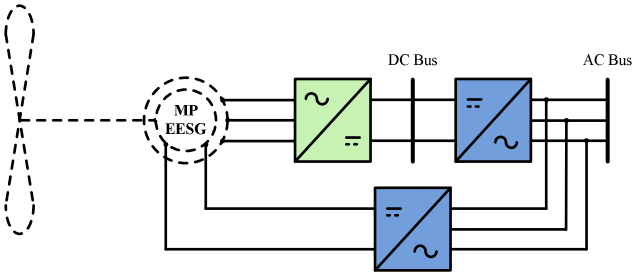

Figure 3-11 Power electronics interface for multi-pole synchronous generators

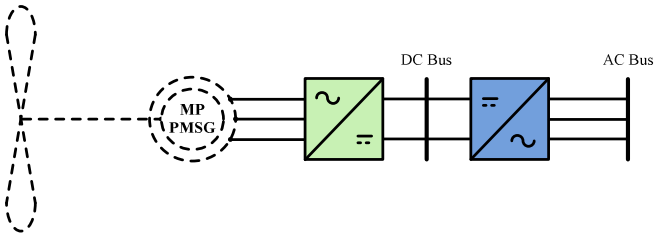

Figure 3-12 Power electronics interface for multi-pole permanent magnet synchronous generator

Typical DFIG based wind turbine is depicted in Figure 3-13. The stator is directly connected to the AC bus and the rotor is interfaced through a back-to-back converter that consists of a rotor side converter (RSC) and a grid side converter (GSC) and a common DC bus [101, 102]. Grid Side Converter (GSC) has a task of maintaining the desired DC bus voltage through proper control. Rotor side converter (RSC) of DFIG has elementary function of active and reactive power control. Stator power is controlled through rotor circuit.

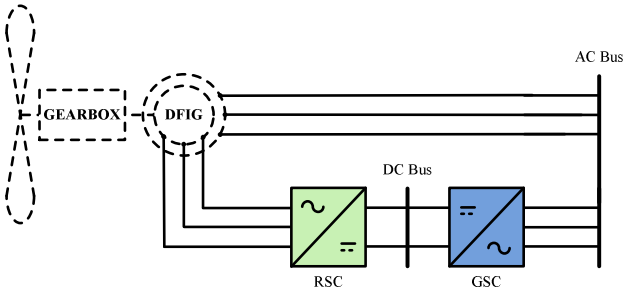

Figure 3-13 Power electronics interface for doubly fed induction generator

3.2.2 Wind turbine modeling

Comprehensive modeling of wind energy conversion system is out of scope of this work. Modeling in this section is done with the sole purpose of understanding the electrical and mechanical behavior of the wind turbine as the central component of WECS and eventually coming up with the design requirements for power electronic interface and control system design. For proper power electronic interface and control system design, it is important to understand the aerodynamic and mechanical behavior of the wind turbines and mechanical and electrical behavior of electrical generator employed in the wind turbine.

Aerodynamics model of the wind turbine normally considers both turbulence and steady state behavior. Nevertheless to obtain the power output characteristics for the purposes of power electronics and control system design only steady state behavior is considered, i.e. the mean power output is determined by the mean wind speed. The mechanical power output of the wind turbine can be described by the following relation;

$$P_m = \frac{1}{2}\rho\pi r^2 c_p(\lambda,\beta) v_w^3 \tag{3.6}$$

where ρ is the air density, r is the rotor blade radius and v_w is the average wind speed. In (3.6), $c_p(\lambda,\beta)$ parameter represents the power coefficient. This coefficient is the function of tip speed ratio, λ, and controllable pitch angle β. This coefficient dictates the maximum power that can be extracted under given conditions. In ideal case this coefficient it 0.5926, meaning that 59.26% of available power in the wind is extractable. This limit is known as the Betz limit. Power coefficient c_p can be calculated for a given turbine design and environment conditions, however most commonly used formula for calculation of this parameter is for 3 blade variable speed turbine [103];

$$c_p(\lambda,\beta) = 0.73\left[\frac{151}{\lambda_i} - 0.58\beta - 0.002\beta^{2.14} - 13.2\right]e^{\frac{-18.4}{\lambda_i}}, \tag{3.7}$$

$$\lambda_i = \frac{1}{\frac{1}{\lambda + 0.02\beta} - \frac{0.03}{\beta^3 + 1}}, \tag{3.8}$$

$$\lambda = \frac{\omega_r r}{v_w}, \tag{3.9}$$

where ω_r is the generators speed of rotation.

Wind turbine model represented by (3.6) - (3.9) has been simulated using Matlab/Simulink and simulation results are shown in Figure 3-14. In the given graph, mechanical power is examined with respect to generator speed of rotation for different cases of wind speed, from 6 m/s up to 12 m/s. All curves exhibit similar behavior indicating that there exists maximum power point (MPP) at specific generator speed of rotation. It is always desired to operate wind turbine at MPP for a given speed of wind. To accomplish this task, control system has to control the speed of generator that corresponds to MPP. Simulation values are given in the Table 3.2.

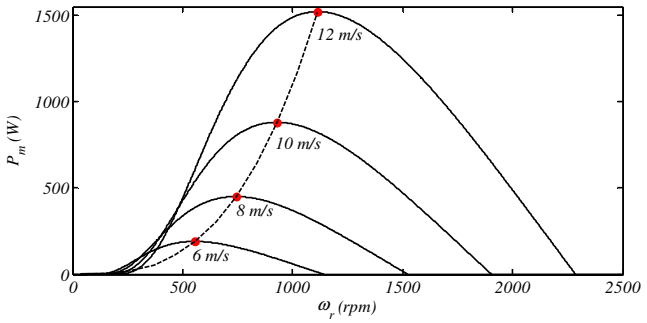

Figure 3-14 Mechanical power curve for different wind speeds

Wind turbine simulation data	
Air density ρ	1.29 kg/m^3
Blade radius r	1 m
Pitch angle β	0^o
Rotor Speed Range ω_r	0 – 2500 rpm
Wind Speed Range v_w	6m/s – 12 m/s

Table 3-2 Wind turbine simulation data

3.2.3 DFIG generator modeling

Among the asynchronous generator used in variable speed turbines Doubly Fed Induction Generator (DFIG) is the most popular option. DFIG is a special type of electrical generator that, when controlled, can track a prescribed torque-speed profile and can output power at any given wind speed. Power rating of the converter for doubly fed induction generator is generally much lower than the power rating of generator itself (about 25%-30%), which makes these generators ideal for WEC applications due to the reduced power rating of necessary electronic converters.

Doubly fed induction generator comprises of a set of three-phase stator windings and a set of three-phase rotor winding. Rotor windings are fed through slip rings. Mathematical model describing the electrical dynamic behavior of DFIG is written for the set of windings on rotor and stator that can be supplied from separate voltage sources. More detailed analysis and modeling of three phase machines can be found in [104]. For each winding in rotor and stator voltage equation is in the form of

$$\begin{aligned} v_i &= R_i i_i + \frac{d\phi}{dt}; \\ \phi_i &= L_i i_i + \sum_k L_{m_{i,k}} i_k . \end{aligned} \tag{3.10}$$

In the above equations, the subscript i is identifying winding under consideration, v_i is the terminal voltage, i_i is the winding current, R_i and L_i are the resistance and self inductance of the winding and $L_{m_{i,k}}$ is the mutual inductance between the winding i and some other rotor or stator winding k. Above compact representation represents 6 different dynamical equations (3 for stator and 3 for rotor). Usually, for three phase machines, winding equations are transformed into some other reference frame. By doing so, dynamic modeling and consequently control of three phase machines is simplified. DFIG dynamical equations are derived in stator synchronously rotating reference frame and expressed in the following form [105],

$$v_{sd} = R_s i_{sd} + L_s \frac{di_{sd}}{dt} - \omega_s \left(L_s i_{sq} + L_m i_{rq} \right) + L_m \frac{di_{rd}}{dt}, \tag{3.11}$$

$$v_{sq} = R_s i_{sq} + L_s \frac{di_{sq}}{dt} + \omega_s \left(L_s i_{sd} + L_m i_{rd} \right) + L_m \frac{di_{rq}}{dt}, \tag{3.12}$$

$$v_{rd} = R_r i_{rd} + L_r \frac{di_{rd}}{dt} - (\omega_s - \omega)\left(L_r i_{rq} + L_m i_{sq} \right) + L_m \frac{di_{sd}}{dt}, \tag{3.13}$$

$$v_{rq} = R_r i_{rq} + L_r \frac{di_{rq}}{dt} + (\omega_s - \omega)\left(L_r i_{rd} + L_m i_{sd}\right) + L_m \frac{di_{sq}}{dt}, \tag{3.14}$$

where $v_{sd}, v_{sq}, v_{rd}, v_{rq}$ are stator and rotor voltages in stator synchronous reference frame, $i_{sd}, i_{sq}, i_{rd}, i_{rq}$ are stator and rotor currents in stator synchronous reference frame, ω_s is stator synchronous speed and ω is electrical speed of rotor, R_s and R_r are stator and rotor resistances respectively, L_s and L_r are stator and rotor self inductances respectively and L_m is the mutual inductance between rotor and stator. All of the above derivation is done in stator voltage oriented synchronous frame and rotor and stator winding turn ratio is assumed to be equal.

Expressions for stator active and reactive power are in the following form,

$$\begin{aligned} P_s &= \frac{3}{2}\left(v_{sd} i_{sd} + v_{sq} i_{sq}\right), \\ Q_s &= \frac{3}{2}\left(v_{sq} i_{sd} - v_{sd} i_{sq}\right). \end{aligned} \tag{3.15}$$

Stator active and reactive powers, on the first look seem to be coupled where both direct and quadrature current components influence both variables. However, if the synchronously rotating frame is oriented with respect to stator voltage, then the quadrature voltage vanish from the equations and independent active and reactive power could be achieved through the control of stator current components. Electromagnetic torque developed by DFIG as the result of currents flowing in rotor and stator becomes,

$$T_e = \frac{3}{2}\frac{p}{2} L_m \left(i_{rd} i_{sq} - i_{rq} i_{sd}\right), \tag{3.16}$$

where p is the number of pole pairs. Often, it is desired that magnetizing current comes solely from voltage formed at the stator – so $i_{rd} = 0$ and above expression becomes,

$$T_e = -\frac{3}{2}\frac{p}{2} L_m i_{rq} i_{sd}. \tag{3.17}$$

During the operation of DFIG developed electromagnetic torque counteracts the mechanical torque developed by wind turbine attached to the shaft of the generator and friction forces to dictate the speed of rotation of generator. The nature of this interaction becomes clearer by looking at the DFIG's equation of motion,

$$\frac{d\omega_m}{dt} = \frac{1}{J}\left(T_m - T_e - b\omega_m\right). \tag{3.18}$$

Where ω_m is the mechanical rotational speed, T_m is the mechanical torque

developed by the wind turbine blades (by sign convention –negative), J is the combined rotational inertia of turbine and generator and b is the damping coefficient.

3.2.4 Power Electronics and Control Requirements for DFIG Based WEC System

As shown in Figure 3-13 power electronics interface for DFIG consists of back-to-back converter placed between AC bus (electrical distribution network) and rotor circuit. Most of back-to-back converters are designed using pairs of three-phase transistors in half bridge configuration. Bridges are coupled through DC link including capacitor. Transistor can be either MOSFET type, with high switching frequency and low power rating or IGBT type with lower switching frequency and higher power rating. Three phase bridges can act as a rectifier or inverter depending on the imposed power sign. Different power electronics topologies are possible for the design of back-to-back converters. For example, it is possible to construct back-to-back converter using so called multilevel inverters. These converters include an array of switching elements and capacitor voltage sources, the output of which generate voltages with stepped waveforms. One of the advantages of this multilevel topology is that the control of the switches permits the addition of the capacitor voltages, which reaches high voltage at the output, while the switches must withstand only reduced voltages. It has been shown that multilevel inverters are viable solution in renewable energy systems as interface medium for sources such as photovoltaic systems or fuel cells or with energy storage devices such as capacitors or batteries [106].

Main control requirements for DFIG based wind turbine can be identified as following;

- Control of active and reactive power delivery;
- Control of amplitude and frequency of stator voltage to match the load requirements in island or grid requirements grid connected applications;
- Control of generators speed to achieve maximum power point tracking;
- DFIG stator and AC bus voltage synchronization.

All of the above mentioned control requirements are achieved through proper control of rotor circuit currents. In general, the rotor current magnitude and frequency are controlled in such a way that stator voltage with fixed magnitude and frequency is generated while angular speed of rotor varies.

3.3 Fuel Cell Based Energy Conversion System

Fuel cell is a device that converts the chemical energy from a fuel into electricity through a chemical reaction. Fuel cell consists of two electrodes – an anode and a cathode - and an electrolyte, arranged in matrix. Operation of fuel cell is similar to the operation battery, however in battery reactants and products are stored while in fuel cell they are continuously fed to cell. During operation hydrogen is fed to anode and air is fed to cathode, electrochemical oxidation and reduction take place at the electrodes to produce electricity. Produced power has DC nature. Heat and water are by-products of generation process.

When compared to conventional generators, fuel cells that use hydrogen have several advantages; they are eco-friendly emitting less CO_2 and NO_X per kilowatt, fuel cells are noiseless and vibration free, since they have no moving parts, they are robust construction wise and they require little maintenance. There are many different types of fuel cells that use variety of fuels like natural gas, propane, landfill gas, anaerobic digester gas, diesel, methanol and hydrogen. However hydrogen is the most common fuel because it can be easily stored and transported, it is efficient and highly versatile.

There are mainly four types of fuel cells with different electrolytes and operating temperatures, which are as follows: (i) Proton exchange membrane fuel cell (PEMFC) operating at 80°C; (ii) Phosphoric acid fuel cell (PAFC) operating at 200°C; (iii) Molten carbonate fuel cell (MCFC) operating at 650°C; and (iv) Solid oxide fuel cell (SOFC) operating at 1,000°C. Further information about fuel cell operation, classification and their utilization in microgrids can be found in [107].

3.3.1 Fuel Cell Modeling and Analysis

Modeling of fuel cell is rather complex since it includes fluid dynamics modeling, electrochemical modeling and thermal modeling. Modeling of fuel cell has been a topic of research of great interest and authors have developed varieties of models including fluid dynamics, electrochemical and thermal phenomena. Many of the present models are done with the purpose of fuel cell design and as such include many details which are not of interest for this thesis. When considering the fuel cell as a component in a microgrid, its electrochemical model is of crucial importance. Electrical characteristics

of fuel cell have to be identified in order to come up with power electronics interface and control system requirements. Electrochemical model of fuel cell is developed with the aim of coming up with the mathematical description of polarization curve.

Understanding of polarization curve of a fuel cell has to be done by identifying the operating regions of fuel cell as the activation region, the ohmic region and the concentration region. Due to the electrical characteristics of the fuel cell, increase of the output current will increase internal voltage drop of the fuel cell and consequently terminal voltage of the device will decrease. The major factors that contribute to the terminal voltage drop are: activation loss, ohmic loss and concentration loss [108].

Operation of fuel cell in the activation region is consequence of light loading and small output currents. In the activation region, electrochemical reactions occurring internally in the fuel cell are typically complex and energy intensive and reflect as nonlinear increase/decrease in the voltage output. On the other hand, in the ohmic region, voltage increase/decrease is relatively linear with respect to change of the loading current. Electrical operation of the fuel cell in ohmic region can be simply seen as voltage source with resistance connected in serial. Increase of the current will cause increased voltage drop across series resistance and consequently terminal voltage will decrease. At very heavy loading of the fuel cells when the output current is large, the output voltage falls down significantly because of the reduction of gas exchange efficiency, it is mainly due to over-flooding of water in catalyst and this region is also called concentration region.

General equation of fuel cell voltage, extensively used in the literature is given by,

$$V_{fc} = V_o - V_{act} - V_{ohm} - V_{conc}. \tag{3.19}$$

Value of fuel cell voltage V_{fc} is defined by open circuit voltage V_o and voltage drops due to the fuel cell operation in different regions of polarization curve, namely, activation voltage drop V_{act}, ohmic voltage drop V_{ohm} and concentration voltage drop V_{conc}. Usually commercial fuel cell is evaluated by the curve that represents voltage of the fuel cell versus the fuel cell current or current density, similar to the PV cell.

The following equation has been proposed by authors in [109] to model the electrochemical phenomena occurring in fuel cell;

$$V_{fc} = \underbrace{x_1}_{V_o} + \underbrace{x_2\left(T_{st} - T_{st}^0\right)}_{\Delta V_{fc}/\Delta T_{st}} + \underbrace{x_3\left(0.5\ln\left(P_{O_2}\right) + \ln\left(P_{H_2}\right)\right)}_{\Delta V_{fc}/\Delta p} - \underbrace{x_4\left(1 - e^{-j/x_5}\right)}_{V_{act}} - \underbrace{x_6 j}_{V_{ohm}} - \underbrace{x_7 j^{(1+x_8)}}_{V_{conc}}. \tag{3.20}$$

Where parameters $x_1 ... x_8$ are determined experimentally for a fuel cell under consideration using method described in [109], T_{st} is the operating stack temperature and T_{st}^0 is the testing temperature of the stack, P_{O_2} and P_{H_2} are the operating pressures of the oxygen and hydrogen respectively and j is the current density defined by,

$$j = \frac{I_{fc}}{A_{fc}}. \tag{3.21}$$

With I_{fc} being the fuel cell current and A_{fc} is the active fuel cell area. Additionally three expressions complete the model of stack voltage,

$$\begin{aligned} V_{fc} &\geq 0, \\ V_{st} &= n_{fc} V_{fc}, \\ I_{st} &= I_{fc}. \end{aligned} \tag{3.22}$$

In the above equation n_{fc} is the number of fuel cells inside the stack.

Simulation of equations (3.20) through (3.22) is done using Matlab/Simulink, Behavior of stack voltage with respect to the stack current is shown in Figure 3-15. Three regions of stack operation are clearly identified on the figure as activation region, ohmic region and concentration region. Change of power with respect to current is given in the Figure 3-16. This graph shows the power curve for the constant operating temperature and constant operating hydrogen and oxygen pressures. It is important to note that fuel cell stack has maximum power point, behavior similar to wind turbine and photovoltaic module. Power curve variation with respect to operating temperature of the stack is shown in the Figure 3-17. Maximum power point varies for different operating temperature. Table 3.3. lists the simulation parameters.

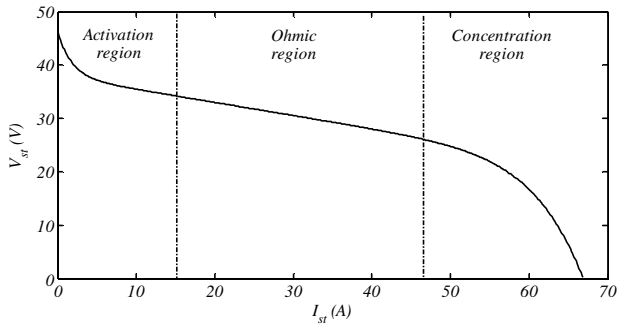

Figure 3-15 *i-v* characteristics of fuel cell stack

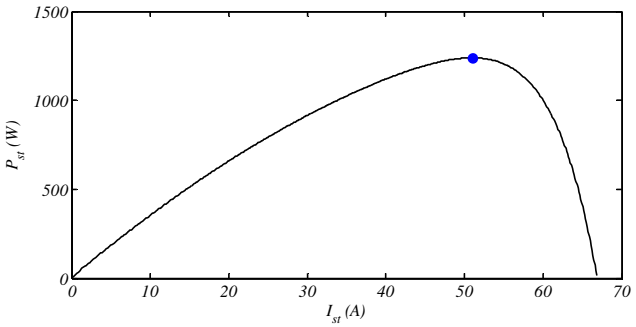

Figure 3-16 Fuel cell stack power curve

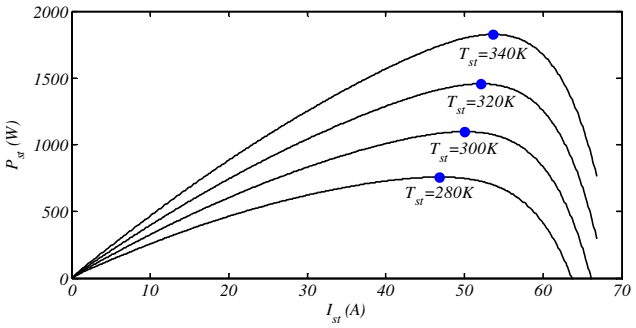

Figure 3-17 Power curve variation with respect to stack temperature

Fuel cell stack and simulation data (Nexa® 1200)	
Rated Power	1200 W
Rated Voltage	24 V
Rated Current	50 A
Rated Temperature T_{st}^{0}	308 K
$\begin{pmatrix} x_1, x_2, x_3, x_4 \\ x_5, x_6, x_7, x_8 \end{pmatrix}$	$\begin{pmatrix} 1.17,\ 0.0076,\ 0.24,\ 0.18 \\ 0.015,\ 0.64,\ 288.59,\ 10 \end{pmatrix}$
P_{O_2}	0.16 bar
P_{H_2}	1.25 bar
n_{fc}	46
A_{fc}	110 cm^2

Table 3-3 1.2kW fuel cell datasheet values and simulation data

3.3.2 Power Electronics and Control Requirements for Fuel Cell System

Power electronics interface for fuel cell is given in the Figure 3-18. Operating regions of the fuel cell and the electrical characteristics associated with these regions give out important insights into the design of power electronic interface. Power

electronics design is similar to the PV module interface design. A DC-DC converter is placed between the output terminals of the fuel cell and the DC bus. For AC bus connected systems additional DC-AC converter is placed between DC and AC buses.

Most basic control requirement for the fuel cell system is the output voltage regulation at a given load. In other words, maximum power point tracking is implemented through the control of a DC-DC converter. For the AC bus connected fuel cell, a control system has to regulate active and reactive power and AC bus voltage magnitude and frequency. Additionally control system is responsible for implementation of protection for both converter and fuel cell and for fuel cell health monitoring.

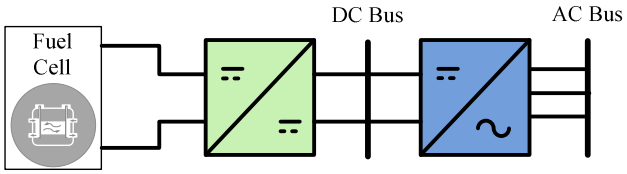

Figure 3-18 Power electronics interface for fuel cell

3.4 Energy Storage System

Distributed generation sources used in microgrid have relatively low generation capacity and use electronic converters at their outputs to generate suitable form of power according to specified power requirements. Compared to conventional generation systems, which are dominated by rotating electrical machines with large rotating mass and damping, DG units have small or no rotating mass and damping. In other words DG sources can be considered as inertialess generation systems. This feature of the DG sources makes them unable to effectively respond to surge power or power mismatch. Energy storage systems appear as an effective solution to these problems in microgrid. Energy storage systems can be controlled to simulate the effect of inertia, naturally found in conventional generation system, with the aim of increasing power reliability and overall microgrid system stability.

Energy storage systems play especially important role in microgrids that integrate renewable energy sources since these sources are largely affected by environmental conditions and their power output is hard to predict. Intermittent power delivery of renewable energy systems has poor effect on overall power reliability and stability of

microgrid system. Properly designed energy storage systems are used to mitigate problems related to the intermittency and instability of power in microgrids.

Most commonly used types of energy storage systems in microgrid are; super-capacitors, batteries, superconducting magnetic energy storage systems, kinetic energy storage in flywheels and hydrogen based energy storage. Due to the importance of energy storage systems in microgrid, these systems have been extensively covered in literature. Literature reviews covering particular applications of ESSs and their comparative advantages and disadvantages can be found in [110-112].

Batteries are devices that store energy in electrochemical form. They consist of cells connected in series and parallel that include conductor electrodes and electrolyte placed together in the sealed container and connected to the external load. Batteries are the most widely used energy storage systems available on market. Their size and capacity ranges from 100W to several megawatts. Batteries provide rapid response for charge and discharge operations. Nevertheless, discharge rate is limited by chemical reactions and the type of battery. Types of batteries used in microgrids are lead-acid, nickel-iron, nickel-cadmium, nickel metal hydride and lithium ion. Their average efficiency is between 60%-80% [113].

Super-capacitors also go by the name ultra-capacitors or double layer capacitors, are storage devices that store energy directly without chemical reaction and have small response time. These devices have much higher energy density and capacitance compared to the regular electrolytic capacitors. Cells forming super-capacitors have capacitance values from 5F to 2700F and rated voltage between 2V-4V. Due to the low output voltage cells are connected in parallel and series to form a module with desired voltage. These devices are relatively expensive, however compared to the other storage systems they have unbeatable characteristic of absorbing and releasing large amounts of energy in very short period of time. New trends in this technology are usage of super-capacitors for temporary high peak power demands, integration with other storage technologies and development of high voltage applications [114].

Flywheel is electromechanical device that stores energy in the form of kinetic energy. Rotating mass is connected to the electrical machine. Electrical machine is used as motor and rotates the flywheel to store kinetic energy when excess energy is available in the system. Energy is extracted from flywheel during power dips through the same mechanism, only rotating machine is used as generator this time. Flywheels are classified to low speed-large inertia and high speed-small inertia. These storage

systems have relatively high efficiency (around 80%), low cycling life, wide operating temperature range and high power/energy density [115-118]. The disadvantages of flywheel systems are large dimensions, high standby loss and noise pollution.

Superconducting magnetic storage systems are storing energy in magnetic field which is created by injection of DC current in superconducting coil at low temperature. Resistive losses of this system are small and their efficiency is high (around 95%) [113]. There is very short time delay during charge or discharge of energy in these systems. The output power is available almost instantaneously and in large quantities. Main disadvantage of these systems is their cost due to refrigeration and expensive coil wires.

In *hydrogen based energy storage systems* excess energy is used to produce hydrogen from water and store it. This system consists of water electrolyzer system, power conversion system, hydrogen storage system and fuel cell. Fuel cell is explained previously as DG source and it is crucial to convert energy from chemical reacting into electrical energy. Electrolyzer and fuel cell have relatively low efficiencies of 60% and 70% respectively [119], so resulting overall efficiency of this kind of storage system is somewhere between 40% - 45%.

Choosing of the proper energy storage for a microgrid is a topic of discussion among the researchers. There are many criteria according to which energy storage system are chosen as the most suitable solution. Definitely, energy storage selection is a subject of system optimization. In this thesis, battery storage system is chosen as further topic of discussion due to the technology maturity, their availability and low cost.

3.4.1 Battery Modeling and Analysis

Modeling of battery can be done by considering the electrochemical processes that are occurring during its operation. Development of such a model is necessary for particular battery design and optimization. From the electrical point of view and from the point of view of microgrid integration of battery, a much simpler model can be developed to serve the purpose of definition of power electronic interface and control system requirements. Model developed for these purposes can be concerned only with electrical behavior of battery during charging and discharging processes. Developed model can be analytical, empirical or result of mixture of these two methods.

General model of battery including the electrical behavior during charging and

discharging processes and state of charge information can be developed by considering the battery voltage equations as;

$$V_b = V_{oc} - V_{pol} - V_{ohm} + V_{\exp}, \tag{3.23}$$

where V_b is the battery output voltage, V_{oc} is the battery open circuit voltage, V_{pol} is the voltage drop during the polarization phase, V_{ohm} is the ohmic voltage drop due to the internal and polarization resistance and $V_{\exp}$ is the exponential voltage of battery.

Depending on the type of the battery (Li-Ion, Lead-Acid, NiMH or NiCd), the charge and discharge models differ. In this thesis the Li-Ion model is given, for models of other types of battery one can refer to [120]. Charge model of Li-Ion battery can be modeled by following expression

$$V_b = V_{oc} - \kappa \frac{Q}{Q - \int i_b dt} \int i_b dt - \kappa \frac{Q}{\int i_b dt - 0.1Q} i_b - R i_b + A e^{-B \int i_b}, \tag{3.24}$$

and discharge model can be modeled by following expression,

$$V_b = V_{oc} - \kappa \frac{Q}{Q - \int i_b dt} \left(\int i_b dt + i_b \right) - R i_b + A e^{-B \int i_b dt}, \tag{3.25}$$

where κ is the polarization coefficient or polarization resistance, Q is the battery capacity, R is the exponential zone constant A is the amplitude of exponential zone and B is the exponential zone time constant. Authors in [120] show the method for calculation of unknown parameters using information from datasheet.

Important parameter to consider for battery is the state of charge. This parameter is 0 when battery is empty and it is 1 when battery is full. State of charge (SOC) is expressed by following equation,

$$SOC = 100 \left(1 - \frac{1}{Q} \int_0^t i_b(t)\, dt \right). \tag{3.26}$$

Model of battery from (3.24) and (3.25) is implemented in Matlab/Simulink for 12V/100Ah Li-Ion battery. Technical specifications of battery are given in the Table 3-4, and simulation results are given in the Figure 3-19. Simulation results show battery discharge characteristics. In other words output voltage behavior is plotted in time when constant current is drawn from battery. Battery is tested for different values of discharge currents (50A, 100A, 150A) and shown on the same graph. As expected higher current values discharge battery faster.

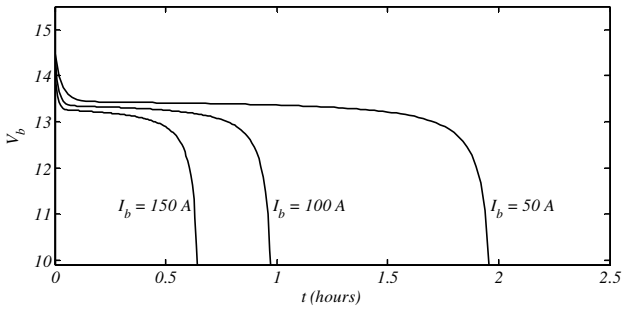

Figure 3-19 Li-Ion battery discharge curve

12V/100Ah Li-Ion battery and simulation data	
Nominal Watt Hours	1320 Wh
Nominal Capacity	100Ah
Nominal Battery Voltage	12 V
Open Circuit Voltage V_{oc}	13.52 V
Internal Resistance R	1.24 mΩ
Polarization Resistance κ	0.503 mΩ
Exponential Zone Amplitude A	1.0325 V
Exponential Zone Time Constant B	0.611 Ah^{-1}

Table 3-4 12V/100Ah Li-Ion battery datasheet values and simulation data

3.4.2 Power Electronics and Control Requirements for Battery Based Storage System

Battery storage units produce or store DC power. Battery storage units are usually connected series/parallel combinations based on the power requirements. Battery storage unit in hybrid source need power electronic interface to operate in a controlled way (controlled charging and discharging process). Hybrid source connected battery needs a DC-DC converter to be interface to a DC bus and for its connection to AC bus it needs additional DC-AC converter. When comparing to the other power electronic interfaces usually used for sources, the battery storage system requires interface that allows bidirectional flow of power from DC bus to it and from it to DC bus. Power electronic interface is shown in the Figure 3-20.

Control system requirements for battery storage unit are somewhat different than for other sources analyzed in this chapter. Battery control system is solely responsible for DC bus voltage regulation. This requirement in the same time means that, battery control system should detect excess power in the DC bus and store it or should detect the deficit of the power in the DC bus and compensate it by discharging battery.

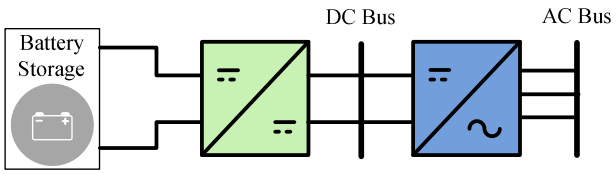

Figure 3-20 Power electronics interface for battery storage

3.5 Hybrid Energy Source in Microgrid

Hybrid energy source (HES), as explained in introductory chapter, consists of multiple energy sources that complement each other in energy delivery. Proper selection of sources, power electronics interfaces (power conversion units) and control strategies to be included in the HES results in the system that is reliable and efficient in energy delivery. From microgrid point of view, HES is an energy source that offers flexible energy control while delivering or storing sustainable and clean energy. It can be said by confidence, that such energy structure, when integrated to a microgrid, increases overall system efficiency.

Integration of distributed generation and storage units into hybrid energy source is done through power electronics interfaces. Throughout this chapter, most typical power electronics interfaces for various different renewable energy sources and battery storage unit were analyzed. Most important conclusion of this analysis is that power electronic interfaces for the sources under considerations are structurally very similar. This fact contributes to, the objective of this thesis – *development of a framework for analysis and control of power electronics interfaces in microgrid connected hybrid energy source.* Analysis of sources in this chapter has showed that for AC bus connected systems power electronics can be designed such that the source dynamics are decoupled from the rest of the system through implementation of a DC bus. In such power electronics interface configuration, there is a common pattern of multi-stage power conversion for all analyzed sources. The same pattern can be demonstrated for other sources commonly found in microgrid but not analyzed in this thesis.

For the purpose of integration of renewable energy sources into HES, their power electronics interfaces are put into a suitable form. Basically, for the power electronic structures from Figure 3-4 – Figure 3-7, Figure 3-13, Figure 3-18 and Figure 3-20 the power converter between DC bus and AC bus is the same, so for the HES integration

purposes it has been combined into a single converter responsible for power conversion between DC and AC buses. Each source is then integrated to the HES through power electronic converter between its output and DC bus (Figure 3-21). Different types of the sources (not considered in this thesis) could be integrated into HES in the same way. For HES structure, following components can be identified; sources, input side converters and controllers, DC bus, output side converter and controller, an AC bus and HES control system. Each element can be described as follows; ***sources*** represent a primary energy sources that can be treated as distributed generation units or as storage units; ***input side converters*** are the power electronic converters responsible for input power conversion; ***input side controllers*** are responsible for input power control and various monitoring tasks; ***DC bus*** acts as an intermediate agent for power transfer between input and output side converters; ***output side converter*** is responsible for power conversion between DC bus and AC bus; ***output side controller*** is an element of this interface that controls the power delivered to the AC bus, synchronizes the HES with an AC bus in terms of voltage magnitude and frequency and monitors the AC bus; ***AC bus*** is generalized bus that can represent a utility grid, microgrid or distribution network for local loads; and ***HES control system*** is mainly responsible for power balancing in the DC bus according to an external power reference demanded by a microgrid. Identification of each of HES elements is necessary to come up with the design requirements. Sources are analyzed and their characteristics are discussed in the previous sections of this chapter so it will not be repeated here.

Input side converter is a power electronics interface connected between source and DC bus. Primary function of this converter is to act as the power conversion agent between source and DC bus. If the source is considered to be DG unit, power flow of this converter is mostly unidirectional and power flows from the source to the DC bus. On the other hand, if the source is considered to be storage unit then power flow of input converter is bidirectional, meaning that power flows from DC bus to the source during the absorption (charging) process as well as from the source to the DC bus during the generation (discharging) process.

Power coming from the source can be of AC or DC nature. Example of distributed generation units that generate DC power are PV and fuel cells, on the other hand, DG units that generate AC power are many, including wind turbines, small hydro-turbines, small gas-turbines and induction/synchronous generators driven by IC engines. Most of the energy storage systems that utilize generation and absorption through single

electrical connection, such as batteries, super-capacitors and superconducting magnetic storage system generate and absorb DC power, while flywheels and pumped water energy storage systems with reversible turbines require the AC power to operate. On the other hand, hydrogen and compressed air based energy storage systems do not generate and absorb power through same electrical connection, so they can be viewed as "useful" loads during the absorption and as DG units during generation process. In that light, fuel cells are using hydrogen to generate DC power and induction/synchronous generator is used in compressed air systems to generate AC power.

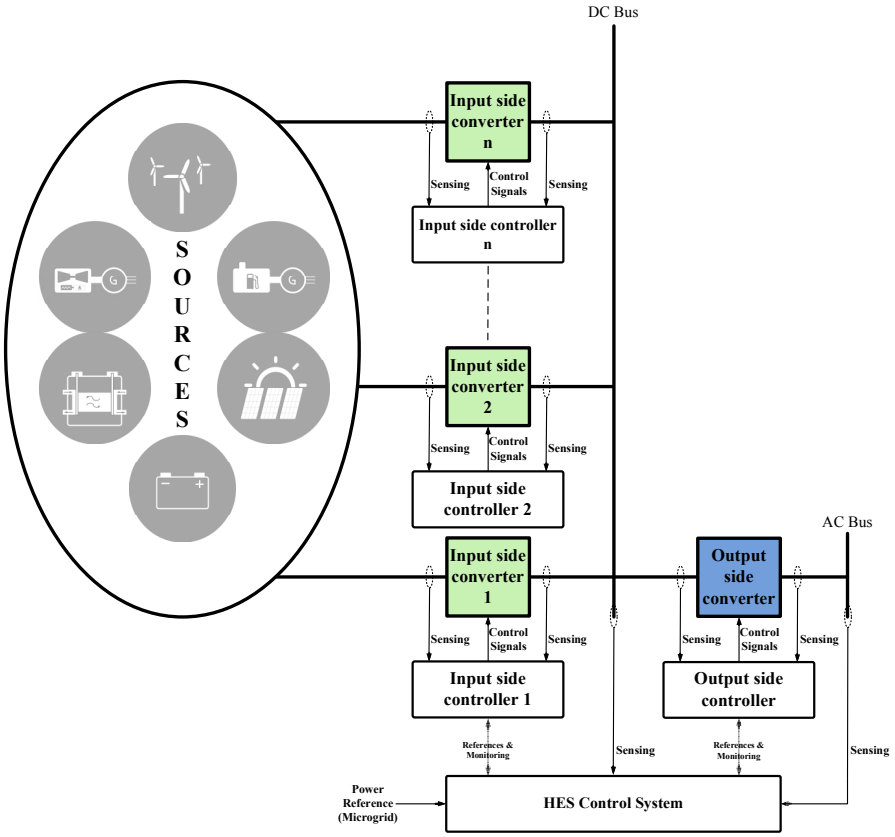

Figure 3-21 HES structure - source integration - power electronics interface

Input side converter can be topologically classified as DC-DC converters or AC-DC converters. It is important to note that power flow in these converters can be either unidirectional or bidirectional depending on whether source is DG unit or storage unit.

To accomplish controlled power conversion, input side converter must include measurement/sensing circuits in its structure. Sensing circuits in the input converter are mostly responsible for voltage and current sensing both at the input and output of the converter. Sensing of voltage and current values at the input and output of this converter

is primarily used by control system to perform control actions and monitoring. Depending on the specific design of input side converter, additional measurement circuits can be incorporated in its structure to measure source associated environmental conditions (e.g. temperature, humidity, etc.).

Input side converter additionally includes protection equipment in its structure. The protection equipment is usually responsible for protection of both converter components and source from various faulty electrical conditions. Protection circuits included in this converter are standard AC and/or DC power protection equipment. Besides hardware protection circuits, certain protection functions can also be software implemented in the input side converter.

The output side converter is connected between DC bus and AC bus and it acts as a power conversion agent between these two buses. During its operation output side converter has to do conversion that is consistent with the demand and supply depending on the availability of power at either bus. This converter must be able to supply both active and reactive power to the AC bus. Likewise, this converter has to be able to import power from AC bus. Thus this converter is bidirectional AC-DC/DC-AC converter.

For the proper operation of this converter monitoring and measurement circuits must be implemented on both DC bus side and on AC bus side. Measurement circuits sense the currents and voltages necessary for power control and AC bus synchronization. Similar to the input side converter, the output side converters includes certain protection equipment in its structure. This protection equipment is used to protect both the converter and the AC bus depending where the fault occurs.

Input side controller tasks are related to the driving and controlling of input side converter. Generally speaking control tasks of input side controller are the control of the input power, protection of the source and protection of the converter. Nevertheless more specific control tasks must be defined according to the type of the source that is being interfaced. Controller requirements for each source under consideration in this thesis are discussed in the previous sections.

Output side controller controls the power that flows from DC bus to the AC bus according to power reference supplied by the HES control system. This controller additionally has a task of synchronization of converter output and AC bus when voltage at the AC bus is defined externally or it is responsible for forming of AC bus when voltage is not defined externally (island mode).

3.5.1 Proposed Hybrid Energy Source

Proposed HES is shown in Figure 3-22. All of the energy sources are integrated using common DC bus. PV and fuel cell sources are integrated through DC-DC converter. Wind source includes DFIG whose rotor circuit may be supplied from DC bus to create conditions for power flow from its stator terminals toward AC bus. Power flow from rotor circuit towards the DC bus is also possible when DFIG rotational speed is larger than its synchronous speed. Battery storage is interfaced to DC bus through bidirectional DC-DC converter. Electrolyzer is interfaced to the DC bus through DC-DC converter. From power electronics and control system point of view, electrolyzer is seen as a controllable DC load and can be used to implement efficient power management strategies.

It is important to note that DFIG system may require high voltage at the DC bus. In the figure it is shown with dashed lines to indicate this. DFIG bus integration could be handled with additional DC-DC converter if it is required.

3.6 Conclusion

In this chapter operation of PV, wind and fuel cell renewable energy sources and battery storage were analyzed and their power electronics and control requirements were identified. In the last section of this chapter set of power electronic and control requirements of overall HES was given and some integration issues associated with HES were discussed.

Main conclusion regarding the analyzed sources is that there exist certain two stage power electronics configurations that can be utilized for the integration of all of the sources into HES. Two stage power electronics configuration consists of input side converter, DC bus, output side converter that is connected to AC bus (microgrid). As a result of this analysis, it has been shown how multiple sources can be integrated into HES (Figure 3-22).

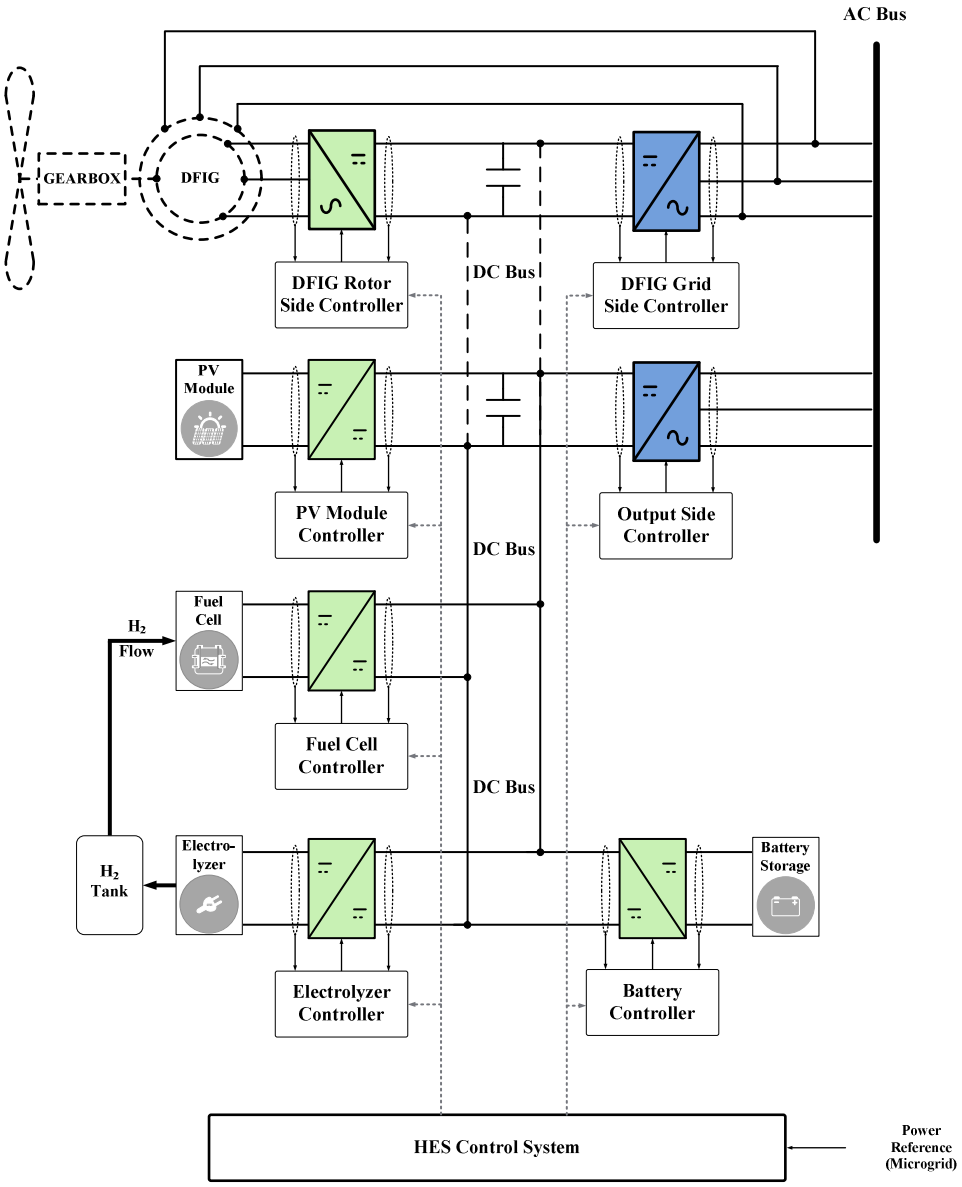

Figure 3-22 Proposed HES structure

4 SWITCHING POWER CONVERTERS – TOPOLOGIES AND CONTROL

The role of a power converter is to interconnect available electric energy sources with loads and to control the rate of energy exchange between source and the load. The form of the available electric energy sources and the form required/desired at the load side may not be the same. The power converters are devices interposed between available sources and the loads – thus an element of the overall power conversion system. Any energy consumed by power converter while performing desired rate of the power conversion control is, in principle, unnecessary loss and consequently, to satisfy application requirements power converter must be made as efficient as possible. From the aspect of efficiency and control of electric power flow the static converters operating in the switching mode represent the best solution.

This chapter presents unified approach to the analysis and control of power converters found in the power electronics interface of hybrid energy source as one of the remaining two objectives specified in Chapter 1. First, generalized converter structure is introduced; the roles and basic operation are identified. Further, DC-DC, AC-DC and DC-AC converters are analyzed and their dynamics are written. Finally the control method based on sliding mode theory is given and unified approach to the control of all of the converters is shown.

4.1 The Role of Switching Converters

In the most general case the source and the energy conversion process (load) may be generating and/or consuming energy (sink - negative power source) – thus power converter has to be able to support bidirectional power (Figure 4-1).

The polyphase AC is a prevailing electric energy distribution system. Hence, a conversion of polyphase AC of some frequency and voltage to polyphase AC of some

other frequency and voltage is the most general type of power conversion. However, the distinct properties possessed by certain power distribution, traditionally the polyphase AC (most often three-phase), single phase AC and DC distribution systems are recognized. This leads to possible four conversion functions that can be implemented, namely: AC-AC, AC-DC, DC-AC and DC-DC (Figure 4-2).

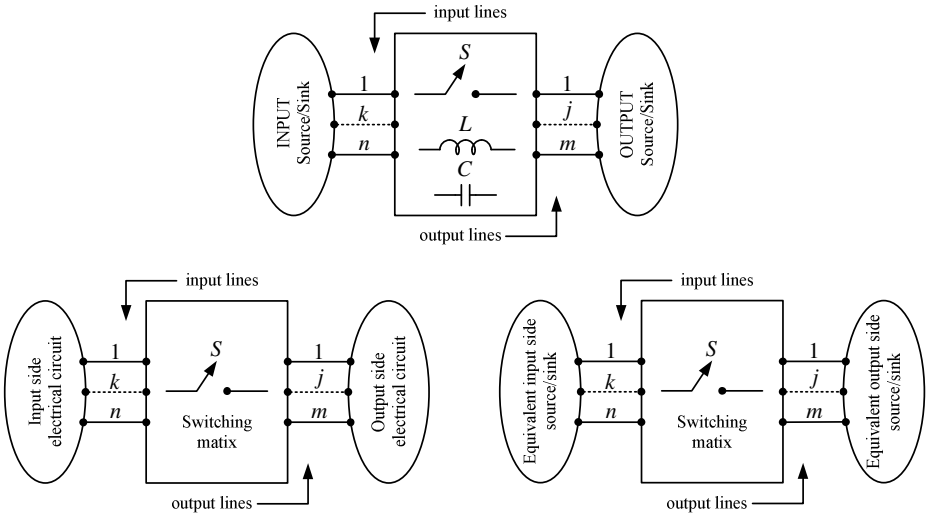

Figure 4-1 The connecting role of a switching converter

For a source interconnected to a given load, no voltage and current could be set independent. That leads to recognition of the two classes of sources: so-called voltage source and the current source.

A voltage source $S_v = \{v_v(t), \forall i_v(t)\}$, with terminal voltage $v_v(t)$ as *independent variable* while the current is the voltage source *dependent variable* determined by the circuitry connected to voltage source terminals.

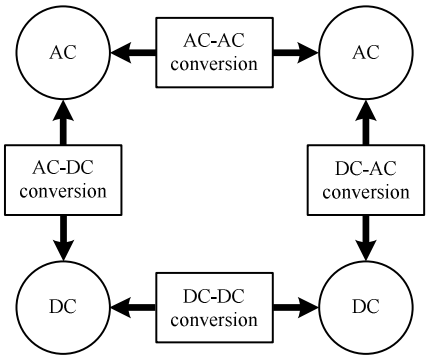

Figure 4-2 The basic conversion functions

A current source, $S_c = \{i_c(t), \forall v_c(t)\}$, with current $i_c(t)$ as *independent variable* while voltage across current source terminals $v_c(t)$ is *dependent variable* determined by the current state of the circuitry connected to current source terminals.

The converter is an interconnecting electrical network facilitating the transformation of current state of the electric power source S_g into the state of the electric power sink $S_s = \Omega(S_g)$. The interconnecting network together with sources and sinks satisfies Kirchhoff's laws and acts in a way that uniqueness of the solutions for the branch currents and node voltages is ensured. The dependent variables on the source and sink terminals need to be determined.

4.2 Switching Matrix

The most general converter interconnects a poly-phase ac source with a poly-phase ac sink. Let $S_g = \{\mathbf{v}_g(t)\}$ be a poly-phase voltage source connected to n input lines, where j[th] input line is connected to independent voltage sources $S_{gj} = \{v_{gj}(t)\}$, $j = 1, 2, ..., n$. Vector $\mathbf{v}_g^T = [v_{g1} ... v_{gn}]$ stands for $n \times 1$ voltage vector. A poly-phase current source $S_s = \{\mathbf{i}_s(t)\}$ is the power sink with each k[th] line is interconnected to $S_{sk} = \{i_{sk}(t)\}$ $k = 1, 2, ..., m$ as independent current sources. Vector $\mathbf{i}_s^T = [i_{s1} \quad ... \quad i_{sm}]$ stands for the $m \times 1$ current vector.

The use of switches as a structural elements of the converters allows considering a converter as the switching matrix as shown in Figure 4-3. The switches arranged in the nodes of a matrix permit that any input line is connected to any output line during some duration of time, by following a selected sequence of "ON" and "OFF" switching states. In an ideal case the transition from one current topology to another is assumed instantaneous. The topologies, resulting from combination of the "ON" and "OFF" states of the switches, that satisfy the Kirchoff's laws - thus allow unique determination of the branch currents and the node's voltage in the current topology will be considered permissible and will form set of converter *permitted configurations*. Due to the finite number of switches in converter matrix the number of *permitted configurations* is also

finite. In a sense the conversion is realized by a variable topology (structure) electric network and the resulting properties depend on the *permitted configurations* and their temporal changes. The analysis of such structures needs to address the average behavior as well as temporal changes of the currents and voltages.

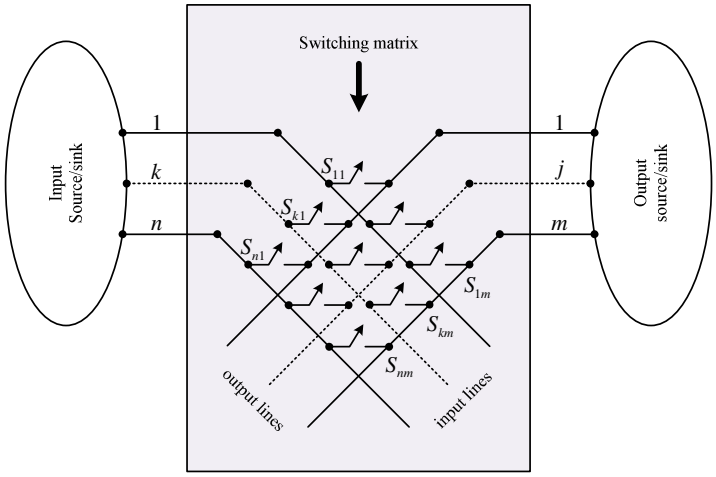

Figure 4-3 The structure of an n-input m-output converter

Let n AC voltage sources $v_{gk}(t), k=1,2,..,n$ be connected to the input lines, and m AC current sinks $i_{sj}(t), j=1,2,..,m$ be connected to the output lines and they are are interconnected by a switching matrix as shown in Fig. 4.3. The switch S_{kj} is placed on the node between $k-th$ input line and $j-th$ output line – thus it can connect or disconnect these two lines. For the given source and sink the output voltages and the input currents are *dependent quantities* that have to be determined.

To satisfy Kirchhoff's law for voltages only one of the switches connecting jth output line to any of the input lines can be closed at any instant of time. If more than one of these switches is closed simultaneously they would short-circuit the input voltage sources to which they are connected. To prevent violation of the Kirchhoff's law for current sources, at least one of the switches connecting jth output line to any of the input lines must be closed at any instant of time. Note that more than one of the output lines may be simultaneously connected to kth input line since this does not violate KCL.

Let state of the switch S_{kj} be described by the binary function $s_{kj}(t)$ (for this function sometimes the term "switching function" will be used),

$$s_{kj}(t)=\begin{cases}1 & \text{if switch } S_{kj} \text{ is ON}\\ 0 & \text{if switch } S_{kj} \text{ is OFF}\end{cases}$$
$$k=1,2,..,n \qquad (4.1)$$
$$j=1,2,...,m$$

4.3 Interconnection of Multiple Voltage or Current Sources to a Line

In Figure 4-4-(a) the interconnection of the *n* input voltage sources to the single output line and in Figure 4-4-(b) interconnection of the *n* input current sources to one output line are depicted. Due to the assumed bilateral energy flow the topologies can be also regarded as interconnection of a single voltage source to n current sinks and interconnection of a single current source to n voltage sinks.

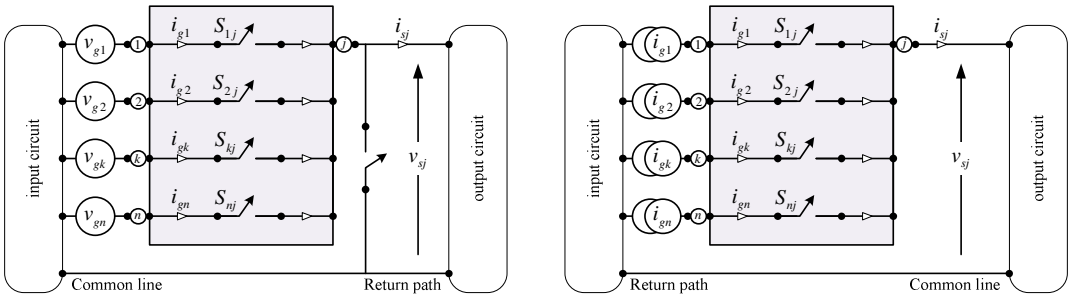

(a) (b)

Figure 4-4 Interconnection of the voltage sources (a) and the current sources (b) to one ouptu line

For structure depicted in Figure 4-4-(a) the KVL will not be violated if the binary functions $s_{lj}(t)$ satisfy the following constraints:

$$\sum_{l=1}^{n} s_{lj}(t)=1, \qquad (4.2)$$

Voltage $v_{sj}(t)$, as a dependent quantity, at any instant of time can be expressed as:

$$v_{sj}(t)=\sum_{k=1}^{n} s_{kj}v_{gk}=\mathbf{s}_j^T\mathbf{v}_g=\mathbf{v}_g^T\mathbf{s}_j$$
$$\mathbf{s}_j^T=\begin{bmatrix}s_{1j} & s_{2j} & .. & s_{nj}\end{bmatrix} \qquad (4.3)$$
$$\mathbf{v}_g^T=\begin{bmatrix}v_{g1} & v_{g2} & .. & v_{gn}\end{bmatrix}$$

The output voltage is a weighted sum of the input voltages and its instantaneous value can never exceed peak value of the one of the input voltages v_{gk}, $k = 1,2,..,n$. Due to the fact that input voltages are given, the desired voltages on the $j-th$ output line must be obtained by proper variation of the switching pattern - determined by the temporal changes of the components of switching vector $\mathbf{s}_j$.

Input line currents can be expressed as a function of the output line current i_{sj} as,

$$\begin{aligned} i_{gk} &= \sum_{l=1}^{n} s_{lj}(t) i_{sj}, \\ \sum_{l=1}^{n} s_{lj}(t) &= 1. \end{aligned} \tag{4.4}$$

It is obvious that switching pattern cannot be independently selected from the desired output voltages and desired input currents – thus design requirements must specify the desired quantities.

For the structure depicted in Figure 4-4-(b) the output line current as dependent quantity can be expressed as,

$$i_{sj}(t) = \sum_{k=1}^{n} s_{kj} i_{gk}. \tag{4.5}$$

In this case at least one of the switches must be closed at any instant of time – thus the constraints can be formulated in the following form,

$$\begin{aligned} 1 \le \sum_{k=1}^{n} s_{kj} &\le n, \\ \text{or} & \\ \sum_{k=1}^{n} s_{kj} &\neq 0. \end{aligned} \tag{4.6}$$

The input voltages are then determined by,

$$\begin{aligned} v_{gk}(t) &= s_{kj} v_{sj}, \\ \sum_{k=1}^{n} s_{kj} &\neq 0 \\ k &= 1,2,...,n. \end{aligned} \tag{4.7}$$

The topology consisting of *n* input voltage sources and *m* output current sources is depicted in Figure 4-5.

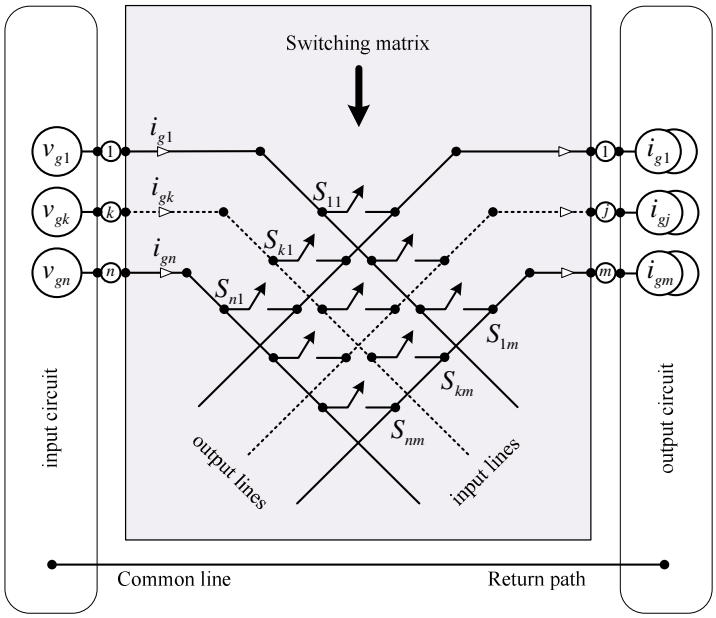

Figure 4-5 Interconnection of the *n* voltage sources and the *m* current sources

By combining all *m* outputs into a vector $\mathbf{v}_s^T = \begin{bmatrix} v_{s1} & v_{s2} & .. & v_{sm} \end{bmatrix}$ the relation $v_{sj}(t) = \sum_{k=1}^{n} s_{kj} v_{gk} = \mathbf{s}_j^T \mathbf{v}_g \quad , \quad j = 1, 2, ..., m$ can be rearranged in the matrix vector form as,

$$\mathbf{v}_\mathbf{s}(t) = \mathbf{M}_\mathbf{v}(t)\mathbf{v}_\mathbf{g}(t). \tag{4.8}$$

Elements of the matrix $\mathbf{M}_\mathbf{v}(t)$ are the switching functions $s_{kj}(t)$. Under the assumption of the lossless operation of the switches the power of the source and the power of the load must be the same. From $P_g = \mathbf{v}_\mathbf{g}^T(t)\mathbf{i}_\mathbf{g}(t)$ and $P_s = \mathbf{v}_\mathbf{s}^T(t)\mathbf{i}_\mathbf{s}(t)$ and (4.8), the vector of the currents in the input lines $\mathbf{i}_\mathbf{g}^T = \begin{bmatrix} i_{g1} & i_{g2} & .. & i_{gn} \end{bmatrix}$ can be expresses as

$$\mathbf{i}_\mathbf{g}(t) = \mathbf{M}_\mathbf{v}^T(t)\mathbf{i}_\mathbf{s}(t) \tag{4.9}$$

The constraint conditions (4.2) can be extended on the matrix $\mathbf{M}_\mathbf{v}$ in the form,

$$\begin{aligned} \mathbf{M}_\mathbf{v}\mathbf{e} &= \mathbf{e}; \\ \mathbf{e}^T &= \begin{bmatrix} 1 & 1 & .. & 1 \end{bmatrix}. \end{aligned} \tag{4.10}$$

Such topology may be regarded as an interaction of the m-current sources and n-voltage sources (reversal of the role of the sources on input and output side). Then relation (4.9) represents the transformation of the source independent variables and relation (4.8) describes the transformation of the output independent variables.

The relationship (4.8) and (4.9) define the transfer of the input variables to the output lines of the switching matrix. The relationship is solely determined by the

operation of the switching matrix. The state of the switches determines the *switching matrix configuration* at any instant of time. The change of the switching matrix configuration determines the *switching pattern* which describes the changes of the dependent quantities on output and the input lines of the switching matrix. This allows treatment of the switching matrix as an element that interconnects the electrical circuits on the input and output lines.

The changes in the configuration can be interpreted as the control of the converter. It is obvious that control is related to the changes in the binary variables s_{kj} and in order to design the desired transformation these binary variables must be determined. For the full specification of the switching pattern one has to find the instant of time when binary functions s_{kj} change its value. For $n \times m$ switching matrix, the switching pattern design – thus selection of the binary functions s_{kj} $k = 1,2,..,n$, $j = 1,2,..,m$ - one can use relationships (4.5) and (4.7). These expressions define $(n+m)$ linear algebraic equations for $n \times m$ unknown binary functions s_{kj} . The change of s_{kj} could be, in general, determined as function of time or a function of the conversion quantities.

Fourier series expansion for periodic function $s_{kj}(t)$ leads to its approximation

$$\lambda_{kj}(t) = a_0 + \sum_{n=1}^{\infty} \left(a_n \cos(n\omega t) + b_n \sin(n\omega t) \right), \tag{4.11}$$

where $\omega = 2\pi/T$ stands for angular frequency. By replacing in configuration matrix $\mathbf{M} \in \Re^{m \times n}$ discontinuous function $s_{kj}(t)$ by its Fourier representation $\lambda_{kj}(t)$ the switching matrix operation can be described by the matrix $\tilde{\mathbf{M}} \in \Re^{m \times n}$ that has time varying but continuous elements. Under the assumption that all variables assigned to sources and sinks are constant during switching interval T, and that $\lambda_{kj}(t)$ is the fundamental or dc component the operation of switching matrix with voltage

$$\begin{aligned} \mathbf{v_s}(t) &= \tilde{\mathbf{M}}_{\mathbf{v}} \left(\lambda_{kj} \right) \mathbf{v_g}, \\ \mathbf{i_g}(t) &= \tilde{\mathbf{M}}_{\mathbf{v}}^{T} \left(\lambda_{kj} \right) \mathbf{i_s}, \end{aligned} \tag{4.12}$$

or current input source,

$$\begin{aligned} \mathbf{i_s}(t) &= \tilde{\mathbf{M}}_{\mathbf{i}} \left(\lambda_{kj} \right) \mathbf{i_g}, \\ \mathbf{v_g}(t) &= \tilde{\mathbf{M}}_{\mathbf{i}}^{T} \left(\lambda_{kj} \right) \mathbf{v_s}. \end{aligned} \tag{4.13}$$

This relationship shows a possibility to treat switching matrix as a universal

transformer where transformation is defined by matrices $\tilde{\mathbf{M}}_{\mathrm{v}}$ and/or $\tilde{\mathbf{M}}_{\mathrm{i}}$. This allows simple treatment of the overall circuit with switching matrix as a generalized transformer inserted between input and output circuitry. Setting a particular "transformation ratio" consists in selecting $n \times m$ continuous functions $\lambda_{kj}(t)$. The general solution cannot be directly found from (4.12) or (4.13) and (4.11), and additional constraints have to be specified for a particular conversion [121,122].

4.4 The Operation of Switching Converters

4.4.1 DC-DC Switching Converters

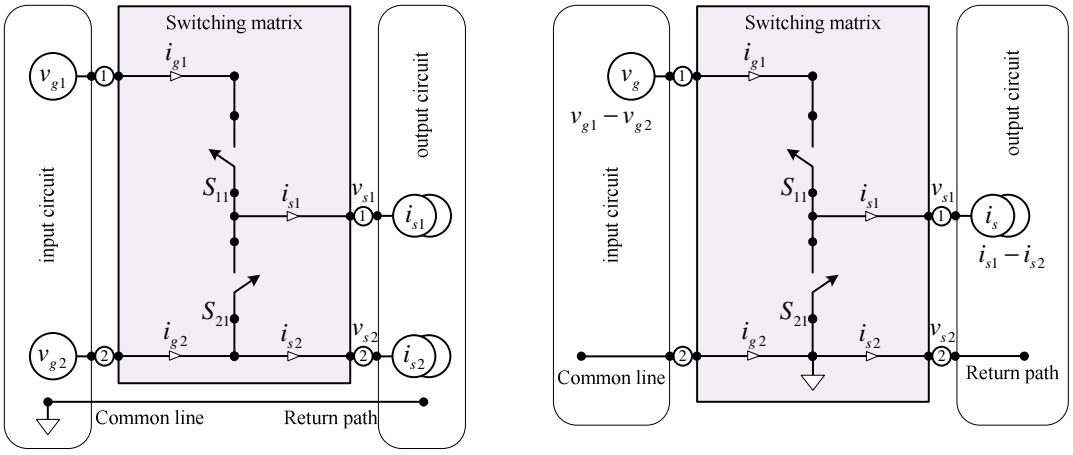

(a) (b)

Figure 4-6 Structure of a single input single output converter with voltage input (a), (b) simplified - single source version

The attribute of DC-DC converters is that the input and output share the common line thus one of the switches is interconnecting the common line to the output. The general structure interconnecting input sources v_{g1} and v_{g2} with current sources i_{s1} and i_{s2} is depicted in Figure 4-6.

The dependent quantities v_{s1} and v_{s2} or in vector form $\mathbf{v}_s = \begin{bmatrix} v_{s1} & v_{s2} \end{bmatrix}^T$ on the output lines can be expressed as

$$\begin{aligned} \mathbf{v_s} &= \mathbf{M_v}\mathbf{v_g}; \\ \mathbf{M_v} &= \begin{bmatrix} s_{11} & s_{21} \\ 0 & 1 \end{bmatrix}; \\ \mathbf{v_s} &= \begin{bmatrix} v_{s1} & v_{s2} \end{bmatrix}^T; \\ \mathbf{v_g} &= \begin{bmatrix} v_{g1} & v_{g2} \end{bmatrix}^T. \end{aligned} \tag{4.14}$$

The dependent quantities on input lines – currents i_{g1} and i_{g2} - as function of the current in output lines i_{s1}, i_{s2} can be expressed as,

$$\begin{aligned} \mathbf{i_g} &= \mathbf{M_v^T}\mathbf{i_s}; \\ \mathbf{i_s} &= \begin{bmatrix} i_{s1} & i_{s2} \end{bmatrix}^T; \\ \mathbf{i_g} &= \begin{bmatrix} i_{g1} & i_{g2} \end{bmatrix}^T. \end{aligned} \tag{4.15}$$

Operational constraints do not allow switches S_{11} and S_{21} be closed concurrently, thus having constraint relationship in the form,

$$s_{11} + s_{21} = 1 \Rightarrow s_{21} = 1 - s_{11} \tag{4.16}$$

With the common line voltage $v_{g2} = 0$ operation can be expressed by

$$\begin{aligned} v_{s1} &= s_{11} v_{g1}; \\ v_{s2} &= 0. \end{aligned} \tag{4.17}$$

$$\begin{aligned} i_{g1} &= s_{11} i_{s1}; \\ i_{g2} &= -s_{11} i_{s1}. \end{aligned} \tag{4.18}$$

Relationships (4.17) and (4.18) show that particular switching matrix has only one independent switch S_{11} as one can readily conclude by circuit analysis.

The dependent quantities cannot exceed the peak values of the corresponding independent quantities. The converter has single "control" input – the switching pattern of the switch S_{11}. Here term control input term points out the fact that the deliberate changes of the state of the switch S_{11} act as a control quantity in determining, for given input and output independent quantities, the changes in the dependent quantities.

Converter with one common line having current sources at its input lines and voltage sources at its output lines is shown in Figure 4-7. The dependent quantities on the output lines can be expressed as

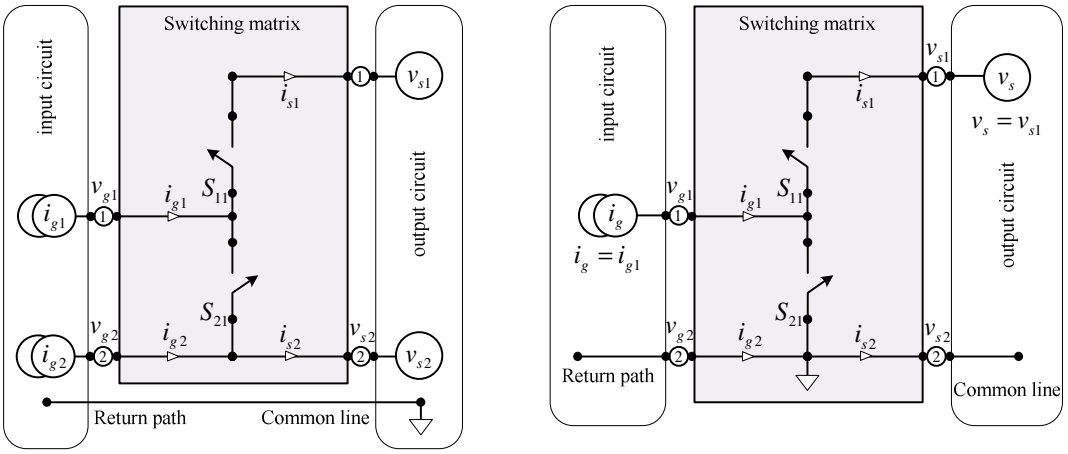

(a) (b)

Figure 4-7 Structure of a single input single output converter with current inputs (a), (b) simplified single source version

$$\mathbf{i_s} = \begin{bmatrix} s_{11} & 0 \\ s_{21} & 1 \end{bmatrix} \mathbf{i_g} = \mathbf{M_i} \mathbf{i_g};$$
$$\mathbf{i_s} = \begin{bmatrix} i_{s1} & i_{s2} \end{bmatrix}^T; \tag{4.19}$$
$$\mathbf{i_g} = \begin{bmatrix} i_{g1} & i_{g2} \end{bmatrix}^T.$$

$$\mathbf{v_g} = \mathbf{M_i}^T \mathbf{v_s};$$
$$\mathbf{v_s} = \begin{bmatrix} v_{s1} & v_{s2} \end{bmatrix}^T; \tag{4.20}$$
$$\mathbf{v_g} = \begin{bmatrix} v_{g1} & v_{g2} \end{bmatrix}^T.$$

By inspection of (4.14) and (4.19) it is easy to confirm that conditions $\mathbf{M_v} = \mathbf{M_i}^T$ are satisfied and the topologies shown in Figure 4-6 and Figure 4-7 are functionally the same - thus with assumption that the switches can support the bilateral energy flow the interchange of the input and output is allowed.

With constraints (4.16) and the properties of the topology expressed by $i_{g2} = -i_{g1}$ and $v_{s2} = 0$, the (4.19) and (4.20) yield

$$\begin{aligned} i_{s1} &= s_{11} i_{g1}; \\ i_{s2} &= -s_{11} i_{g1}. \end{aligned} \tag{4.21}$$

$$\begin{aligned} v_{g1} &= s_{11} v_{s1}; \\ v_{g2} &= 0. \end{aligned} \tag{4.22}$$

The dependent quantities are expressed the same way as in the structure with voltage sources.

4.4.2 DC-AC and AC-DC Single Phase Switching Converters

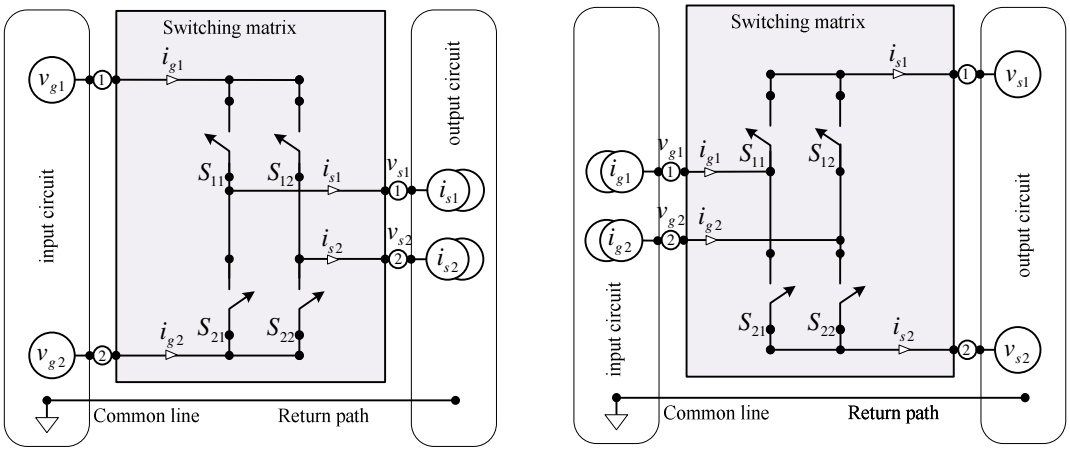

(a) (b)

Figure 4-8 Converters with two input and two output lines, voltage sources at the input and current sinks at the ouput (a) and vie versa (b)

By combining two of switching matrices depicted in Figure 4-6 one can easily obtain a switching matrix that interconnect two input and two output sources as shown in Figure 4-8-(a). To avoid violation of the KVL and/or KCL switches (S_{11} and S_{21}) or (S_{12} and S_{22}) cannot be simultaneously closed or open. By treating branches (S_{11}, S_{21}) and (S_{12}, S_{22}) as independent switching matrices, the output voltages v_{s1} and v_{s2} can be treated independently and from (4.14)and (4.16) determined as $v_{s1} = s_{11}(t)\left(v_{g1} - v_{g2}\right)$ and $v_{s2} = s_{12}(t)\left(v_{g1} - v_{g2}\right)$. The voltages v_{s1} and v_{s2} stand for independent voltage sources that can be interconnected to the output circuitry. Analysis of the circuits with two input and two output lines can be done as combination of the two converters analyzed in the previous sections.

The direct analysis of the switching matrix shown in Figure 4-8-(a) allows express the dependent quantities on the output side as ,

$$\mathbf{v_s} = \begin{bmatrix} v_{s1} \\ v_{s2} \end{bmatrix} = \begin{bmatrix} s_{11} & s_{21} \\ s_{12} & s_{22} \end{bmatrix} \begin{bmatrix} v_{g1} \\ v_{g2} \end{bmatrix} = \mathbf{M_{v2}} \mathbf{v_g};$$
$$\mathbf{M_{v2}} = \begin{bmatrix} s_{11} & s_{21} \\ s_{12} & s_{22} \end{bmatrix}, \tag{4.23}$$

where $\mathbf{v_g} = \begin{bmatrix} v_{g1} & v_{g2} \end{bmatrix}^T$ stands for the voltage input vector, $\mathbf{v_s} = \begin{bmatrix} v_{s1} & v_{s2} \end{bmatrix}^T$ stands

for the output voltage vector, and $\mathbf{M}_{\mathbf{v2}}$ stands for the transformation matrix describing operation of the topology with 2 input and 2 output lines.

The current on the input lines can be expressed as $\mathbf{i_g} = \mathbf{M}_{\mathbf{v2}}^T \mathbf{i_s}$ where $\mathbf{i_g} = \begin{bmatrix} i_{g1} & i_{g2} \end{bmatrix}^T$ stands for the current vector on the input side of converter (dependent quantity), $\mathbf{i_s} = \begin{bmatrix} i_{s1} & i_{s2} \end{bmatrix}^T$ stands for the output current vector (independent quantity).

For switching matrix with two input and two output lines the constraints have the following form,

$$\begin{aligned} s_{11} + s_{21} = 1 \Rightarrow s_{21} = 1 - s_{11}, \\ s_{12} + s_{22} = 1 \Rightarrow s_{22} = 1 - s_{12}. \end{aligned} \tag{4.24}$$

If the input voltage is measured from line 2, thus $v_{g2} = 0$ and $v_g = v_{g1}$ the voltages on the output lines can be expressed in the following form,

$$\begin{aligned} \begin{bmatrix} v_{s1} \\ v_{s2} \end{bmatrix} = \begin{bmatrix} s_{11} \\ s_{12} \end{bmatrix} v_g; \\ \mathbf{v_s} = \mathbf{s}_s^{2\to 2} v_g. \end{aligned} \tag{4.25}$$

The relationship (4.25) clearly shows that the voltages on the output lines, measured from the common point, act as two independent voltage sources each "controlled" by its switching pattern.

The output circuit is connected between output lines 1 and 2 thus the equivalent voltage that acts on this circuit can be written as,

$$\begin{aligned} v_s &= v_{s1} - v_{s2}; \\ &= (s_{11} - s_{12})(v_{g1} - v_{g2}); \\ &= v_g (s_{11} - s_{12}). \end{aligned} \tag{4.26}$$

Similarly the input current can be expressed as,

$$\begin{aligned} i_g &= i_{g1}; \\ &= s_{11} i_{s1} + s_{12} i_{s2}; \\ &= i_s (s_{11} - s_{12}). \end{aligned} \tag{4.27}$$

The dependent quantities - voltage acting on the output circuitry v_s and current in input lines i_g - depend on the input and output independent quantities and the difference between switching pattern in the branches of the switching matrix.

The same topology can be analyzed with current sources at input side and the voltage sources at the output side (Figure 4-8-(b)). Direct application of the generalized

switching matrix description the line currents on the output can be expressed in the following form

$$\begin{aligned}\mathbf{i_s} &= \begin{bmatrix} i_{s1} \\ i_{s2} \end{bmatrix} = \begin{bmatrix} s_{11} & s_{21} \\ s_{12} & s_{22} \end{bmatrix} \begin{bmatrix} i_{g1} \\ i_{g2} \end{bmatrix} \\ &= \mathbf{M_{i2}} \mathbf{i_g} \\ &= \mathbf{M_{v2}^T} \mathbf{i_g} \end{aligned} \tag{4.28}$$

The line voltages on the input can be expressed in the following form

$$\begin{aligned}\mathbf{v_g} &= \begin{bmatrix} v_{g1} \\ v_{g2} \end{bmatrix} = \begin{bmatrix} s_{11} & s_{12} \\ s_{21} & s_{22} \end{bmatrix} \begin{bmatrix} v_{s1} \\ v_{s2} \end{bmatrix} \\ &= \mathbf{M_{i2}^T} \mathbf{v_s} \\ &= \mathbf{M_{v2}} \mathbf{v_s} \end{aligned} \tag{4.29}$$

Insertion of the values of the switching variables s_{11} and s_{12} into (4.28) and (4.29) the span of the changes of the dependent quantities can be expressed as

$$i_s = \begin{cases} i_g & \text{if} \quad s_{11} = 1 \,\&\, s_{21} = 0 \\ 0 & \text{if} \quad s_{11} = 1 \,\&\, s_{21} = 1 \; or \; s_{11} = 0 \,\&\, s_{21} = 0 \\ -i_g & \text{if} \quad s_{11} = 0 \,\&\, s_{21} = 1, \end{cases} \tag{4.30}$$

$$v_g = \begin{cases} v_s & \text{if} \quad s_{11} = 1 \,\&\, s_{21} = 0 \\ 0 & \text{if} \quad s_{11} = 1 \,\&\, s_{21} = 1 \; or \; s_{11} = 0 \,\&\, s_{21} = 0 \\ -v_s & \text{if} \quad s_{11} = 0 \,\&\, s_{21} = 1. \end{cases} \tag{4.31}$$

4.4.3 DC-AC and AC-DC Three Phase Converters

The three phase is a dominant way of the electrical distribution. This section discusses interaction of a three phase sources with other type of electric power sources.

The topology depicted in Figure 4-9 consists of the branches (S_{11}, S_{21}), (S_{12}, S_{22}) and (S_{13}, S_{23}), thus it is an interconnection of the three converters shown in Figure 4-6.

The switches in one branch cannot be simultaneously closed due to the requirement to meet the KVL or cannot be simultaneously open without violating KCL, so all the possible state of the switches for structure depicted in can be summarized as in Table 4-1.

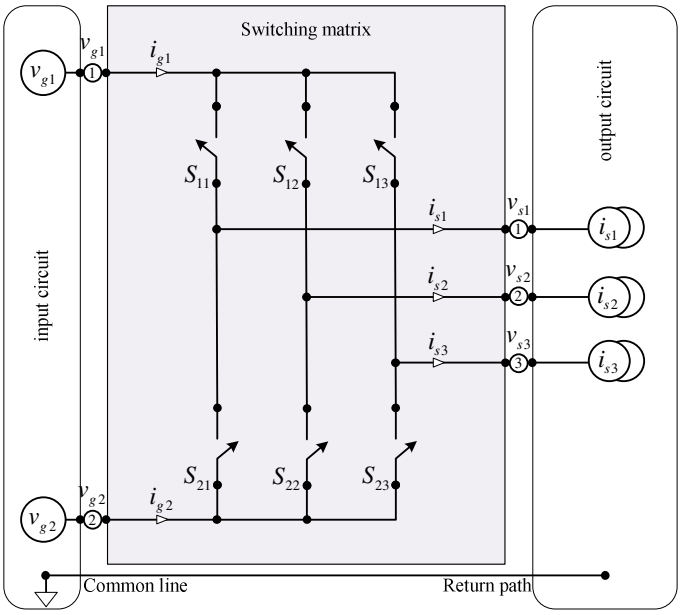

Figure 4-9 Converter with two input lines and three output lines, voltage sources at the input and current sinks at the output

Matrix Configuration	State of switches						Value of switching variable					
	S_{11}	S_{21}	S_{12}	S_{22}	S_{13}	S_{23}	s_{11}	s_{21}	s_{12}	s_{22}	s_{13}	s_{23}
1	ON	OFF	OFF	ON	OFF	ON	1	0	0	1	0	1
2	ON	OFF	ON	OFF	OFF	ON	1	0	1	0	0	1
3	OFF	ON	ON	OFF	OFF	ON	0	1	1	0	0	1
4	OFF	ON	ON	OFF	ON	OFF	0	1	1	0	1	0
5	OFF	ON	OFF	ON	ON	OFF	0	1	0	1	1	0
6	ON	OFF	OFF	ON	ON	OFF	1	0	0	1	1	0
7	ON	OFF	ON	OFF	ON	OFF	1	0	1	0	1	0
8	OFF	ON	OFF	ON	OFF	ON	0	1	0	1	0	1

Table 4-1 State of the switches for structure depicted in Figure 4-9

The voltages on output lines can be expressed as

$$\mathbf{v_s} = \begin{bmatrix} v_{s1} \\ v_{s2} \\ v_{s3} \end{bmatrix} = \begin{bmatrix} s_{11} & s_{21} \\ s_{12} & s_{22} \\ s_{13} & s_{23} \end{bmatrix} \begin{bmatrix} v_{g1} \\ v_{g2} \end{bmatrix} = \mathbf{M_{v3}} \mathbf{v_g} \tag{4.32}$$

The equation (4.32) describes, as expected, three voltage sources acting on the output lines of the switching matrix.

The input currents are determined by transposing the matrix $\mathbf{M_{v3}}$ to obtain

$$\mathbf{i_g} = \begin{bmatrix} i_{g1} \\ i_{g2} \end{bmatrix} = \begin{bmatrix} s_{11} & s_{12} & s_{13} \\ s_{21} & s_{22} & s_{23} \end{bmatrix} \begin{bmatrix} i_{s1} \\ i_{s2} \\ i_{s3} \end{bmatrix} = \mathbf{M}_{\mathbf{v3}}^{T} \mathbf{i_s} \tag{4.33}$$

To avoid violation of KLV and KLC, switching variables $s_{kj}(t)$, $k = 1,2$, $j = 1,2,3$ are constrained by

$$\begin{aligned} s_{11} + s_{21} &= 1 \Rightarrow s_{21} = 1 - s_{11} \\ s_{12} + s_{22} &= 1 \Rightarrow s_{22} = 1 - s_{12} \\ s_{13} + s_{23} &= 1 \Rightarrow s_{23} = 1 - s_{13} \end{aligned} \tag{4.34}$$

The same relationships are valid if topology is analyzed with reversed input and output sides (current sources as inputs and voltage source at output) thus describing the operation of the AC-DC three phase converter with current inputs. In this case the switching constraints are the same as in (4.34).

Relations (4.32) and (4.33) define quantities on the output lines. In order to determine the voltages across the load side sources one need to know the topology determining the interconnection on load side. In general there are three possibilities: (a) all load side sources are connected to the return path - thus they act as three independent loads, (b) load side sources are interconnected to a common point (usually called neutral) which is not connected to the ground. Such interconnection is known as so-called star connection (Figure 4-10-(a)) and (c) load side sources are interconnected in so-called delta connection (Figure 4-10-(b)).

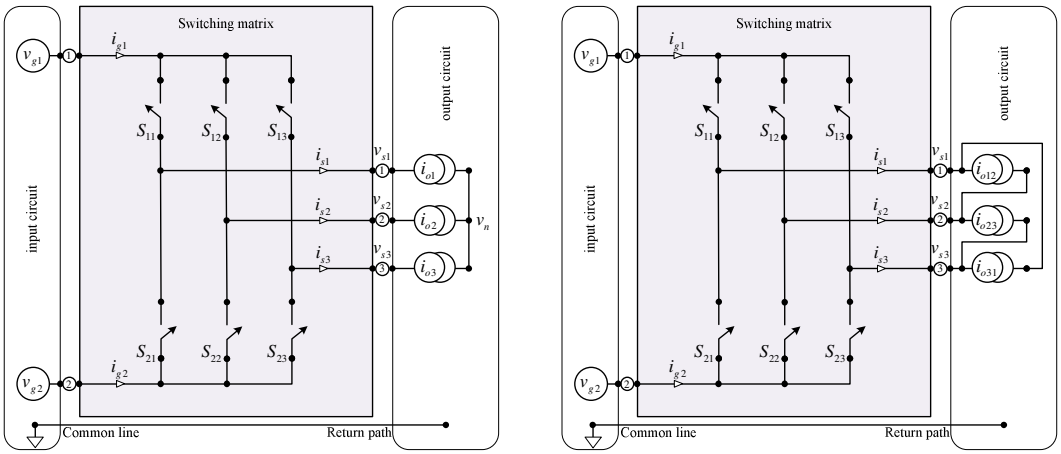

(a) (b)

Figure 4-10 Converter with star connection on the load side (a) and delta connection on load side (b)

Assuming that the voltage of the common point is denoted as v_n , the voltages across the loads - usually called load phase voltages - can be expressed as

$$\begin{aligned} v_{o1} &= v_{s1} - v_n \\ v_{o2} &= v_{s2} - v_n \\ v_{o3} &= v_{s3} - v_n \end{aligned} \tag{4.35}$$

The load currents satisfy the following constraints

$$i_{o1} + i_{o2} + i_{o3} = i_{s1} + i_{s2} + i_{s3} = 0 \tag{4.36}$$

For the case of symmetrical load, the voltages of neutral point can be expressed as

$$v_n = \tfrac{1}{3}\left(v_{s1} + v_{s2} + v_{s3}\right) = \tfrac{1}{3}\left[\mathbf{e}^{1\times 3}\right]^T \mathbf{v_s} \tag{4.37}$$

where $\mathbf{e}^T = \begin{bmatrix} 1 & 1 & 1 \end{bmatrix}$ stands for unit vector. Insertion of the (4.32) into (4.37) yields

$$v_n = \frac{1}{3}\begin{bmatrix} \left(s_{11} + s_{12} + s_{13}\right) & \left(s_{21} + s_{22} + s_{23}\right) \end{bmatrix}\begin{bmatrix} v_{g1} \\ v_{g2} \end{bmatrix} \tag{4.38}$$

From (4.35) and (4.38) load phase voltages in star connection can be expressed in the following form:

$$\begin{bmatrix} v_{o1} \\ v_{o2} \\ v_{o3} \end{bmatrix} = \frac{1}{3}\begin{bmatrix} 2 & -1 & -1 \\ -1 & 2 & -1 \\ -1 & -1 & 2 \end{bmatrix}\begin{bmatrix} v_{s1} \\ v_{s2} \\ v_{s3} \end{bmatrix} = \mathbf{A_Y v_s} \tag{4.39}$$

Insertion of (4.32) into (4.39) yields

$$\begin{bmatrix} v_{o1} \\ v_{o2} \\ v_{o3} \end{bmatrix} = \frac{1}{3}\begin{bmatrix} 2 & -1 & -1 \\ -1 & 2 & -1 \\ -1 & -1 & 2 \end{bmatrix}\begin{bmatrix} s_{11} & s_{21} \\ s_{12} & s_{22} \\ s_{13} & s_{23} \end{bmatrix}\begin{bmatrix} v_{g1} \\ v_{g2} \end{bmatrix} = \mathbf{A_Y M_{v3} v_g} \tag{4.40}$$

The load phase voltages depend on the matrix operation ($\mathbf{M_{v3} v_g}$) and the load connection defined by matrix $\mathbf{A_Y}$. If load is in delta connection Figure 4-10-(b), the phase voltages measured across the phase sources i_{o12}, i_{o23} and i_{o31} can be expressed in the following form:

$$\begin{aligned} \begin{bmatrix} v_{o12} \\ v_{o23} \\ v_{o31} \end{bmatrix} &= \begin{bmatrix} 1 & -1 & 0 \\ 0 & 1 & -1 \\ -1 & 0 & 1 \end{bmatrix}\begin{bmatrix} v_{s1} \\ v_{s2} \\ v_{s3} \end{bmatrix} = \mathbf{A_\Delta v_s} \\ &= \mathbf{A_\Delta} \underbrace{\begin{bmatrix} s_{11} & s_{21} \\ s_{12} & s_{22} \\ s_{13} & s_{23} \end{bmatrix}}_{\mathbf{M_{v3}}} \underbrace{\begin{bmatrix} v_{g1} \\ v_{g2} \end{bmatrix}}_{\mathbf{v_g}} = \mathbf{A_\Delta M_{v3} v_g} \end{aligned} \tag{4.41}$$

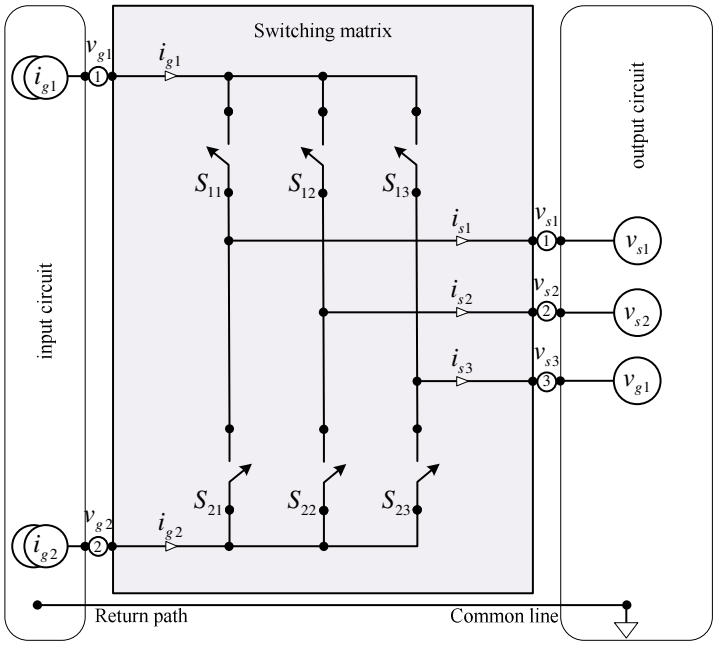

Figure 4-11 Converters with two input and three output lines, current source and voltage sink at output

A converter with current source at input and three phase voltage source at output is shown in Figure 4-11. The dependent quantities (currents in the output lines and voltages on input lines) can be expressed as,

$$\mathbf{i_s} = \begin{bmatrix} i_{s1} \\ i_{s2} \\ i_{s3} \end{bmatrix} = \begin{bmatrix} s_{11} & s_{21} \\ s_{12} & s_{22} \\ s_{13} & s_{23} \end{bmatrix} \begin{bmatrix} i_{g1} \\ i_{g2} \end{bmatrix} = \mathbf{M_{v3}} \mathbf{i_g} \tag{4.42}$$

$$\mathbf{v_g} = \begin{bmatrix} v_{g1} \\ v_{g2} \end{bmatrix} = \begin{bmatrix} s_{11} & s_{12} & s_{13} \\ s_{21} & s_{22} & s_{23} \end{bmatrix} \begin{bmatrix} v_{s1} \\ v_{s2} \\ v_{s3} \end{bmatrix} = \mathbf{M}_{\mathbf{v3}}^{T} \mathbf{v_s} \tag{4.43}$$

Equation (4.42) describes three current sources acting on the output lines of the converter. The results obtained for the general switching matrix operation links directly the $\mathbf{M_i}$ and $\mathbf{M_v}$ matrices. The result can be verified by comparing the results for voltage source and current source converters.

To avoid violation of KVL and KCL, switching variables $s_{kj}(t)$ $k = 1, 2$, $j = 1, 2, 3$ are constrained by

$$\begin{aligned} s_{11} + s_{12} + s_{13} &= 1 \\ s_{21} + s_{22} + s_{23} &= 1 \end{aligned} \tag{4.44}$$

At least one of the switches connecting input line 1 or 2 to an output line must be

ON. The same relationship is valid if the topology in Figure 4-11 is analyzed as switching matrix with three input and two output lines e.g. as an AC-DC converter.

The analysis of the switching matrix operation shows that it can be treated as generalized transformer acting on the independent variables of the sources interconnected to its input and output lines in an electrical circuit. In Figure 4-12 the topologies with equivalent input side voltage and current sources are shown. In both cases the action of the switching matrix as a transformer allows calculation of the relevant voltages and currents in input and output circuits.

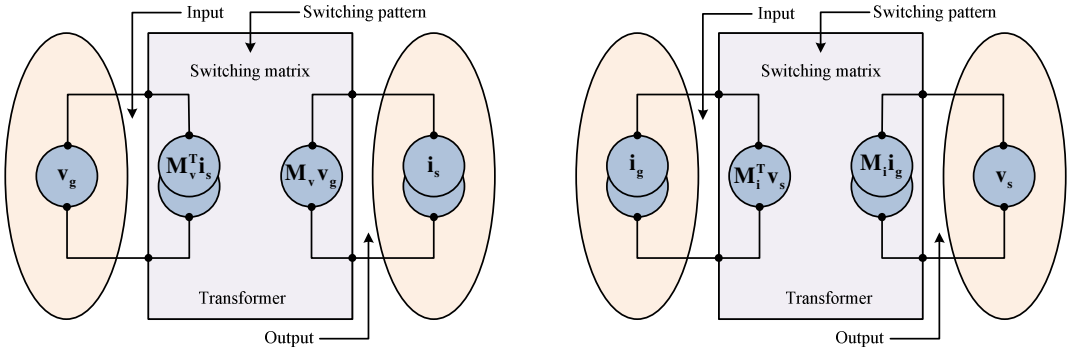

Figure 4-12 Switching matrix as a transformer

4.5 Dynamics of Switching Converters

In preceding sections basic properties of the interaction of the switches and ideal sources were revealed and basic functional characteristics of elementary switching matrix were shown. The topology of the converters, besides of the sources employs energy storing elements (see Figure 4-1). Energy storing elements introduce dynamics in the energy processing due to the capabilities to accumulate energy. By developing a way of deriving the input and output properties of switching matrix derivation of dynamical models of switching converters may follow the standard procedure for electric circuitry modeling. Switching matrix than is an element of the topology with defined relationship between quantities on its input and output lines.

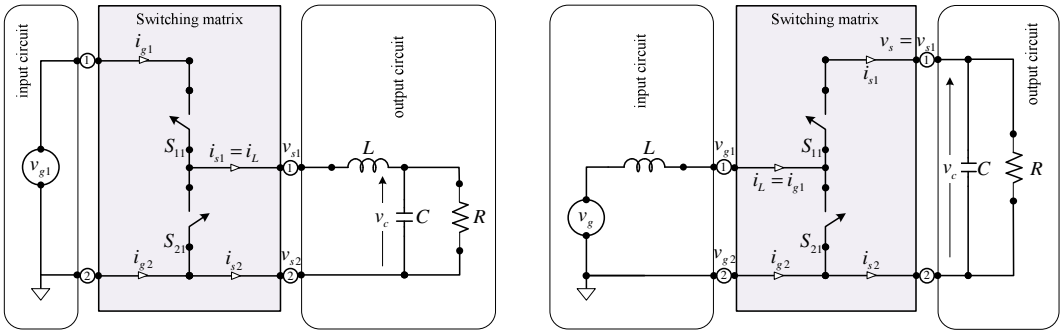

(a) (b)

Figure 4-13 Converters with no energy storing elements on input side (a) and converters with dynamics on both input and output side (b)

4.5.1 Dynamics of DC-DC Converters

In general energy storing elements (*L,C*) may be placed on the output side of the converter or on the input and output side of the converter or they may be structured in such a way that they are shared between input and output side as depicted in structures in Figure 4-13.

The dynamics of the output circuit in Figure 4-13-(a) can be written directly, by selecting the inductor current i_L and the capacitor voltage as system state variables as;

$$\begin{aligned} \frac{d}{dt}\left(Li_L\right) &= v_{s1} - v_C, \\ \frac{d}{dt}\left(Cv_C\right) &= i_L - i_R. \end{aligned} \tag{4.45}$$

By taking into account the operation of the switching matrix and the fact that $v_{s1} = v_{g1} \cdot s_{11}$, $v_{s2} = 0$ and $i_{g1} = -i_{g2} = i_{s1} \cdot s_{11}$ (4.45) can be rewritten as

$$\begin{aligned} \frac{d}{dt}\left(Li_L\right) &= v_{g1} \cdot s_{11} - v_C, \\ \frac{d}{dt}\left(Cv_C\right) &= i_L - \frac{v_C}{R}. \end{aligned} \tag{4.46}$$

This description should be completed by the switching pattern for s_{11}. Under assumption that switching is periodic with period T_s one can write,

$$s_{11} = \begin{cases} 1 & \text{for} \quad kT_s \le t \le \left(kT_s + d_{11}T_s\right) \\ 0 & \text{for} \quad \left(kT_s + d_{11}T_s\right) < t \le T_s \end{cases} \quad k = 1, 2, \ldots \tag{4.47}$$

The inductor voltage and the capacitor current for converter in Figure 4-13-(b)

can be derived as

$$\begin{aligned} \frac{d}{dt}\left(Li_L\right) &= v_g - v_{g1}, \\ \frac{d}{dt}\left(Cv_C\right) &= i_{s1} - i_R. \end{aligned} \tag{4.48}$$

The voltage on the common line is $v_{g2} = 0$ and the current in the common line is $i_{g2} = -i_{g1} = -i_L$. From previous section we know that voltage on the input line v_{g1} and the current on the output line i_{s1} can be written as $v_{g1} = v_{s1}s_{11} = v_C s_{11};\ i_{s1} = i_{g1}s_{11} = i_L s_{11}$. So inserting these expressions into (4.48) yields,

$$\begin{aligned} \frac{d}{dt}\left(Li_L\right) &= v_g - v_C s_{11}, \\ \frac{d}{dt}\left(Cv_C\right) &= i_L s_{11} - \frac{v_C}{R}. \end{aligned} \tag{4.49}$$

This description should be completed by the switching pattern for s_{11}

$$s_{11} = 1 - s_{12} = \begin{cases} 1 & \text{for} \quad kT_s \le t \le \left(kT_s + d_{11}T_s\right) \\ 0 & \text{for} \quad \left(kT_s + d_{11}T_s\right) < t \le T_s \end{cases} \quad k = 1, 2, \ldots \tag{4.50}$$

In the power electronics literature as a rule the switching function for switch s_{12} is used in the mathematical description of this converter. Then the model (4.49) becomes,

$$\begin{aligned} \frac{d}{dt}\left(Li_L\right) &= v_g - v_C\left(1 - s_{12}\right), \\ \frac{d}{dt}\left(Cv_C\right) &= i_L\left(1 - s_{12}\right) - \frac{v_C}{R}. \end{aligned} \tag{4.51}$$

4.5.2 DC-AC and AC-DC Single Phase Switching Converters

The voltage source converter with two input and two output lines (Figure 4-14) can be treated in very similar way. The dynamics of the output circuit can be written directly, by selecting the inductor current i_L and the capacitor voltage as system state variables. Then by inspection we can write:

$$\begin{aligned} \frac{d}{dt}\left(Li_L\right) &= \left(v_{s1} - v_{s2}\right) - v_C, \\ \frac{d}{dt}\left(Cv_C\right) &= i_L - i_R. \end{aligned} \tag{4.52}$$

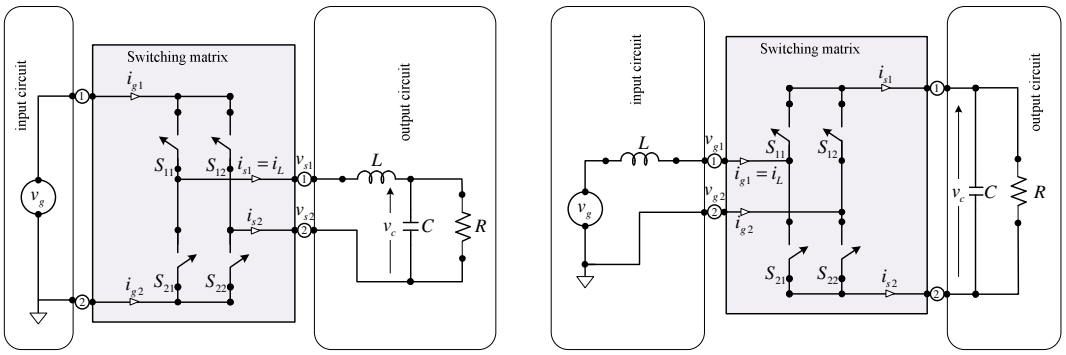

(a) (b)

Figure 4-14 Voltage source converter (a) and current source converter (b) with two input and two output lines

By taking into account the operation of the switching matrix as described by (4.25) and the fact that the voltage on the switching matrix output lines is defined by $v_{s1}-v_{s2}=(s_{11}-s_{12})v_g$ and we can write,

$$\begin{aligned}\frac{d}{dt}(Li_L)&=(s_{11}-s_{12})v_g-v_C,\\ \frac{d}{dt}(Cv_C)&=i_L-\frac{v_C}{R}.\end{aligned}\tag{4.53}$$

This description should be completed by the switching pattern for s_{11} and s_{12}. Model (4.53) appears to have two independent switching patterns - or two binary control inputs - acting in the first equation. It could be easily verified that converter has four topologies but they results in three possible values of the voltage $v_{s1}-v_{s2}=(s_{11}-s_{12})v_g$ as shown in (4.31).

For converter with current input in Figure 4-14-(b) if,

$$\begin{aligned}v_{g1}&=(s_{11}-s_{21})(v_{s1}-v_{s2})=(s_{11}-s_{21})v_C,\\ i_{s1}&=(s_{11}-s_{21})i_L,\end{aligned}\tag{4.54}$$

then dynamics become;

$$\begin{aligned}\frac{d}{dt}(Li_L)&=v_g-v_C(s_{11}-s_{21}),\\ \frac{d}{dt}(Cv_C)&=i_L(s_{11}-s_{21})-\frac{v_C}{R}.\end{aligned}\tag{4.55}$$

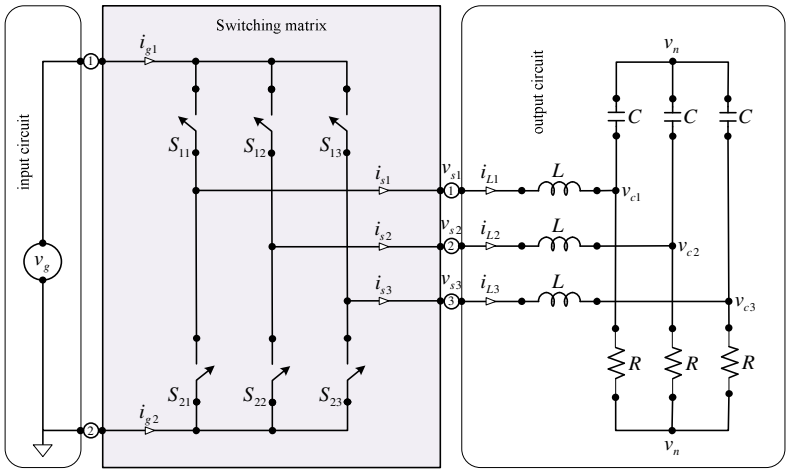

Figure 4-15 Voltage source 3-phase converter (buck inverter)

4.5.3 Three-Phase Switching Converters

In this section dynamics of the most common three phase converters will be analyzed to demonstrate the procedures and operational properties.

From Figure 4-15 it is easy to write the voltages across inductors as,

$$\frac{d}{dt}\left(Li_{Li}\right) = v_{si} - v_{Ci} = v_g s_{1i} - v_{Ci}, \quad i = 1,2,3. \tag{4.56}$$

All of the voltages will be determined with respect to one reference point. With star connection of the load, transformation (4.39) should be applied to right-hand side of (4.56). This transformation leads to following equations,

$$\frac{d}{dt}\left(\mathbf{L}\mathbf{i}_{\mathbf{L}}\right) = v_g \mathbf{A}_{\mathbf{Y}} \mathbf{s}_{\mathbf{s}}^{2\to 3} - \mathbf{A}_{\mathbf{Y}} \mathbf{v}_{\mathbf{C}}, \tag{4.57}$$

where $\mathbf{i}_{\mathbf{L}}^T = \begin{bmatrix} i_{L1} & i_{L2} & i_{L3} \end{bmatrix}$ is inductors current vector, $\mathbf{L} = diag\left(L\right)$ is diagonal inductance matrix, $\mathbf{s}_{\mathbf{s}}^{2\to 3} = \begin{bmatrix} s_{11} & s_{12} & s_{13} \end{bmatrix}^T$ is vector that defines operation of the switches, and $\mathbf{v}_{\mathbf{C}}^T = \begin{bmatrix} v_{C1} & v_{C2} & v_{C3} \end{bmatrix}$ is capacitor voltage vector. Note that this transformation means that the measurements are taken with point "0" on the input side as a reference. Equation (4.57) can be written in expanded form as,

$$L\frac{di_{Li}}{dt} = v_L = -\left(v_{Ci} - \frac{1}{3}\sum_{j=1}^{3} v_{Cj}\right) + v_g\left(s_{1i} - \frac{1}{3}\sum_{j=1}^{3} s_{1j}\right), \quad i = 1,2,3. \tag{4.58}$$

The components of the s_{1j}, $j = 1,2,3$ control are defined as:

$$s_{1j}(t)=\begin{cases}1 & \text{for} \quad S_{1j}=ON \;\&\; S_{2j}=OFF \\ 0 & \text{for} \quad S_{1j}=OFF \;\&\; S_{2j}=ON\end{cases}, \quad j=1,2,3. \tag{4.59}$$

The change of the voltages of the output capacitors can be obtained as,

$$\frac{d}{dt}\left(\mathbf{C}\mathbf{v}_{\mathbf{C}}\right)=\mathbf{i}_{\mathbf{L}}-\mathbf{R}^{-1}\mathbf{v}_{\mathbf{C}}, \tag{4.60}$$

where $\mathbf{C}=diag\left(C\right)$ and $\mathbf{R}=diag\left(R\right)$ are diagonal matrices of capacitances and load resistances. Model (4.58)-(4.60) represent a sixth order dynamical system linear with respect to control vector $\mathbf{s}_s^{2\to 3}$. The comparison with corresponding expressions for DC-DC buck converter shows the same properties of the two converters regarding the transformations of the variables. The basic behavior is determined by the switching matrix and the sources connected to the input and output terminals of the switching matrix. The gains that switching matrix introduces in the system are less than 1 for all independent variables connected to the input or output terminals.

The voltages across inductor for converter depicted in Figure 4-16 are $v_L=v_g-\left(v_{g1}-v_{g2}\right)=v_g-\mathbf{v}_C^T\mathbf{s}^{2\to 3}$, and the dynamics of the inductor current are,

$$\frac{d}{dt}\left(Li_L\right)=v_L=v_g-\mathbf{v}_{\mathbf{C}}^T\mathbf{s}^{2\to 3}. \tag{4.61}$$

The change of the voltages of the output capacitors can be obtained as:

$$\begin{aligned}&\mathbf{i}_{\mathbf{C}}=i_L\mathbf{s}^{2\to 3}-\mathbf{R}^{-1}\mathbf{A}_{\mathbf{Y}}\mathbf{v}_{\mathbf{C}};\\ &\frac{d}{dt}\left(\mathbf{C}\mathbf{v}_{\mathbf{C}}\right)=i_L\mathbf{s}^{2\to 3}-\mathbf{R}^{-1}\mathbf{A}_{\mathbf{Y}}\mathbf{v}_{\mathbf{C}},\end{aligned} \tag{4.62}$$

where $\mathbf{C}=diag\left(C\right),\mathbf{R}=diag\left(R\right)$ and $\mathbf{i}_{\mathbf{C}}^T=\left[i_{C1}\quad i_{C2}\quad i_{C3}\right]$ vector of capacitor currents.

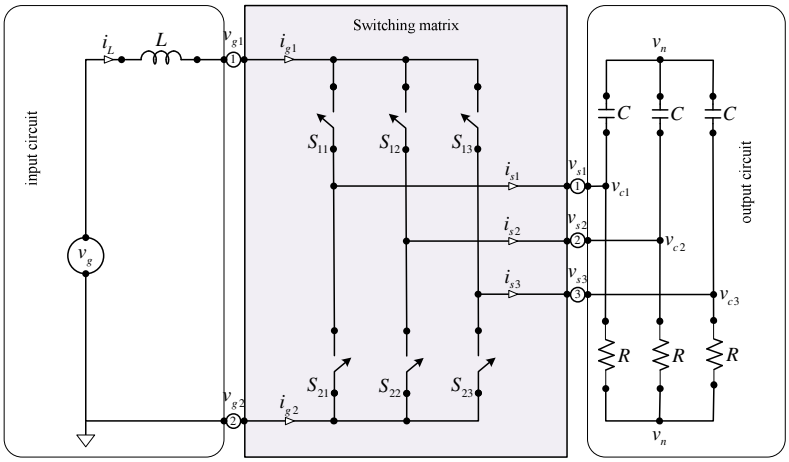

Figure 4-16 Current source 3-phase converter (boost inverter)

Model (4.61) and (4.62) represent a sixth order dynamical system linear with respect to control vector $\mathbf{s}^{2\to 3}$. The comparison with corresponding expressions for DC-DC boost converter shows the same properties of the two converters regarding the transformations of the variables.

Structure of three phase buck rectifier is depicted in Fig. 4.17. The time derivative of the inductor current can be calculated as,

$$\frac{d}{dt}\left(Li_L\right) = v_L = \mathbf{v}_\mathbf{g}^T \mathbf{s}^{3\to 2} - v_C \tag{4.63}$$

where i_L is inductor current, $\mathbf{v}_g^T = \begin{bmatrix} v_{g1} & v_{g2} & v_{g3} \end{bmatrix}$ is input voltage vector, v_C is output capacitance voltage, $\mathbf{s}^{3\to 2} = \begin{bmatrix} s_{11} & s_{21} & s_{31} \end{bmatrix}^T$ and L is inductance. The change of the voltages of the output capacitors can be obtained as,

$$\frac{d}{dt}\left(Cv_C\right) = i_C = i_L - \frac{v_C}{R}. \tag{4.64}$$

where C and R are capacitance and resistance. This model is similar as the model obtained for DC-DC buck converter. The difference is in inner product $\mathbf{v}_g^T \mathbf{s}^{3\to 2}$ instead of a simple scalar product as it stands in DC-DC converter. Input current is influenced by all components of the control and this raises the problem of MISO systems control.

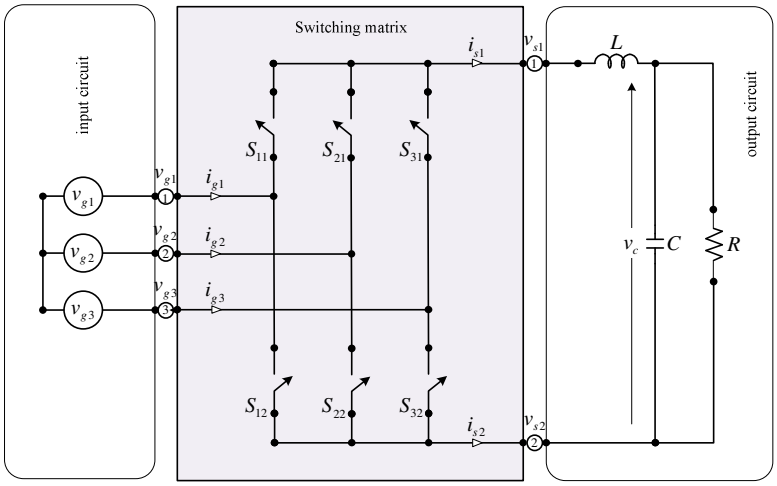

Figure 4-17 Structure of three phase buck rectifier

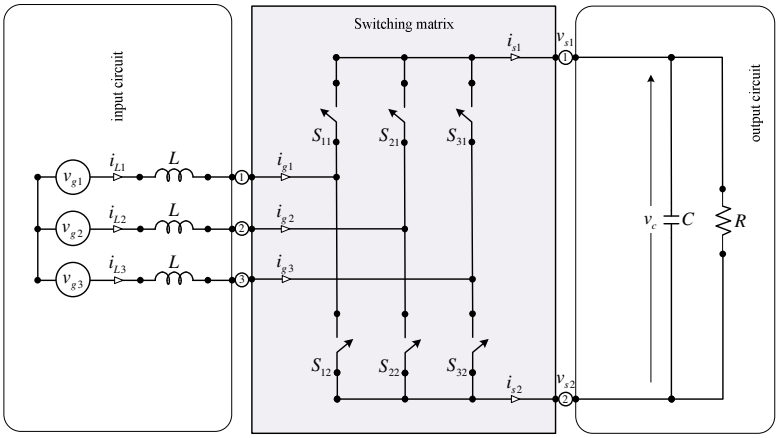

Figure 4-18 Structures of three phase boost rectifier

A structure of three phase boost rectifier is depicted in Figure 4-18. The time derivative of the inductor current can be calculated as,

$$\frac{d}{dt}\left(\mathbf{L}\mathbf{i}_{\mathbf{L}}\right)=\mathbf{v}_{\mathbf{g}}-\mathbf{A}_{\mathbf{Y}}\mathbf{s}^{3\to 2}v_C, \tag{4.65}$$

where $\mathbf{i}_L^T=\begin{bmatrix}i_{L1} & i_{L2} & i_{L3}\end{bmatrix}$ is inductor current, v_C is output capacitance voltage, $\mathbf{s}^{3\to 2}=\begin{bmatrix}s_{11} & s_{21} & s_{31}\end{bmatrix}^T$ and $\mathbf{L}=diag\left(L\right)$ is inductance.

The change of the voltages of the output capacitors can be obtained as:

$$\frac{d}{dt}\left(Cv_C\right)=\mathbf{i}_{\mathbf{L}}^T\mathbf{s}^{3\to 2}-\frac{v_C}{R} \tag{4.66}$$

where C and R are capacitance and resistance of the output circuitry. This model is similar as the model obtained for DC-DC boost converter.

Till now we had been looking at converters in which energy storage elements are placed at the output lines of the switching matrix (so-called buck converters) and converters in which storage elements are placed on input and output side of the switching matrix (so-called boost converters) as depicted in Figure 4-19 and Figure 4-20.

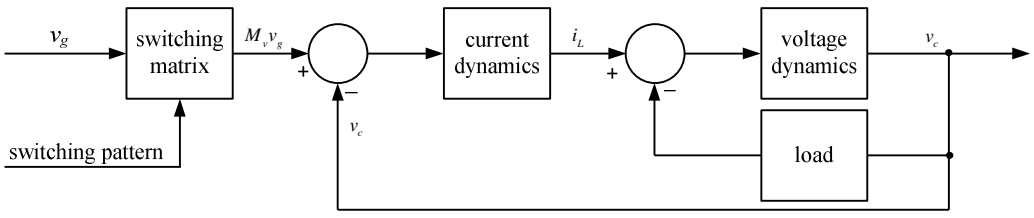

Figure 4-19 Dynamic structures of the buck converters

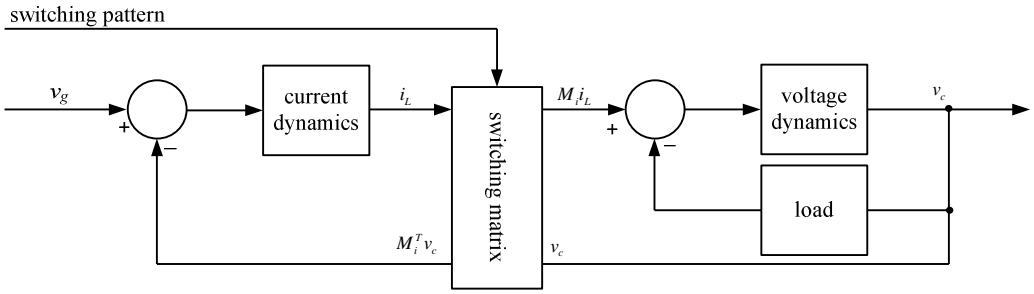

Figure 4-20 Dynamic structures of the boost converters

By inspection of the above given mathematical models of converters, the dynamics of the converters can be written in the form

$$\frac{d\mathbf{x}}{dt} = \mathbf{f}(\mathbf{x}) + \mathbf{B}(\mathbf{x})\mathbf{u}(\mathbf{s}) + \mathbf{H}\mathbf{v}_\mathbf{g} \tag{4.67}$$

where $\mathbf{x} \in \Re^n$ stands for the state vector of inductor currents and capacitor voltages, $\mathbf{f}(\mathbf{x}) \in \Re^n$ stands for a vector function of converter states, $\mathbf{B}(\mathbf{x}) \in \Re^{n\times m}$ stands for the control distribution matrix, $\mathbf{u}(\mathbf{s}) \in \Re^m$ stands for the control vector which depend on the switching matrix operation, $\mathbf{H} \in \Re^{n\times l}$ stands for the input voltage $\mathbf{v}_g \in \Re^l$ distribution matrix. The components of the control vector are periodic functions (with period T) defined on a duty cycle as:

$$u_i(\mathbf{s}) = \begin{cases} 1 & \text{for} \quad t \le \tau \le t + \mu_i(\mathbf{x})T \\ 0 & \text{for} \quad t + \mu_i(\mathbf{x})T \le \tau \le T \end{cases}, \quad i = 1,...,m, \quad \sum_{i=1}^{m} \mu_i(\mathbf{x}) = 1, \tag{4.68}$$

with average $\tilde{u}_i(\mathbf{s}) = \mu_i(\mathbf{x})$. The nonlinear system described by (4.67) and (4.68), is linear in discontinuous control. For such systems averaged motion could be derived by applying Filippov's method [123] for averaged motion of systems with discontinuous right hand side. Direct application of Filippov results leads to the averaged motion in the form

$$\frac{d\tilde{\mathbf{x}}}{dt} = \mathbf{f}(\tilde{\mathbf{x}}) + \mathbf{B}(\tilde{\mathbf{x}})\tilde{\mathbf{u}}(\mathbf{s}) + \mathbf{H}\mathbf{v}_\mathbf{g} \tag{4.69}$$

where $\tilde{\mathbf{u}}(\mathbf{s})$ stands for average control input with components $\tilde{u}_i(\mathbf{s}) = \mu_i(\tilde{\mathbf{x}})$. Model (4.69) allows calculation of the steady state operation of switching power converters from $\mathbf{0} = \mathbf{f}(\tilde{\mathbf{x}}) + \mathbf{B}(\tilde{\mathbf{x}})\tilde{\mathbf{u}}(\mathbf{s}) + \mathbf{H}\mathbf{v}_\mathbf{g}$.

4.6 Control of DC-DC Switching Converters

Control of the power converters in general could be designed as continuous (based on model (4.69) and then switching patter is derived by applying a PWM. In this approach well known methods of continuous system design are directly applicable.

Another possibility is to apply methods of the variable structure systems and directly design switching pattern while enforcing desired dynamics of the closed loop. The simplest design procedure consists of two steps;

- select control u such that inductor current tracks its reference;
- select the current reference so that voltage satisfies prescribed closed loop dynamics.

Application of this procedure for DC-DC buck converters leads to selection of current tracking error as $\sigma = i_L^{ref}(t) - i_L$ (where $i_L^{ref}(t)$ is a continuous function). From $d\sigma/dt = 0$ one can find an fictitious control input that, if applied at instant t_0 (determined as a time when error function reaches its zero value for the first time $\sigma(t_0) = 0$,) will assure that the $d\sigma/dt = 0, \forall t > t_0$. That control input, denoted as s_{11eq} could be determined in the following form:

$$\frac{d\sigma}{dt} = \frac{d\left(i_L^{ref} - i_L\right)}{dt} = \frac{di_L^{ref}}{dt} + \frac{v_C}{L} - \frac{v_g}{L} s_{11eq} = 0$$
$$s_{11eq} = \frac{1}{v_g}\left(L\frac{di_L^{ref}}{dt} + v_C\right) \tag{4.70}$$

From operational conditions of the buck converter the $0 \le s_{11eq} \le 1$ can be easily verified. Substituting this control to the original equations of the system one can obtain:

$$\frac{dv_C}{dt} = \frac{i_L^{ref}}{C} - \frac{v_C}{RC}, \quad i_L(t) = i_L^{ref}(t). \tag{4.71}$$

Dynamics of the system reduces to the first order linear system with reference current as input and capacitance voltage as output. Reference current could be selected using standard design procedures for linear systems. If for example, reference current is selected as $i_L^{ref} = v_C/R + C\frac{d}{dt}v_C^{ref} - Ck\left(v_C - v_C^{ref}\right); k > 0$ the voltage error dynamics will be described by $\frac{d}{dt}\left(v_C - v_C^{ref}\right) + k\left(v_C - v_C^{ref}\right) = 0$. The proposed design leads to first order dynamics in the closed loop but implementation of the s_{11eq} as a continuous control

input cannot be realized due to the fact that s_{11} is discontinuous. This leads to the application of Pulse Width Modulation (PWM) in the control system. The role of PWM is to generate discontinuous signal which has average value equal to s_{11eq}.

Approach based on the deliberate introduction of sliding mode into the control system leads to direct selection of the switching pattern - thus avoiding usage of the PWM generator. The procedure follows the same steps with small modification in the realization. The $d\sigma/dt$ can be expressed as

$$\frac{d\sigma}{dt}=\frac{v_g}{L}\left(s_{11eq}-s_{11}\right);\quad \frac{v_g}{L}>0 \tag{4.72}$$

In order to ensure stability of solution $\sigma(t)=0$, one may use Lyapunov stability concept which leads to selection of s_{11} such that $\sigma\dot{\sigma}<0$. By selecting

$$s_{11}=\begin{cases}1 & if\ \sigma>0\\ 0 & if\ \sigma<0\end{cases}. \tag{4.73}$$

The condition $\sigma\dot{\sigma}<0$ is satisfied, and after finite time, $\sigma=0$, $\dot{\sigma}=0$ and consequently $\tilde{s}_{11}=s_{11eq}$ and desired closed loop transient is enforced.

For boost DC-to-DC converter the same procedure leads to:

$$\begin{aligned}&\frac{d\sigma}{dt}=\frac{d\left(i_L^{ref}-i_L\right)}{dt}=\frac{di_L^{ref}}{dt}+\frac{v_C}{L}\left(1-s_{12eq}\right)-\frac{v_g}{L}=0,\\ &1-s_{12eq}=\frac{1}{v_C}\left(-L\frac{di_L^{ref}}{dt}+v_g\right);\quad 0\le\left(1-s_{12eq}\right)\le 1\end{aligned}. \tag{4.74}$$

and insertion of this equation to the system model leads to,

$$\frac{C}{2}\frac{dv_C^2}{dt}+\frac{L}{2}\frac{d\left(i_L^{ref}\right)^2}{dt}=v_g i_L^{ref}-\frac{v_C^2}{R},\quad i_L=i_L^{ref}. \tag{4.75}$$

The system structure is describing energy conservation law for the circuits. From the control point of view it could be regarded as a linear first order system with square of the output voltage as output and inductor current as control input

It is easy to conclude that condition $\sigma\dot{\sigma}<0$, and thus current tracking, is satisfied if $1-s_{12}$ is selected as

$$\left(1-s_{12}\right)=\begin{cases}1 & if\ \sigma>0\\ 0 & if\ \sigma<0\end{cases}. \tag{4.76}$$

4.7 AC-DC and DC-AC Single Phase Switching Converter Control

Control of DC-AC single phase buck converters described by (4.53) can be designed the same way as shown for DC-DC converters. The reference current may be selected from second equation in (4.53) to ensure first order dynamics in the voltage control loop as $i_L^{ref} = v_C/R + C\frac{d.}{dt}v_C^{ref} - Ck\left(v_C - v_C^{ref}\right); k>0$. The dynamics of the current loop can be expressed as.

$$\frac{d\sigma}{dt} = \frac{d\left(i_L^{ref} - i_L\right)}{dt} = \frac{v_g}{L}\left(\left(L\frac{di_L^{ref}}{dt} + v_C\right)\frac{1}{v_g} - \left(s_{11} - s_{12}\right)\right), \quad \frac{v_g}{L} > 0. \tag{4.77}$$

The operational conditions of the converter are met if $\left(s_{11} - s_{12}\right)_{eq}$ obtained from $\dot{\sigma} = 0$ satisfy

$$-1 \le \left(s_{11} - s_{12}\right)_{eq} = \left(L\frac{di_L^{ref}}{dt} + v_C\right)\frac{1}{v_g} \le 1. \tag{4.78}$$

The sliding mode conditions $\sigma\dot{\sigma} < 0$ will be satisfied if $\left(s_{11} - s_{12}\right)$ is selected as,

$$\left(s_{11} - s_{12}\right) = \begin{cases} 1 & if\ \sigma > 0 \\ -1 & if\ \sigma < 0 \end{cases}. \tag{4.79}$$

From the analysis of the converter operation we have concluded that $\left(s_{11} - s_{12}\right)$ can take three distinctive values $(-1, 0, 1)$. The above solution uses only two of them thus not all possibilities are used in the design of the switching pattern. This leads to excessive switching frequency.

From $\dot{\sigma} = \frac{v_g}{L}\left(\left(s_{11} - s_{12}\right)_{eq} - \left(s_{11} - s_{12}\right)\right)$ a switching pattern that will enforce condition $\sigma\dot{\sigma} < 0$ could be specified as function of $\left(s_{11} - s_{12}\right)$ and $\left(s_{11} - s_{12}\right)_{eq}$ as follows:

$$\left(s_{11} - s_{12}\right) = \begin{cases} 1 & \text{if} \quad \left(s_{11} - s_{12}\right)_{eq} > 0 \quad \text{and} \quad \sigma > 0 \\ 0 & \text{if} \quad \left(s_{11} - s_{12}\right)_{eq} > 0 \quad \text{and} \quad \sigma < 0 \end{cases} \tag{4.80}$$

$$\left(s_{11} - s_{12}\right) = \begin{cases} 0 & \text{if} \quad \left(s_{11} - s_{12}\right)_{eq} < 0 \quad \text{and} \quad \sigma > 0 \\ -1 & \text{if} \quad \left(s_{11} - s_{12}\right)_{eq} < 0 \quad \text{and} \quad \sigma < 0 \end{cases} \tag{4.81}$$

This solution shows a way of using information on equivalent control in selecting switching pattern.

4.8 AC-DC and DC-AC Three Phase Switching Converters Control

As previously shown three phase converters are interconnecting a DC and AC sources (sinks). That poses a problem of the operational and control tasks specification for the DC and AC side of converter and thus the power flow in the system.

On the DC side either voltage or current could be set as control variables, not both together, thus only one control task could be defined from the DC side requirements.

The AC side in addition to the magnitude of the voltage or current may also have specification for the phase shift between voltage and current (a reactive and active power ratio). That means in the AC side there are up to two requirements, a magnitude and displacement of the voltage (current). For given voltage and current vectors, $\mathbf{v},\mathbf{i}$ are displaced by an angle ϕ , apparent power is expressed as $S^2 = P^2 + Q^2 = \|\mathbf{v}\|\|\mathbf{i}\|$, active power is defined as $P = \mathbf{v}^T\mathbf{i} = \|\mathbf{v}\|\|\mathbf{i}\|\cos(\phi) = S\cos(\phi)$, and the reactive power is defined as $Q = \pm\sqrt{S^2 - P^2} = \|\mathbf{v}\|\|\mathbf{i}\|\sin(\phi) = S\sin(\phi)$. The active and reactive powers may be expressed in the following form $P = \mathbf{v}^T\mathbf{i} = \|\mathbf{v}\|\|\mathbf{i}\|\cos(\phi) = \|\mathbf{v}\| i_d$ and $Q = \|\mathbf{v}\|\|\mathbf{i}\|\sin(\phi) = \|\mathbf{v}\| i_q$, where $i_d = \|\mathbf{i}\|\cos(\phi)$ and $i_q = \|\mathbf{i}\|\sin(\phi)$ are components of the current vector collinear i_d and orthogonal i_q to the voltage vector respectively. This shows that in the case voltage is given or constrained we still have possibility to change angular shift and components i_d and i_q of the current (or P and Q) with maximum current (or apparent power) as constraint.

On the other hand, the operation of the electrical machines shows similar features. If one is looking from the mechanical variables control then, projection of the machine dynamics to the rotor flux frame of references, would lead to similar analysis. The component of the current collinear with determine flux magnitude and the component of the current orthogonal to flux would determine torque - thus the mechanical motion.

From the above analysis in a way to design control in three phase converters (both DC-AC and AC-DC) one needs to project the dynamics expressed in the terms of phase variables in a rotating frame of references which is related to selected vector (voltage, flux, etc.). This transformation is generally done in two steps. First mapping corresponding equations of motion into orthogonal stationary ($\alpha,\beta,0$) frame of

references by matrix $\mathbf{A}_{abc}^{\alpha\beta 0}$ and then mapping description presented in ($\alpha,\beta,0$) frame of references into synchronously rotating ($d,q,0$) frame of references defined by matrix $\mathbf{A}_{\alpha\beta 0}^{dq0}$. These two mappings could be represented by the following matrix,

$$\mathbf{F}_{\mathbf{abc}}^{\mathbf{dq0}}(\theta_r)=\mathbf{A}_{\boldsymbol{\alpha\beta 0}}^{\mathbf{dq0}}(\theta_r)\mathbf{A}_{\mathbf{abc}}^{\boldsymbol{\alpha\beta 0}}=\frac{\sqrt{2}}{\sqrt{3}}\begin{bmatrix}\cos\theta_r & \sin\theta_r & 0\\ -\sin\theta_r & \cos\theta_r & 0\\ 0 & 0 & 1\end{bmatrix}\begin{bmatrix}1 & -\frac{1}{2} & -\frac{1}{2}\\ 0 & \frac{\sqrt{3}}{2} & -\frac{\sqrt{3}}{2}\\ \frac{\sqrt{2}}{2} & \frac{\sqrt{2}}{2} & \frac{\sqrt{2}}{2}\end{bmatrix}. \tag{4.82}$$

For the balanced three-phase systems "*0*" component is always equal to zero so the transformation (4.82) from stationary three-phase (a,b,c) to orthogonal two-phase (α,β) and synchronous frame of reference (d,q) could be simplified and mapping between these frames of reference is defined by matrix $\mathbf{A}_{\mathbf{abc}}^{\boldsymbol{\alpha\beta}}$ for (a,b,c) to (α,β) and $\mathbf{A}_{\boldsymbol{\alpha\beta}}^{\mathbf{dq}}$ for (α,β) to (d,q).

$$\mathbf{F}(\theta_r)=\mathbf{A}_{\boldsymbol{\alpha\beta}}^{\mathbf{dq}}(\theta_r)\mathbf{A}_{\mathbf{abc}}^{\boldsymbol{\alpha\beta}}=\frac{\sqrt{2}}{\sqrt{3}}\begin{bmatrix}\cos\theta_r & \sin\theta_r\\ -\sin\theta_r & \cos\theta_r\end{bmatrix}\begin{bmatrix}1 & -\frac{1}{2} & -\frac{1}{2}\\ 0 & \frac{\sqrt{3}}{2} & -\frac{\sqrt{3}}{2}\end{bmatrix}. \tag{4.83}$$

Matrix $\mathbf{F}(\theta_r)$ is defining the nonlinear transformation between three phase (a,b,c) and synchronous orthogonal (d,q) frames of reference. For all three-phase converters the (d,q) frame of reference is determined in such a way that it is synchronous with the three-phase side of a converter (input side for rectifiers and output side for inverters). In the presented models notation is used as follows: $\mathbf{v}_\mathbf{c}^T=\begin{bmatrix}v_{cd} & v_{cq}\end{bmatrix}$ the capacitance voltage vector, $\mathbf{i}_\mathbf{L}^T=\begin{bmatrix}i_{Ld} & i_{Lq}\end{bmatrix}$ inductor current vector and $\mathbf{u}_\mathbf{dq}^T=\begin{bmatrix}u_d & u_q\end{bmatrix}$ is the control vector, v_g is amplitude of input voltage *R,L,C* – converter parameters.

4.8.1 Three phase buck inverter

Applying the coordinate transformation to the mathematical model developed for three phase buck inverter with θ_r determined as a output voltage vector position in ($\alpha,\beta,0$) frame of references one can easily calculate,

$$\begin{aligned}\frac{dv_{cd}}{dt}&=-\frac{v_{cd}}{RC}+\omega_r v_{cq}+\frac{i_{Ld}}{C};\\ \frac{dv_{cq}}{dt}&=-\frac{v_{cq}}{RC}-\omega_r v_{cd}+\frac{i_{Lq}}{C};\end{aligned} \tag{4.84}$$

$$\begin{aligned}\frac{di_{Ld}}{dt} &= -\frac{v_{cd}}{L} + \omega_r i_{Lq} + \frac{V_g}{L}u_d;\\ \frac{di_{Lq}}{dt} &= -\frac{v_{cq}}{L} - \omega_r i_{Ld} + \frac{V_g}{L}u_q;\end{aligned} \tag{4.85}$$

$$\begin{aligned}\frac{d\theta_r}{dt} &= \omega_r;\\ \mathbf{u_{dq}} &= \mathbf{F}(\theta_r)\mathbf{u},\end{aligned} \tag{4.86}$$

where $\frac{d\theta_r}{dt} = \omega_r$ is the angular velocity of the desired output, voltage, $\mathbf{v_c}^T = \begin{bmatrix} v_{cd} & v_{cq} \end{bmatrix}$ and $\mathbf{i_L}^T = \begin{bmatrix} i_{Ld} & i_{Lq} \end{bmatrix}$ are the output voltage and the inductor current vectors respectively. The control in stationary (a,b,c) frame of reference is determined from,

$$u_i(t) = \begin{cases} 1 & \text{with switch} \quad S_{1i} = \text{ON} \quad \text{and} \quad \text{S}_{2i} = \text{OFF} \\ 0 & \text{with switch} \quad S_{1i} = \text{OFF} \quad \text{and} \quad \text{S}_{2i} = \text{ON} \end{cases}; \quad i = 1,2,3. \tag{4.87}$$

For particular value of the θ_r transformation (4.82) results in the seven values of the control vector as depicted in Figure 4-23. It is easy to verify that above model in vector form can be described by (4.88) and that this expression fully resembles the DC-DC buck converter.

$$\begin{aligned}\frac{d\mathbf{v_c}}{dt} &= \mathbf{f_v}\left(v_c, i_L\right);\\ \frac{d\mathbf{i_L}}{dt} &= \mathbf{f_i}\left(v_c, i_L\right) + \mathbf{B_u}\left(v_g\right)\mathbf{u_{dq}};\\ \mathbf{u}_{dq} &= \mathbf{F}(\theta_r)\mathbf{u}.\end{aligned} \tag{4.88}$$

4.8.2 Three phase boost inverter

By applying mapping (4.82) on mathematical description of the model of boost inverter, one can obtain the following description,

$$\begin{aligned}\frac{dv_{cd}}{dt} &= -\frac{v_{cd}}{RC} + \omega_r v_{cq} + \frac{i_L}{C}u_d;\\ \frac{dv_{cq}}{dt} &= -\frac{v_{cq}}{RC} - \omega_r v_{cd} + \frac{i_L}{C}u_q;\end{aligned} \tag{4.89}$$

$$\frac{di_L}{dt} = -\frac{v_{cd}}{L}u_d - \frac{v_{cq}}{L}u_q + \frac{v_g}{L}; \tag{4.90}$$

$$\begin{aligned} &\frac{d\theta_r}{dt} = \omega_r; \\ &\mathbf{u_{dq}} = \mathbf{F}(\theta_r)\mathbf{u}, \end{aligned} \tag{4.91}$$

where $\frac{d\theta_r}{dt} = \omega_r$ is the angular velocity of the desired output voltage, $v_c^T = \begin{bmatrix} v_{cd} & v_{cq} \end{bmatrix}$ and i_L are the output voltage and the inductor current respectively. The components of switching functions vector us can have values from the set $S_u^3 = \{u_i : -1, 0, 1\}$. The above description can be rewritten in the form of (4.92). It can be noticed that such description has the same structure as model of DC-DC boost converter.

$$\begin{aligned} &\frac{d\mathbf{v_c}}{dt} = \mathbf{f_v}(v_c) + \mathbf{B_v}(i_L)\mathbf{u_{dq}}; \\ &\frac{di_L}{dt} = f_i(v_g) + \mathbf{B_u}(v_c)\mathbf{u_{dq}}; \\ &\mathbf{u}_{dq} = \mathbf{F}(\theta_r)\mathbf{u}. \end{aligned} \tag{4.92}$$

4.8.3 Three phase buck rectifier

In the (*d,q*) frame of references, with d-axis collinear with the voltage supply vector $\mathbf{v_g}$, the mathematical model of buck rectifier can be written as,

$$\frac{dv_c}{dt} = -\frac{v_c}{RC} + \frac{i_L}{C}; \tag{4.93}$$

$$\frac{di_L}{dt} = -\frac{v_c}{L} + \frac{v_g}{L}u_d; \tag{4.94}$$

$$\begin{aligned} &\mathbf{i}_{gdq} = i_L\mathbf{u}; \\ &\mathbf{i}_{gdq}^T = \begin{bmatrix} i_{gd} & i_{gq} \end{bmatrix}; \end{aligned} \tag{4.95}$$

$$\begin{aligned} &\frac{d\theta_r}{dt} = \omega_r; \\ &\mathbf{u_{dq}} = \mathbf{F}(\theta_r)\mathbf{u}, \end{aligned} \tag{4.96}$$

where $\frac{d\theta_r}{dt} = \omega_r$ is the angular velocity of the input voltage, v_c is the output voltage, i_L is the inductor current. Above given mathematical model can be written in the following, generalized form;

$$\begin{aligned}
&\frac{dv_c}{dt} = f_v\left(v_c, i_L\right);\\
&\frac{di_L}{dt} = f_i\left(v_c\right) + \mathbf{B_u}\left(v_g\right)\mathbf{u_{dq}};\\
&\mathbf{u_{dq}} = \mathbf{F}(\theta_r)\mathbf{u}.
\end{aligned} \tag{4.97}$$

4.8.4 Three phase boost rectifier

By selecting the orthogonal frame of references (*d,q*) with d-axis collinear with the voltage supply vector $\mathbf{v_g}$, the dynamics of a boost rectifier can be described by

$$\frac{dv_c}{dt} = -\frac{v_c}{RC} + \frac{i_{Ld}u_d + i_{Lq}u_q}{2C}; \tag{4.98}$$

$$\begin{aligned}
&\frac{di_{Ld}}{dt} = \omega_r i_{Lq} - \frac{v_c}{2L}u_d + \frac{v_g}{L};\\
&\frac{di_{Lq}}{dt} = -\omega_r i_{Ld} - \frac{v_c}{2L}u_q;
\end{aligned} \tag{4.99}$$

$$\begin{aligned}
&\frac{d\theta_r}{dt} = \omega_r;\\
&\mathbf{u_{dq}} = \mathbf{F}(\theta_r)\mathbf{u},
\end{aligned} \tag{4.100}$$

where $\frac{d\theta_r}{dt} = \omega_r$ is the angular velocity of the source voltage, v_c is the output voltage, $i_L^T = \begin{bmatrix} i_{Ld} & i_{Lq} \end{bmatrix}$ is the vector of the input current

$$\begin{aligned}
&\frac{dv_c}{dt} = f_v\left(v_c\right) + \mathbf{B_v}\left(i_L\right)\mathbf{u_{dq}};\\
&\frac{d\mathbf{i_L}}{dt} = \mathbf{f_i}\left(v_g, i_L\right) + \mathbf{B_u}\left(v_c\right)\mathbf{u_{dq}};\\
&\mathbf{u_{dq}} = \mathbf{F}(\theta_r)\mathbf{u}.
\end{aligned} \tag{4.101}$$

Combining the descriptions of various types of converters described above, unified model of the three phase converters can be derived in the following form;

$$\begin{aligned}
&\frac{d\mathbf{v_c}}{dt} = \mathbf{f_v}\left(v_c, i_L\right) + \mathbf{B_v}\left(i_L\right)\mathbf{u_{dq}};\\
&\frac{d\mathbf{i_L}}{dt} = \mathbf{f_i}\left(v_g, i_L, v_c\right) + \mathbf{B_u}\left(v_c, v_g\right)\mathbf{u_{dq}};\\
&\mathbf{u_{dq}} = \mathbf{F}(\theta_r)\mathbf{u}.
\end{aligned} \tag{4.102}$$

The structure of three phase converters is depicted in Figure 4-21. The same properties as for DC-DC converters are apparent.

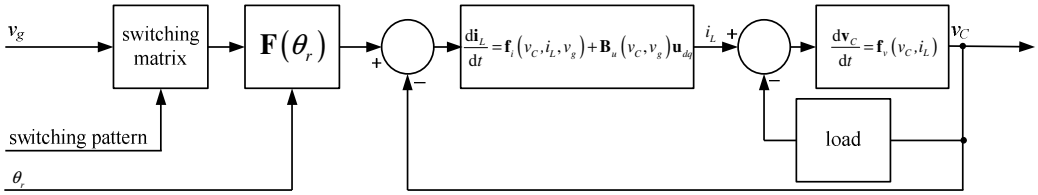

(a)

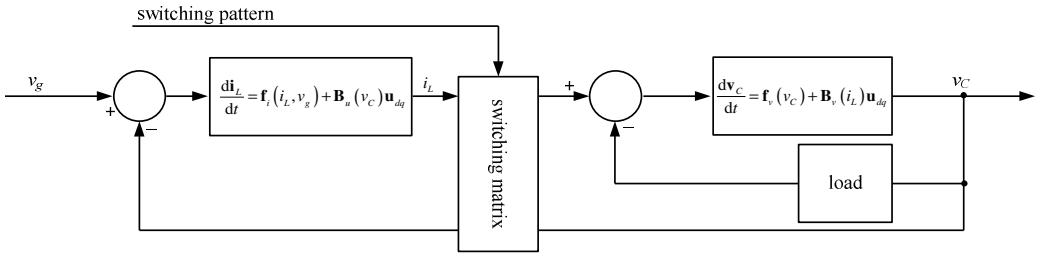

(b)

Figure 4-21 The dynamical structure of the (a) buck and (b) boost three phase converters

4.8.5 The Design of a Converter Control System

The structures of the buck and boost converters depict the fundamental properties of the converters acting as the voltage source. The output voltage can be controlled by the appropriate change of the inductor current. Here, the differences between buck and boost structures are apparent. For the buck converters, the current must be changed if the operation conditions changes.

Buck Converter:

$$\begin{aligned}\frac{d\mathbf{v_c}}{dt}&=\mathbf{f_v}\left(v_c,i_L\right)\\ \frac{d\mathbf{i_L}}{dt}&=\mathbf{f_i}\left(v_c,i_L\right)+\mathbf{B_u}\left(v_g\right)\mathbf{u_{dq}}\\ \mathbf{u_{dq}}&=\mathbf{F}(\theta_r)\mathbf{u}\end{aligned} \tag{4.103}$$

Boost Converter:

$$\begin{aligned}
\frac{d\mathbf{v_c}}{dt} &= \mathbf{f_v}\left(v_c\right) + \mathbf{B_v}\left(i_L\right)\mathbf{u_{dq}} \\
\frac{d\mathbf{i_L}}{dt} &= \mathbf{f_i}\left(i_L, v_g\right) + \mathbf{B_u}\left(v_c\right)\mathbf{u_{dq}} \\
\mathbf{u_{dq}} &= \mathbf{F}(\theta_r)\mathbf{u}
\end{aligned} \tag{4.104}$$

Control vector mapping:

$$\begin{aligned}
\mathbf{F}(\theta_r) &= \mathbf{A}_{\alpha\beta}^{dq}\mathbf{A}_{abc}^{\alpha\beta}, \\
\mathbf{A}_{\alpha\beta}^{dq} &= \begin{bmatrix} \cos\theta_r & \sin\theta_r \\ -\sin\theta_r & \cos\theta_r \end{bmatrix}, \\
\mathbf{A}_{abc}^{\alpha\beta} &= \frac{\sqrt{2}}{\sqrt{3}}\begin{bmatrix} 1 & -1/2 & -1/2 \\ 0 & \sqrt{3}/2 & -\sqrt{3}/2 \end{bmatrix}, \\
\mathbf{u}_{dq} &= \mathbf{F}\left(\theta_r\right)\mathbf{u}_{abc}.
\end{aligned} \tag{4.105}$$

Mathematical models of the switching converters could be presented in regular form [124] with discontinuous control influencing the change of the currents and currents being treated as “virtual control” in the voltage dynamics. The structure of the boost converters is more complicated with control entering all the equations of the system. Despite the differences in the dynamical structure, the control system design for buck and boost converters may follow the two-step procedure:

- Select control u such that inductor current tracks its reference;
- Select the current reference (virtual control) so that capacitance voltage satisfy prescribed dynamical behavior

This procedure is not so obvious for the boost structures since control enters both equations. In this framework the above procedure for boost converters requires calculation of the control to track current reference (so-called equivalent control), substitution of the equivalent control to the voltage equation and then taking current reference as ”virtual control” input. Three phase converters structurally differ from their DC counterparts in the number of energy storage elements and in the structure of the switching matrix. These converters interconnect a DC and AC sources. The dynamical structure of the systems remains the same as for DC converters except that the there-phase are MIMO systems. That allows design of the control in the same two-step procedure as applied for DC converters.

In Figure 4-22 the number of *dof* that could be specified by the operation of the interconnected switching matrix is shown. As it can be seen the number of independent

control parameters that could be specified for both DC-DC and AC-DC structures is two while the switching matrix has three independent controls.

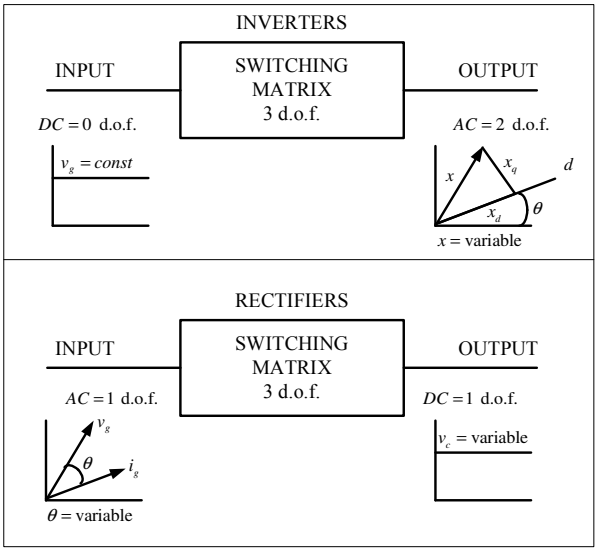

Figure 4-22 The assignment of the degrees of freedom in control for three-phase switching matrix.

4.8.6 Current Control in Three Phase Converters

The switching matrix in DC to AC and AC to DC three phase converters has six switches. The state of the switches may be represented by a sector with six elements each defining a state of the corresponding switch. For buck inverter and boost rectifier, due to electrical circuit constraints for buck inverter and boost rectifier, there are 8 permissible configurations of the switches;

$$S_1=[100011],\quad S_2=[110001],\quad S_3=[010101],\quad S_4=[011100],$$
$$S_5=[001110],\quad S_6=[101010],\quad S_7=[111000],\quad S_8=[000111].$$

For boost inverter and buck rectifier there are 9 permissible switch configurations,

$$S_1=[100001],\quad S_2=[010001],\quad S_3=[010100],\quad S_4=[001100],\quad S_5=[001010],$$
$$S_6=[100010],\quad S_7=[100100],\quad S_8=[010010],\quad S_9=[001001];$$

These combination of the switches in $(\alpha,\beta,0)$ frame of references, for star and delta interconnection, is shown Figure 4-23-(a) and (b).

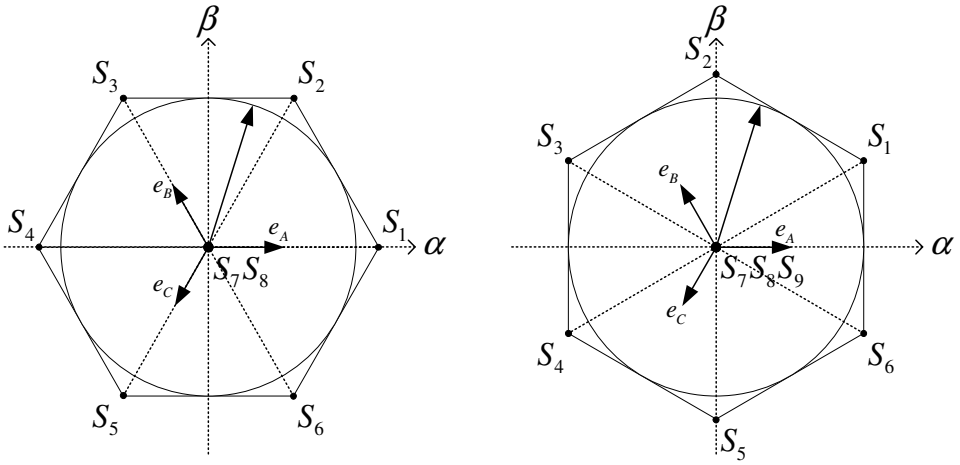

Figure 4-23 Possible values of S_i (i=1,2,...,9) with star connected load (a) and delta connected load (b)

Let us now look at design of the switching pattern for the three phase converters in more details. Current control is based on the sliding mode existence in the manifold $\boldsymbol{\sigma}^T = \left[\mathbf{i}_L^{ref}(t) - \mathbf{i}_L\right]^T = 0$ where vector $\boldsymbol{\sigma}^T = \left[\sigma_d \quad \sigma_q\right]^T$ with $\sigma_d = i_{Ld}^{ref}(t) - i_{Ld}$, $\sigma_q = i_{Lq}^{ref}(t) - i_{Lq}$ and $i_{Ld}^{ref}(t)$, $i_{Lq}^{ref}(t)$ are continuous functions to be determined later.

Design of the current controller is based on the system description (4.103)-(4.105) where matrix $\mathbf{B}_u$ is diagonal. The structure of function $\mathbf{f}_i$ and matrix $\mathbf{B}_u$ could be easily found from mathematical models of converters. The time derivative of $\boldsymbol{\sigma}^T = \left[\sigma_d \quad \sigma_q\right]^T$ is determined as

$$\begin{aligned} \frac{d\boldsymbol{\sigma}_{dq}}{dt} &= \frac{d\mathbf{i}_{Ldq}^{ref}}{dt} - \frac{d\mathbf{i}_{Ldq}}{dt} \\ &= \frac{d\mathbf{i}_{Ldq}^{ref}}{dt} - \mathbf{f}_i - \mathbf{B}_u\mathbf{u}, \\ \mathbf{u}^T &= \left[u_d \quad u_q\right]; \end{aligned} \tag{4.106}$$

Equivalent control can be calculated as $\mathbf{B}_u^{-1}\left[d\mathbf{i}_{Ldq}^{ref}/dt - \mathbf{f}_i\right] = \mathbf{u}_{eq}$ and (4.106) becomes

$$\frac{d\boldsymbol{\sigma}_{dq}}{dt} = \mathbf{B}_u\left[\mathbf{u}_{eq} - \mathbf{u}(S_i)\right], \quad i = (1,...,9). \tag{4.107}$$

Control vectors could take values from the discrete set $S=\{S_1,S_2,S_3,S_4,S_5,S_6,S_7,S_8,S_9\}$ as depicted in Figure 4-23-(b). All realizable values of the

equivalent control lie inside the hexagon spanned by the elements of the set S. The rate of change of error is proportional to the differences between the vector of equivalent control and the realizable control vectors. For a particular combination of errors all permissible vectors S_i that satisfy the sliding mode existence conditions could be determined from $\dot{\sigma}_d\sigma_d < 0$ and $\dot{\sigma}_q\sigma_q < 0$ or $sign\left(u_{eq} - u_{dq}\left(S_i\right)\right) = -sign\left(\sigma_{dq}\right)$ as shown in Figure 4-24 Permissible control vectors (a), selection of permissible control for given combination of the signs of control errors (b).

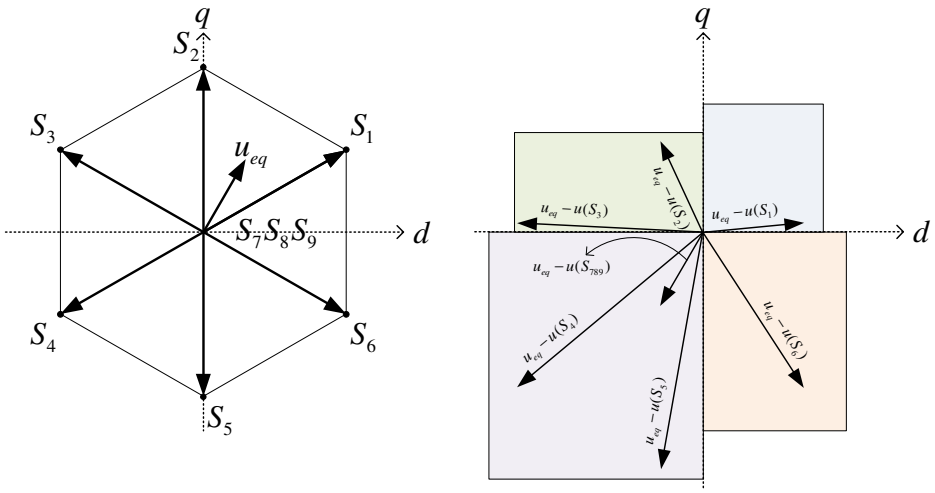

(a) (b)

Figure 4-24 Permissible control vectors (a), selection of permissible control for given combination of the signs of control errors (b)

For some combinations of errors there are more than one permissible vector that leads to an ambiguous selection of the control and consequently existence of more than one solution for the selection of switching pattern. The same could be concluded from $\operatorname{rank}\mathbf{F}(\theta_r) = \operatorname{rank}\left(\mathbf{A}_{\alpha\beta}^{\mathbf{dq}}\mathbf{A}_{\mathbf{abc}}^{\alpha\beta}\right) = 2$. Ambiguity in selection of the control vector based on selected u_d and u_q allows us to have a number of different PWM algorithms that satisfy sliding mode conditions in (d,q) frame of references. In early works related to electrical machine control, expression (4.106) is augmented with the an additional requirement $\vartheta(t) = 0$ to have the form

$$\begin{bmatrix} \dfrac{d\boldsymbol{\sigma}_{\mathbf{dq}}}{dt} \\ \dfrac{d\vartheta}{dt} \end{bmatrix} = \begin{bmatrix} \dfrac{d\mathbf{i}_{\mathbf{L}}^{ref}}{dt} - \mathbf{f}_{\mathbf{i}} \\ f_{\vartheta} \end{bmatrix} - \begin{bmatrix} \mathbf{B}_u\mathbf{F}(\theta_r) \\ \mathbf{b}_{\vartheta}^T \end{bmatrix}\mathbf{u}\left(S_i\right) \tag{4.108}$$

$$\frac{d\boldsymbol{\sigma}_N}{dt} = \mathbf{f}_N - \mathbf{B}_N \mathbf{u}(S_i); \qquad \mathbf{u}^T(S_i) = \begin{bmatrix} u_a & u_b & u_c \end{bmatrix}. \tag{4.109}$$

where vector $\mathbf{b}_\vartheta$ should be selected so that rank $\mathbf{B}_N = 3$. The simplest solution is $\dot{\vartheta}(t) = u_a + u_b + u_c$, then matrix $\mathbf{B}_N$ will have full rank. To determine the switching pattern, the simplest way is to use the nonlinear transformation $\boldsymbol{\sigma}_s = \mathbf{B}_N^{-1}\boldsymbol{\sigma}_N$, and then the sliding mode conditions are satisfied if the control is selected as,

$$sign\left(u_j(S_i)\right) = -sign(\sigma_{sj}), \quad -1 \le u_{eqj} \le 1. \tag{4.110}$$

This line of reasoning with some variations has been the most popular in designing the sliding mode based switching pattern [125].

Another solution implicitly applied in most of the so-called space vector PWM algorithms is based on the simple idea [126] using transformation $\mathbf{u}_{abc} = \left(\mathbf{A}_{\alpha\beta}^{dq}\mathbf{A}_{abc}^{\alpha\beta}\right)^T \mathbf{u}_{dq}$ to the (*a,b,c*) reference frame. Then components u_a, u_b, u_c of $\mathbf{u}$ are selected according to the following rule

$$S_i = \left\{ \begin{array}{c} sign\left(u_a(S_i)\right) = sign\left(u_d\cos\theta_r - u_q\sin\theta_r\right) \\ sign\left(u_b(S_i)\right) = sign\left(u_d\cos\left(\theta_r - 2\pi/3\right) - u_q\sin\left(\theta_r - 2\pi/3\right)\right) \\ sign\left(u_c(S_i)\right) = sign\left(u_d\cos\left(\theta_r - 4\pi/3\right) - u_q\sin\left(\theta_r - 4\pi/3\right)\right) \end{array} \right\}, \quad i = 1,...,9; \tag{4.111}$$

In the application of above algorithms switching is realized using hysteresis which directly determines the current ripple to be equal to the half of the hysteresis width. For the given current ripple (constant hysteresis width) the time between two switching for each component is directly proportional to $\left[u_{jeq} - u_j(S_i)\right], (j = d,q), (i = 1,..,9)$.

A new class of the switching algorithms based on the simple requirement that control should be selected to give the minimum rate of change of control error could be designed for which the same error will be achieved with less switching effort. The algorithm can be formulated in the following form,

$$S_i = \left\{ \begin{array}{c} \min\left\|\mathbf{u}_{eq}(t) - \mathbf{u}\ (S_i)\right\| \\ \& \\ sign\left\{\left[u_{eqd} - u_d(S_i)\right]\cdot\sigma_d(t)\right\} = -1 \\ \& \\ sign\left\{\left[u_{eqq} - u_q(S_i)\right]\cdot\sigma_q(t)\right\} = -1 \end{array} \right\}, \quad i = (1,2,\ .....\ ,8,9). \tag{4.112}$$

All of the above algorithms naturally include so-called over-modulation functionality. Due to the specifics of three-phase balanced systems the number of independent controls for the switching matrix is higher than the dimension of the controlled current vector This is the basic reason that three-phase PWM, under many different names, is still attractive as a research topic.

In the sliding mode dynamics of current the control loop is reduced to $\boldsymbol{\sigma}^T = \left[\mathbf{i}_L^{ref}(t) - \mathbf{i}_L\right]^T = \mathbf{0}$ or $i_{Ld}^{ref}(t) = i_{Ld}$ and $i_q^{ref}(t) = i_q$ with equivalent control being determined as $\mathbf{B}_u^{-1}\left[d\mathbf{i}_L^{ref}/dt - \mathbf{f}_i\right] = \mathbf{u}_{eq}$. In order to complete the design of converters and electrical machines the reference currents must be determined.

For buck converters and electrical machines with reference currents interpreted as virtual control inputs the description could be easily transformed to the following form;

$$\begin{aligned} \frac{d\mathbf{v}_c}{dt} &= \mathbf{f}_v(v_c, i_L); \\ \frac{d\mathbf{i}_\mathbf{L}}{dt} &= \mathbf{f}_\mathbf{o}(v_c, i_L) + \mathbf{B}_\mathbf{i}(i_L, v_g)\mathbf{i}^{ref} \end{aligned} \tag{4.113}$$

where vector $\mathbf{v}_c^{\,T} = \left[v_{cd} \quad v_{cq}\right]$ represent the output voltage vector. For the buck inverter both components of the reference current could be determined from the specification of the voltage loop, but for buck rectifiers only the *d*-component of the source current can be determined from the voltage loop specification. The *q*-component of the source current does not influence the output voltage and thus represent current circulating between supply sources and creating reactive power flow from sources. The same is directly applicable for a DC machine supplied by the three-phase rectifier. The outer loop control requirements for converters could be defined as in equations (4.114)-(4.116);

Buck three-phase inverter:
$$\begin{aligned} \sigma_d &= v_{cd}^{ref} - v_{cd}; \\ \sigma_q &= v_{cq}^{ref} - v_{cq}; \end{aligned} \tag{4.114}$$

Buck three-phase rectifier:
$$\begin{aligned} \sigma_d &= v_c^{ref} - v_c; \\ \sigma_q &= i_{Lqav}^{ref} - i_{Lqav}; \end{aligned} \tag{4.115}$$

Boost three-phase rectifier:
$$\begin{aligned} \sigma_d &= \mu\left(v_{c,ref}^2 - v_c^2\right); \\ \sigma_q &= i_{Lqav}^{ref} - i_{Lqav}; \end{aligned} \tag{4.116}$$

The reference current can be selected following the discrete time sliding mode control design. For all of the systems under consideration it can be written in a unified

form as $\mathbf{i}_k^{ref} = \mathbf{i}_{k-1}^{ref} - \left(\mathbf{G}\mathbf{B}_i T\right)^{-1}\left(\left(\mathbf{E}+T\mathbf{D}\right)\boldsymbol{\sigma}_k - \boldsymbol{\sigma}_{k-1}\right)$; $\mathbf{G} = \{\partial\boldsymbol{\sigma}/\partial x\}$, where T is the sampling interval. The realization of this control algorithm requires information on the sliding functions and the plant gain matrix. The selected structure is only one of the several possible solutions, applying other design procedures many of which are developed in the framework of motion control systems may derive other structures.

5 INTERCONNECTION OF THE HYBRID ENERGY SOURCE AND A MICROGRID

In previous chapters HES design requirements were identified, and main focus was put on the analysis and control of power electronic interfaces necessary for HES operation. Important aspects of interconnection of the HES and a microgrid are discussed in this chapter and technical discussion regarding HES is concluded. Throughout this chapter, the final objective of this thesis, *identification of requirements for interconnection of the hybrid energy source and a microgrid*, is achieved. Firstly, power control and power management for HES is explained and main guidelines to the design are discussed. Power control and management discussion reveals that renewable energy sources receive their power set values from MPPT algorithm and that the power control of output side converter is very important in implementation of overall control system. Following the section on power control and management, sections covering output side converter control and MPPT algorithm are given.

5.1 HES Control System – Power Management

A hybrid energy source can be viewed as an interconnection of different energy sources as shown in the Figure 5-1. The Σ in Figure 5-1 represents the power summation power point of the HES. For the hybrid source discussed in this thesis power summation point is DC bus in the system. For HES many different combination of the energy sources and energy storage systems can be used. From a structural point of view, they have no difference. In Figure 5-1 power is delivered to (or absorbed from) the load (grid, microgrid, local loads). Components of HES can be categorized based on their way of handling power. They fall into three categories, namely, components that generate power (G), components that store energy (S) and components that convert power (C).

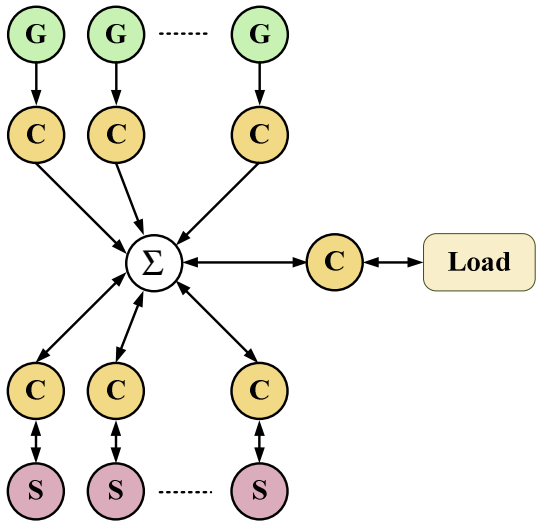

Figure 5-1 Functional structure of HES attached to the load that can consume or generate power

In this thesis we have been discussing the HES containing PV and wind renewable energy sources, fuel cell that uses fuel (hydrogen) to generate energy and battery storage unit. Other than these, incorporation of device for hydrogen production (electrolyzer) is also possible.

Other than their relatively low efficiency and high cost, the controllability of the electrical production is the main drawback of renewable energy generators, like wind turbines and photovoltaic moduless, because of the uncontrollable meteorological conditions. In consequence, their connection into the utility network can lead to grid instability or even failure if they are not properly controlled. Moreover, the standards for interconnecting these systems to the utility become more and more critical and require the HES systems to provide certain services, like frequency and voltage regulations of the local grid.

The structure of the HES considered in this thesis is shown in Figure 5-2. Wind energy conversion systems and PV work like passive generators. Because of the intermittent and fluctuant power flow they cannot offer any ancillary services to the electrical system in a microgrid application, where stable active- and reactive-power requirements should be attributed to the generators. As solutions HES is complemented with fuel cell and a battery as a element that can play both source and storage role and the electrolyzer as a energy converter and storage system. This way HES can use available renewable energy sources on their optimal points of exploitation, battery as a fast energy source to cover fast changes in the power requirements and electrolyzer with

storage as a high capacity storage system. *Energy storage* is used to compensate or absorb the difference between the generated wind power and the required microgrid power, and *power management strategies* are implemented to control the power exchange among different sources and to provide some services to the grid.

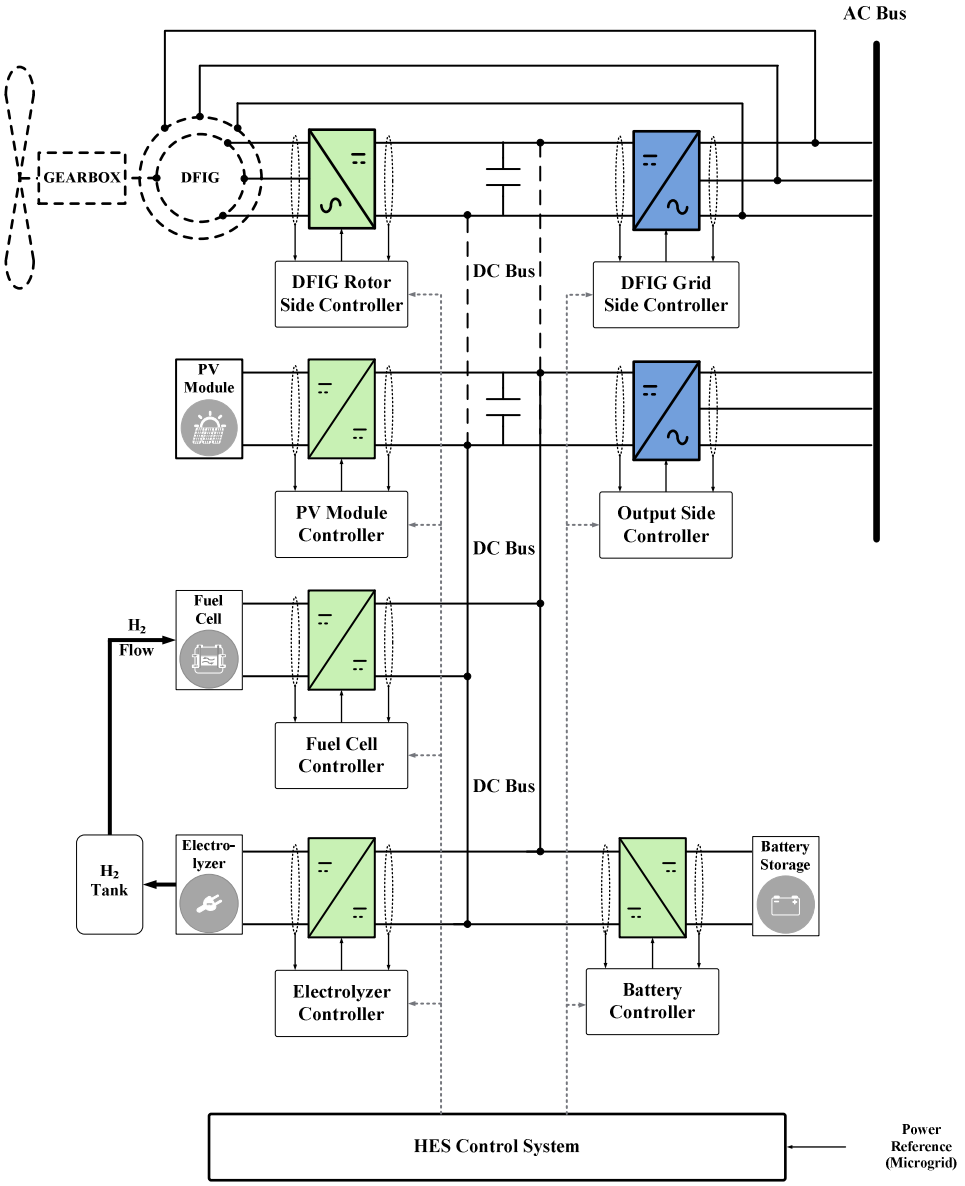

Figure 5-2 Structure of a HES consisting of PV, WT, FC and storage system

In this section power management strategies of the studied HES will be discussed. Power management strategies are implemented in order to control the power at the summation point-DC bus (see Figure 5-1) and to satisfy microgrid power requirements. These requirements are formulated as real- and reactive-power references, which are

calculated by a centralized secondary control center in order to coordinate power dispatch of several plants in a control area. This area corresponds to a microgrid and is limited due to the high level of reliability and speed required for communications and data transfer.

5.1.1 Structure of HES Control System

Power converters introduce control inputs for power conversion system and its interconnections to the grid. The structure of control system is depicted in Figure 5-3.

The *Switching Converter Unit (SCU)* is designed for each power converter. The structures and the algorithms for different converters and different operational modes are discussed in Chapter 4. The SCU can receive different commands and deliver desired current flow in the branch they are connected.

The *Automatic Control Unit (ACU)* is designed for each energy source and its power conversion system in such a way that source is working in desired (in many cases the maximum power) mode. The operational mode of the energy source would then be treated as a reference for the switching converter control.

The *Power Control Unit (PCU)* is aiming to perform the power balancing of the entire HES in order to satisfy the microgrid requirements. These requirements are real- and reactive-power flow, which are obtained from the secondary control center. In a PCU, some power-balancing algorithms are implemented to coordinate the power flows of different energy sources. The different power-balancing algorithms correspond to a number of possible operating modes of the HES or some optimization algorithms.

In order to focus on the power-balancing strategies of the HES, the control schemes of the power conversion systems through different power converters is already discussed in Chapter 4 and it will not be repeated here.

The energy sources are interconnected to the DC bus and then via DC-AC converter to the AC bus (microgrid, grid, local loads). The wind system, PV system and fuel cell systems are controlled to follow maximum available power conversion via MPPT algorithms. Both wind and PV are stochastic energy sources, but the fuel cell is a source that may change its power by changing the fuel input, thus it can play a role of the controllable source, but it dynamics are not very fast. The battery is energy source/sink that can be charged and discharged very fast, thus it can play a role of either

source or a sink with instantaneous power change capability. The DC bus capacitor is defining DC bus voltage and is balanced by the current from energy sources and current to the microgrid. This allows us to look at the HES control system as shown in Figure 5-3.

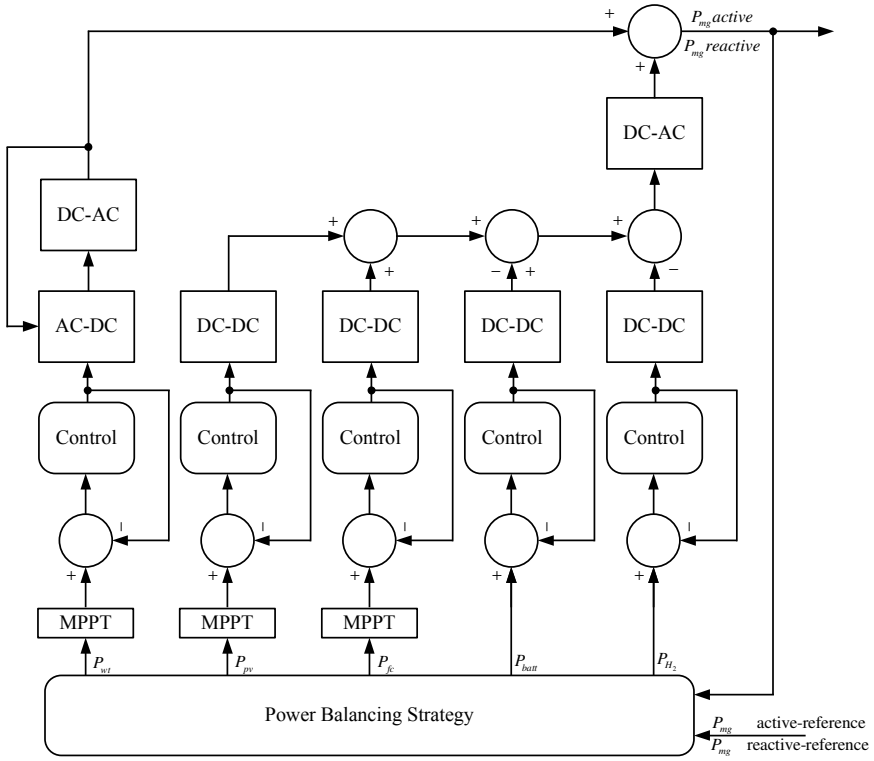

Figure 5-3 Control system structure of a HES consisting of PV, wind, FC and storage system

5.1.2 Power Control Level

The power exchanges are controlled by deriving related power references. The sources' powers, the exchanged power with the DC bus capacitor and the required grid power are taken into account here. For the energy storage systems, the powers are calculated by multiplying the measured currents and the measured voltages. For the wind and PV, an MPPT strategy is used to extract the maximum power of the available energy. The output of the DC bus voltage control loop is the current reference of the DC bus capacitor, and its product with the measured DC bus voltage gives the power reference for the DC bus voltage regulation. The powers, which are exchanged with the microgrid, can be calculated from measured data. In order to focus on the power

exchanges with the different sources around the DC bus, the instantaneously exchanged power with the choke, the losses in the filters and in the power converters are neglected.

5.1.3 Power Sharing Level

The power sharing level is used to implement the power balancing strategies in order to coordinate the various sources in the HES (Figure 5-3). It plays a very important role in the control system, because the power exchanges lead directly to the stability of the HES and impact the DC bus voltage. Change of the energy stored in the DC bus capacitor E_{DC} (or resulted power into the DC bus capacitor P_{DC} can be expressed as function of the P_{wt} power from the wind turbine, P_{pv} power generated by PV module, P_{fc} power generated from the fuel cell, P_{batt} power exchanged with battery (note that it can act as storage or a source), P_{H_2} power consumed by the electrolysis and stored as H_2 and P_{dc-ac} power delivered to the microgrid from the DC bus (via the output side converter). Power reference to the output side converter can be calculated as,

$$P_{dc-ac}^{ref} = P_{mg}^{ref} - P_{wt} \tag{5.1}$$

Power control of DC-AC output side converter has been discussed as the outer loop control of cascade control structure in Chapter 4 and will be further discussed in this Chapter. We can assume that power of DC-AC converter is regulated such that $P_{dc-ac} = P_{dc-ac}^{ref}$. Under these conditions the power exchange on the DC bus can be expressed as,

$$\frac{dE_{DC}}{dt} = Cu_{DC}\frac{du_{DC}}{dt} = P_{DC} = P_{pv} + P_{fc} \pm P_{batt} - P_{H_2} - P_{dc-ac} \tag{5.2}$$

From this expression one can derive many strategies to keep balanced power flow and the desired DC bus voltage. The operational requirements and constraints are opening a set of different strategies. Among the sources that are acting as generators the wind and PV sources have stochastic nature and their time profile cannot be controlled, but if good statistical data are available, their average behavior could be estimated. These sources, from the control point of view, may be regarded as "disturbances" and reasonable strategy of their usage is to tap maximum power they can deliver at any

instant of time. That strategy then operates these two sources by their individual MPPT. The fuel cell and electrolyzer are two main energy exchangers due to simple fact that large quantity of hydrogen can be stored. The fuel cell conversion processes dictate slow dynamics of the energy conversion thus the battery plays a role of fast power source that can act almost instantaneously in changing the current flow.

According to a chosen power flow many power balancing strategies can be implemented. Here we will make short analysis of the two of them:

1) The ***microgrid following strategy*** in which the power exchanged with microgrid is variable and regarded as a control input along with power exchanged with storage elements.

2) The ***source following strategy*** in which the microgrid active power is set as reference determined by the system controller and the DC bus voltage is regulated by the available sources and storage units

5.1.3.1 Microgrid Following Strategy

In this scenario a HES operational point is determined and then available power is delivered to the microgrid. The operational point of the HES means setting of $P_{pv}, P_{fc}, P_{batt}, P_{wt}, P_{H_2}$ and then changing P_{dc-ac}^{ref} in order to maintain the desired DC bus voltage u_{DC}. The operational point of the HES may be set according to many scenarios one of them being the maximum power tracking of the renewable sources (PV and wind) and desired operational point of the fuel cell (can also be MPPT) and energy storage. These scenarios may be derived by different cost functions and their derivation is outside of the scope of this work. The main methods in setting operational point of the HES can be divided in three groups [130]:

- *Rule-based method*

Rule based strategy is easy to implement. It has been widely used in industry due to the low computational load required. However, the control strategy is not mathematically formulated, the optimality of power management strategy is difficult to evaluate.

- *Instantaneous optimization method*

The main idea in energy management strategy based on the instantaneous optimization method is to define a cost function to be minimized at each instant. This

cost function depends only on the system variables at the current time. Due to the self-sustaining requirements (in some period of time) of electrical energy storage, the variation of stored energy status has to be taken into account as part of cost function. Different approaches have been proposed to deal with this issue.

- *Optimal control methods*

The third type of strategy level control is based on different techniques in optimization theory, such as calculus of variation, Pontryagin's Minimum Principle, and Bellman's Dynamic Programming. These optimization techniques are mathematically well formulated. They choose the optimal control policy over the whole operating period. However, the difficulties for applying this type of control to a real time HES come from the unknown future power requirement and limitations. When the problem is stochastic optimal control, a stochastic model is needed.

These mathematical approaches are valuable tools to obtain good insight into the problem and its optimal solution. They can be used as a reference to evaluate other approaches. In some cases the optimal solution can help defining simple and implementable rule-based strategy.

5.1.3.2 Source Following Strategy

In this strategy the microgrid power is set as reference determined by the system controller, within operational capability of the HES and the microgrid requirements. Then the power exchange and the DC bus voltage are regulated by the available sources and storage units. The operational point of the HES is then determined from the requirement of the balanced power flow needed to maintain DC bus voltage u_{DC} and with P_{dc-ac} as disturbance in the system. The operational point of the HES may be realized with different distribution of the needed power flow between sources and the storage units. The maximum power tracking of the renewable sources may not be always possible but it should be maintained as much as possible. The HES operational point tracking would need careful selection of the methods in setting operational point.

The realization of the power flow rests on the proper control of the power converters. In both scenarios these converters should be controlled as current sources with either DC bus or microgrid being assumed to be voltage sources.

5.2 MPPT Algorithm

In Chapter 3 it has been shown that PV module, wind turbine and fuel cell sources exhibit very similar behavior related to the extractable power. Furthermore, for the given electrical and environmental conditions, analysis of sources has shown that there exists a single maximum power point. Main goal of the MPPT algorithm is to control the power of the system and keeps it in the maximum point despite the environmental disturbances.

5.2.1 MPP in renewable energy sources

For a PV module, the output power behavior with respect to module current is depicted in Figure 5-4-(a). At the given irradiance and temperature conditions there exists a maximum power point. Since the value of power at the maximum changes with changing environmental conditions (for irradiance change effect see Figure 5-4-(b)), a control of PV module current should be done such that maximum power is always extracted from the module.

Fuel cell electrical characteristics are similar to the ones exhibited by a PV module. Behavior of output power with respect to the fuel cell current is depicted in Figure 5-5-(a). At the given environmental conditions (oxygen and hydrogen pressures and fuel cell stack temperature) there exists a maximum power point. Change of MPP with respect to the temperature change of fuel cell is depicted in Figure 5-5-(b). Change of MPP imposes a requirement on control system to achieve MPP tracking by controlling the fuel cell output current.

Finally, for a wind turbine similar behavior is observed for a generator output power. The change of power with respect to the generator speed, for constant wind speed, is shown in Figure 5-6-(a). Existence of MPP is clearly seen on this graph. However, changing wind speed causes changing value of MPP (Figure 5-6-(b)). For a MPP tracking to be achieved, generator speed needs to be controlled.

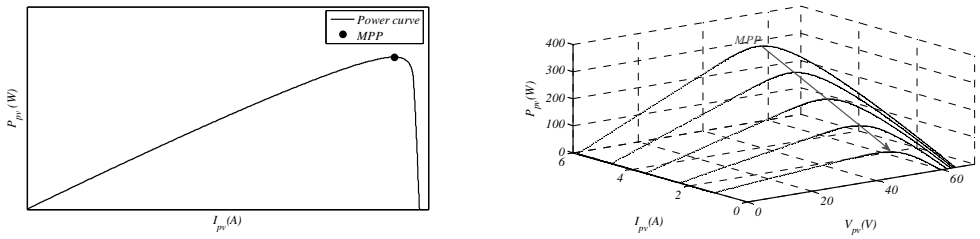

(a) (b)

Figure 5-4 PV power vs. PV current (a); MPP for changing irradiance (b)

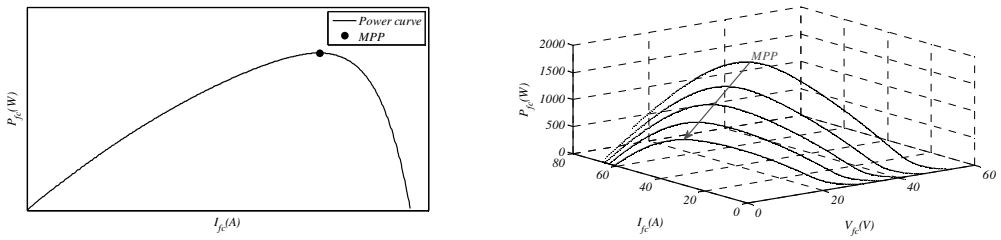

(a) (b)

Figure 5-5 FC power vs. FC current (a); MPP for changing stack temp. (b)

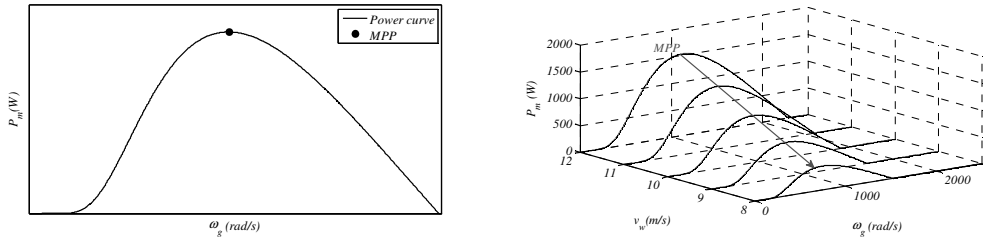

(a) (b)

Figure 5-6 WT power vs. generator speed (a); MPP for changing wind speed (b)

All of the shown power curves exhibit similar behavior with respect to individual source related variables. Thus, same MPPT algorithm can be applied in all three cases. Literature review about the MPPT algorithms has shown that there exist many different approaches to this problem. In general solutions can be grouped into online and offline algorithms. Offline algorithms are mostly based on the development of empirical relation between the controllable variable and output power. Offline algorithms show severe disadvantages mostly due to the complexity of development of empirical relations. Online algorithms, on the other hand, are much better solutions in terms of overall performance. In online algorithm usually the instantaneous values of the output power are used to generate control signals. Most popular online MPPT algorithms are perturbation and observation method (P&O), extremum seeking control method (ESC) and the incremental conductance method (IncCond) [127]. All of these algorithms have very poor precision and depend on the calculation of derivative of power.

5.2.2 Sliding mode based optimization algorithm

Maximum power point tracking for renewable energy sources is a maximization problem. Such problem can be treated using sliding mode optimization algorithm originally developed for anti-lock breaking system in cars [128]. This algorithm doesn't depend on the calculation of derivative of power and inherits the robustness due to the implementation of sliding mode control. Optimization algorithm is developed for the systems in following dynamical form,

$$\dot{x} = u, \tag{5.3}$$

with output $y = f(x)$ is assumed differentiable function and its derivative different than zero everywhere except at the point where $y = \max(y)$. For system in (5.3) u should be found such that it results in x that drives the function y to its maximum value. To achieve this, optimization algorithm is developed by constructing an error between some monotonically increasing function g and output of the system as,

$$\sigma = g - y. \tag{5.4}$$

Based on this error, sliding surfaces are chosen to be,

$$\begin{aligned} s_1 &= \sigma; \\ s_2 &= \sigma + \delta, \end{aligned} \tag{5.5}$$

and control input u is defined as,

$$u = u_0 sign(s_1 s_2). \tag{5.6}$$

The reference function g is defined by (5.7) as,

$$\dot{g} = \rho + v(s_1, s_2). \tag{5.7}$$

In the above equations δ, u_0, ρ are positive constants. And $v(s_1, s_2)$ is the three-element relay defined as,

$$v = \begin{cases} -M & \text{for} \quad s_1 - \Delta > 0, s_2 > 0 \\ 0 & \text{for} \quad (s_1 + \Delta)(s_2 - \Delta) < 0, \\ M & \text{for} \quad s_1 < 0, s_2 + \Delta < 0 \end{cases} \tag{5.8}$$

With $M > 0, M \gg \rho$ conditions. In the above equation 2Δ is the width of relay hysteresis. For easier visualization, control input u and relay function v are depicted in Figure 5-7 and Figure 5-8 respectively.

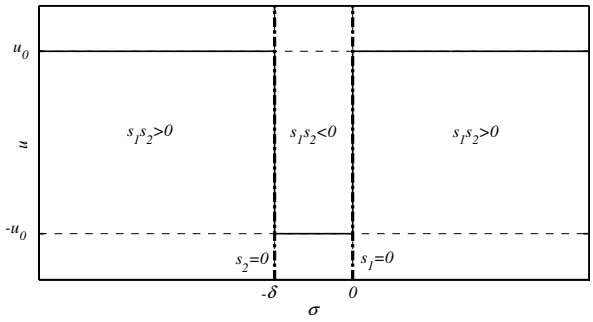

Figure 5-7 Control input *u*

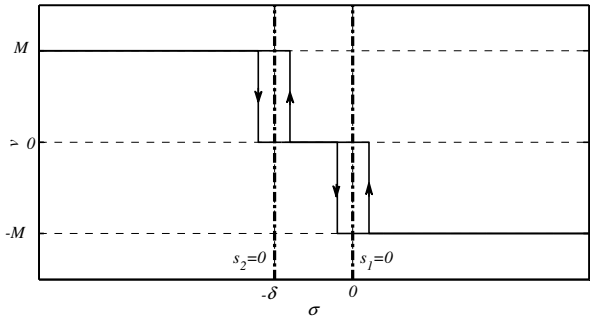

Figure 5-8 Three element relay *v*

In these figures three regions of operation are identified. When $\sigma<-\delta$ or $\sigma>0$ control effort is positive and controller forces the error to decrease by driving system output closer to the reference value. Once the value of error is in the region where $-\delta<\sigma<0$ holds, control effort is negative and from this point on, controller exhibits the typical behavior of sliding mode and control input changes its sign according at the boundaries defined by either sliding surface. Reference modification is done using three element relay depicted in Figure 5-8. This element modifies reference such that it is always monotonically increasing function so that output will always move toward its maximum value. At the region around maximum point, algorithm exhibits oscillatory behavior. Optimization algorithm based on sliding mode is depicted in the Figure 5-9.

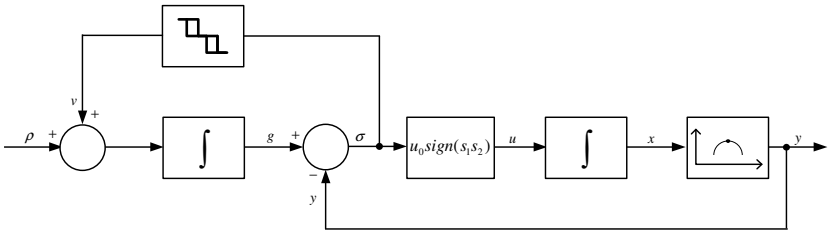

Figure 5-9 Optimization algorithm block diagram

5.2.3 Application of sliding mode based optimization algorithm for MPPT

Algorithm presented in the previous subsection is simple and doesn't require knowledge of derivative of output function $y = f(x)$. However, algorithm exhibits certain undesired switching behavior (chattering) due to the implementation of sliding mode. This problem is addressed by introduction of smooth functions in the place of sign function in controller and relay function in three element relay. Smooth functions can be specified as sigmoid functions in the form,

$$\begin{aligned} h_1(s_1) &= \frac{2}{1+e^{-ks_1}} - 1; \\ h_2(s_2) &= \frac{2}{1+e^{-ks_2}} - 1. \end{aligned} \tag{5.9}$$

In the above expressions, k is the design parameter specifying the rate of change of sigmoid functions. When $k \to \infty$, expressions in (5.9) become sign functions. Three element relay v and control input u are then redefined using functions from (5.9) as;

$$u = u_0 h_1 h_2. \tag{5.10}$$

$$v = \frac{M}{2}\left(-h_1 - h_2\right). \tag{5.11}$$

Graphical comparison between (5.6) and (5.8) and newly defined function from (5.10) and (5.11) is given in the Figure 5-10. With implementation of newly defined u and v strictly speaking sliding mode is lost, however for maximization problem, the rest of the algorithm can be applied without any change.

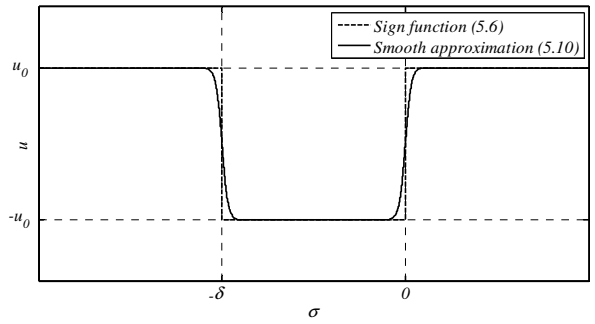

(a)

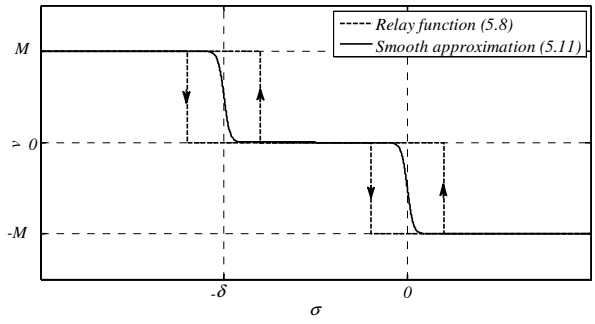

(b)

Figure 5-10 Control input u (a) and three element relay v (b) redefined using sigmoid functions

Maximum power point tracking for renewable energy sources under consideration in this thesis can be achieved using sliding mode based optimization algorithm. This conclusion can be drawn from the analysis of systems and their output behavior. For PV system, this optimization algorithm can be applied in the following way,

$$\begin{aligned}
&\frac{di_{pv}^{ref}}{dt} = u_{pv}; \quad P_{pv} = f\left(i_{pv}\right);\\
&u_{pv} = u_0 h_1 h_2; \quad v_{pv} = \frac{M}{2}\left(-h_1 - h_2\right);\\
&\sigma_{pv} = g_{pv} - P_{pv}; \quad \dot{g}_{pv} = \rho + v_{pv};\\
&s_1 = \sigma_{pv}; \quad s_2 = \sigma_{pv} + \delta;\\
&h_1(s_1) = \frac{2}{1+e^{-ks_1}} - 1; \quad h_2(s_2) = \frac{2}{1+e^{-ks_2}} - 1,
\end{aligned} \tag{5.12}$$

with the parameters $M, u_0, \rho, k, \delta > 0$. MPPT algorithm generates reference output current of PV module (i_{pv}^{ref}). Output current of PV module is in fact input current of a DC-DC converter, and control system must control this current.

In Chapter 4 current control of DC-DC converters was discussed. A control approach was developed to control current flowing through inductor in converter. For boost DC-DC converters, current flowing through inductor is in the same time the input current of the converter, for buck DC-DC converter this is not the case, however there exists a straightforward relation between inductor current and converter input current and can be easily calculated.

Control block diagram of PV module controller is shown in Figure 5-11. MPPT block generates PV output reference current, i_{pv}^{ref}, according to the algorithm described by (5.12). Block H represents a relation between reference PV module output current

and converter inductor current reference i_L^{ref} . Inductor current controller is denoted by C_i and developed in Chapter 4. Inductor current dynamics are described by general form $\frac{di_L}{dt} = f_i + b_i u$. Inductor current controller enforces that $i_L^{ref} = i_L$ and consequently $i_{pv}^{ref} = i_{pv}$. In this manner maximum power point tracking is realized.

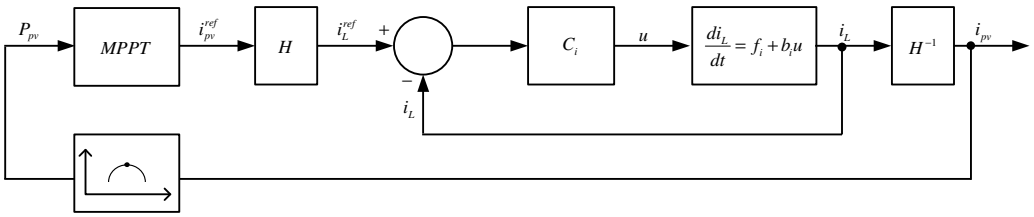

Figure 5-11 Control block diagram for PV with DC-DC converter and MPPT

For a fuel cell, controller is very similar to that one of PV module so its description will not be explicitly given for convenience. The MPPT algorithm is described with the following set of equations,

$$\begin{aligned}
&\frac{di_{fc}^{ref}}{dt} = u_{fc}; \quad P_{fc} = f\left(i_{fc}\right); \\
&u_{fc} = u_0 h_1 h_2; \quad v_{fc} = \frac{M}{2}\left(-h_1 - h_2\right); \\
&\sigma_{fc} = g_{fc} - P_{fc}; \quad \dot{g}_{fc} = \rho + v_{fc}; \\
&s_1 = \sigma_{fc}; \quad s_2 = \sigma_{fc} + \delta; \\
&h_1(s_1) = \frac{2}{1+e^{-ks_1}} - 1; \quad h_2(s_2) = \frac{2}{1+e^{-ks_2}} - 1,
\end{aligned} \tag{5.13}$$

with the design parameters $M, u_0, \rho, k, \delta > 0$.

MPPT of wind turbine is developed with different variables of interest. Additionally need for speed control appears. The MPPT algorithm for wind turbine is described by,

$$\begin{aligned}
&\frac{d\omega_g^{ref}}{dt} = u_{wt}; \quad P_m = f\left(\omega_g\right); \\
&u_{wt} = u_0 h_1 h_2; \quad v_{wt} = \frac{M}{2}\left(-h_1 - h_2\right); \\
&\sigma_{wt} = g_{wt} - P_m; \quad \dot{g}_{wt} = \rho + v_{wt}; \\
&s_1 = \sigma_{wt}; \quad s_2 = \sigma_{wt} + \delta; \\
&h_1(s_1) = \frac{2}{1+e^{-ks_1}} - 1; \quad h_2(s_2) = \frac{2}{1+e^{-ks_2}} - 1,
\end{aligned} \tag{5.14}$$

with the design parameters $M, u_0, \rho, k, \delta > 0$.

Controller block diagram is shown in Figure 5-12. MPPT block generates the reference generator rotational speed ω_g^{ref} according to the algorithm given in(5.14). Reference generator speed is controlled by speed controller denoted as C_ω, this controller can be designed as in [129]. Speed controller results in reference electromagnetic torque T_e^{ref} which is used to calculate i_{Lq}^{ref} using (3.17). Current i_{Lq} is controlled using control techniques described in Chapter 4. Current i_{Lq} generates electromagnetic torque and consequently changes the generator speed. In overall current controller achieves that $i_{Lq} = i_{Lq}^{ref}$, which in the same time means that $T_e = T_e^{ref}$ and speed controller achieves that $\omega_g = \omega_g^{ref}$. In this manner maximum power point tracking for wind turbine is realized.

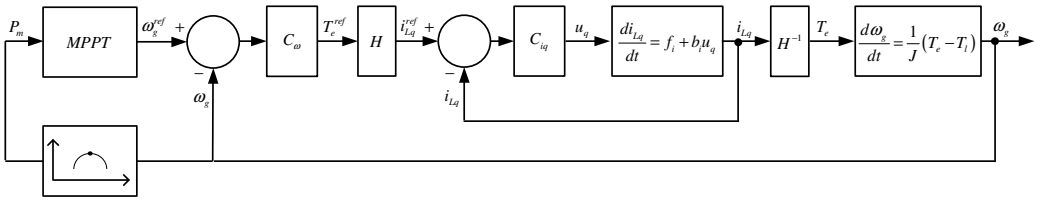

Figure 5-12 Control block diagram for wind turbine with MPPT

5.3 Output side converter control and grid synchronization

The converter interfacing DC bus with AC bus plays a major role in the power exchange between HES and AC bus. Let us assume that AC bus is representing microgrid. By interfacing a DC and AC sources this converter may have a role of the inverter (or AC source) and a rectifier (a DC source) thus it can transfer energy from DC bus to microgrid or from the microgrid to DC bus. As shown in previous sections the switching matrix with two input (or output) lines and three output (or input) lines - so called buck inverter or boost rectifier - may control a bilateral power flow. Before discussing control system design let us analyze possible power flow that this converter may be required to realize. This analysis would serve as a control task specification. The single line diagram of the DC bus to microgrid interconnection is given in Figure 5-13.

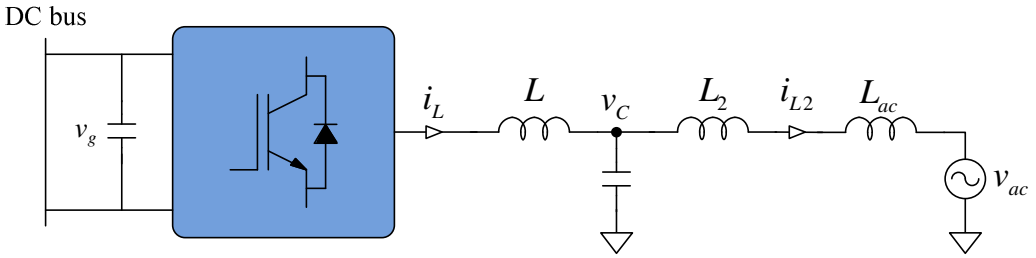

Figure 5-13 A single line diagram of the DC bus to microgrid interconnection

The dynamical model of the system in the grid voltage frame of references can be written as,

$$\begin{aligned}
\frac{di_{Ld}}{dt} &= -\frac{v_{Cd}}{L} + \omega_g i_{Lq} + \frac{v_{DC}}{L} u_d; \\
\frac{di_{Lq}}{dt} &= -\frac{v_{Cq}}{L} - \omega_g i_{Ld} + \frac{v_{DC}}{L} u_q; \\
\frac{d\theta_g}{dt} &= \omega_g; \\
\mathbf{u_{dq}} &= \mathbf{F}(\theta_g)\mathbf{u_{abc}},
\end{aligned} \tag{5.15}$$

$$\begin{aligned}
(L_2 + L_{ac})\frac{di_{L2d}}{dt} &= v_{Cd} - v_{acd}; \\
(L_2 + L_{ac})\frac{di_{L2q}}{dt} &= v_{Cq} - v_{acq}; \qquad v_{acq} = 0,
\end{aligned} \tag{5.16}$$

$$\begin{aligned}
\frac{dv_{Cd}}{dt} &= -\frac{i_{L2d}}{C} + \omega_g v_{Cq} + \frac{i_{Ld}}{C}; \\
\frac{dv_{Cq}}{dt} &= -\frac{i_{L2q}}{C} - \omega_g v_{Cd} + \frac{i_{Lq}}{C},
\end{aligned} \tag{5.17}$$

where ω_g is the angular velocity of the desired output voltage, $v_C^T = \begin{bmatrix} v_{Cd} & v_{Cq} \end{bmatrix}$ and $i_L^T = \begin{bmatrix} i_{Ld} & i_{Lq} \end{bmatrix}$, $i_{L2}^T = \begin{bmatrix} i_{L2d} & i_{L2q} \end{bmatrix}$ are the output voltage and the inductor current vectors respectively. The control in stationary (a,b,c) frame of reference is determine by

$$u_i(t) = \begin{cases} 1 & \text{with switch} \quad S_{1i} = ON \quad \text{and} \quad S_{1i} = OFF \\ 0 & \text{with switch} \quad S_{1i} = OFF \quad \text{and} \quad S_{2i} = ON \end{cases}; \quad i = 1,2,3. \tag{5.18}$$

If the DC bus voltage is controlled by other converters then the output side converter can be regarded as a source with apparent power $S^2 = P^2 + Q^2 = \|\mathbf{v}\|\|\mathbf{i}\|$, $P = \mathbf{v}^T\mathbf{i} = \|\mathbf{v}\|\|\mathbf{i}\|\cos(\varphi) = S\cos(\varphi)$ and $Q = \pm\sqrt{S^2 - P^2} = \|\mathbf{v}\|\|\mathbf{i}\|\sin(\varphi) = S\sin(\varphi)$. The voltage is determined by the microgrid, thus in that voltage frame of references the active and reactive powers may be expressed in the following form $P = \mathbf{v}^T\mathbf{i} = \|\mathbf{v}\|\|\mathbf{i}\|\cos(\varphi) = \|\mathbf{v}\|i_d$ and

$Q = \|\mathbf{v}\|\|\mathbf{i}\|\sin(\varphi) = \|\mathbf{v}\| i_q$, where $i_d = \|\mathbf{i}\|\cos(\varphi)$ and $i_q = \|\mathbf{i}\|\sin(\varphi)$ are components of the current vector collinear i_d and orthogonal i_q to the voltage vector respectively. With given maximum current (thus maximum apparent power) the converter may be theoretically required to deliver to the microgrid active and reactive power in ratio satisfying constraints $S^2 = P^2 + Q^2 = \|\mathbf{v}\|\|\mathbf{i}\|$, thus currents $i_d^{ref} = \|\mathbf{i}\|\cos(\varphi)$ and $i_q^{ref} = \|\mathbf{i}\|\sin(\varphi)$ can be specified to attain desired power.

In structure under examination the current $\mathbf{i_{L2}}$ is defining power delivered to microgrid. From given active and reactive power the reference currents i_{L2d}^{ref} and i_{L2q}^{ref} can be easily determined. Then $\mathbf{e_{iL2}} = \mathbf{i_{L2}^{ref}} - \mathbf{i_{L2}}$ can be expressed as

$$\begin{aligned} \frac{d\mathbf{e_{L2}}}{dt} &= \frac{d\mathbf{i_{L2}^{ref}}}{dt} - \frac{d\mathbf{i_{L2}}}{dt} = \underbrace{\left(\left(L_2 + L_{ac}\right)\frac{d\mathbf{i_{L2}^{ref}}}{dt} + \mathbf{v_g} \right)}_{\mathbf{v_{dis}}} \frac{1}{\left(L_2 + L_{ac}\right)} - \frac{\mathbf{v_C}}{\left(L_2 + L_{ac}\right)} \\ &= \frac{\mathbf{v_{dis}} - \mathbf{v_C}}{\left(L_2 + L_{ac}\right)} \end{aligned} \tag{5.19}$$

The $\mathbf{v_{dis}}$ act as a disturbance in the current control loop and the output capacitor voltage $\mathbf{v_C}$ is a control input. If $\mathbf{v_C}$ is selected as

$$\mathbf{v_C} = \left(\left(L_2 + L_g\right)\frac{d\mathbf{i_{L2}^{ref}}}{dt} + \mathbf{v_g} \right) + k\mathbf{e_{L2}} = \mathbf{v_C^{ref}} \tag{5.20}$$

Then the HES current supplied to the microgrid would have error dynamics governed by

$$\frac{d\mathbf{e_{L2}}}{dt} + k\mathbf{e_{L2}} = 0; \quad k > 0. \tag{5.21}$$

With $\mathbf{v_C^{ref}}$ defined as in (5.20) the current $\mathbf{i_L}$ could be determined from converter output voltage control loop. The voltage control error $\mathbf{e_{vC}}$ can be expressed as

$$\frac{d\mathbf{e_{vC}}}{dt} = \frac{d\mathbf{v_C^{ref}}}{dt} - \frac{d\mathbf{v_C}}{dt} = \left(-\frac{\mathbf{i_{L2}}}{C} + \omega_g \mathbf{P}\mathbf{v_C} \right) + \frac{\mathbf{i_L}}{C}; \quad \mathbf{P} = \begin{bmatrix} 0 & 1 \\ -1 & 0 \end{bmatrix}. \tag{5.22}$$

For the closed loop dynamics $\frac{d\mathbf{e_{vC}}}{dt} + k_1\mathbf{e_{vC}} = 0, k_1 > 0,$ inductor current should be

$$\mathbf{i_L} = \left(\mathbf{i_{L2}} - \omega_g C\mathbf{P}\mathbf{v_C}\right)\frac{1}{C} + Ck_1\mathbf{e_{vC}} = \mathbf{i_L^{ref}} \tag{5.23}$$

With reference current determined as in (5.23) we can now apply current control algorithm already discussed in Chapter 4. It is now obvious that we can directly specify

active and reactive power as input to the controller without any change of its structure. In this way this converter may act as active or reactive power source. This allows its usage as a power compensator or higher harmonics filter. It is only necessary to be able to express desired controlled variable in the terms of active and reactive power (or components of the current collinear and orthogonal to the grid voltage vector). Classical active filter configuration of output side converter is shown in Figure 5-14.

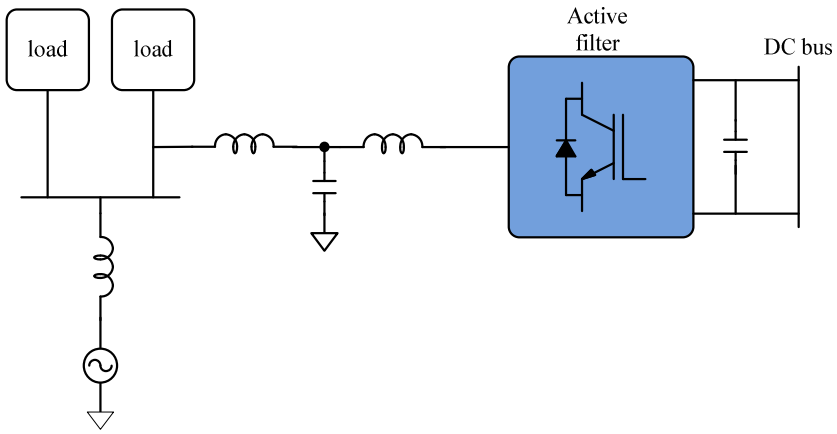

Figure 5-14 Output side converter as active filter in microgrid

5.4 Conclusion

This chapter concludes the technical discussion about the HES power electronic interfaces and control system. In this chapter three basic topics are covered, MPPT for renewable energy sources, output side converter control and HES power control and power balancing strategies. Developed MPPT algorithm discussed in this chapter is modification of optimization algorithm based on sliding mode control as described in [128]. Algorithm has been modified by replacing discontinuous control and optimization functions with smooth and differentiable functions and algorithm is modified so it can be applied for each renewable source under consideration. Regarding the output converter control it has been shown that additional dynamics introduced by the output filter must be taken into consideration when designing control system. Together with the control strategies developed in Chapter 4 a control system design of output side converter has been completed. Finally the power management strategies are presented for the sake of completeness of this thesis. Power management in HES is active topic of research and it is explained in this chapter only roughly.

6 EXPERIMENTAL AND SIMULATION RESULTS

This chapter contains the experimental results that verify the most important finding of this thesis. To solidify the verification simulation results are given along. Basic DC-DC converters were simulated and experimentally verified. Control of DC-DC converters presented in Chapter 4 is verified both in simulations and experiments. Experiments related to the renewable energy sources are done and relevant results are presented. Finally experimental results concerning the control of three phase switching converters are given together with simulation and experimental verification of switching algorithm from Chapter 4.

6.1 Experimental Results of Control of DC-DC Converters

6.1.1 DC-DC Converters Experimental Setup

For the experimental purposes, two most common DC-DC converters, buck and boost were designed and implemented. Schematic of the designed DC-DC buck converter is shown in the Figure 6-1. Switches in switching matrix are implemented using combination of MOFET and Schottky diodes to allow bidirectional power transfer. Inductor current and capacitor voltage are measured quantities. Current is measured using Hall effect current sensors. Voltage is measured by custom designed sensor. Voltage sensor consists of resistor divider and signal conditioning stage. DC-DC converter is run from digital controller that includes analog to digital converters and switch modulators. Switch signals are supplied to the gate terminal of the MOSFET using appropriate gate driver circuits. Implemented buck converter is shown in Figure 6-2. Current and voltage sensors are shown in Figure 6-3-(a) and Figure 6-3-(b), respectively.

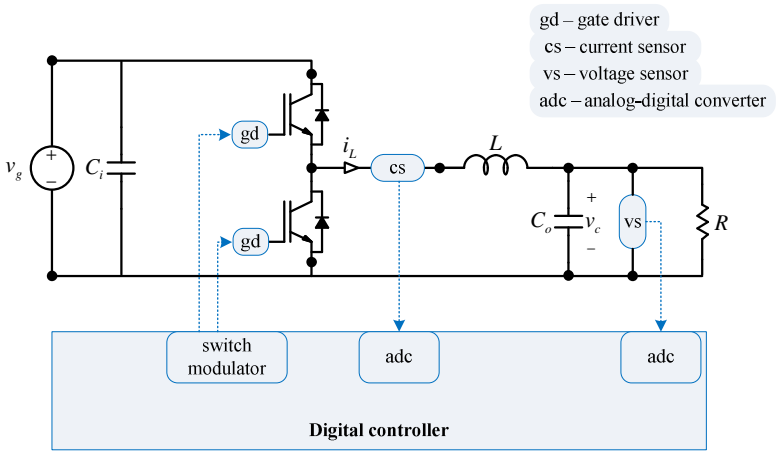

Figure 6-1 Buck converter implementation schematic

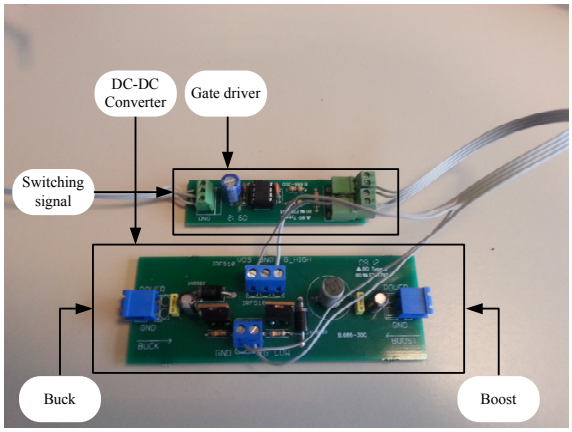

Figure 6-2 DC-DC converter power topology implementation

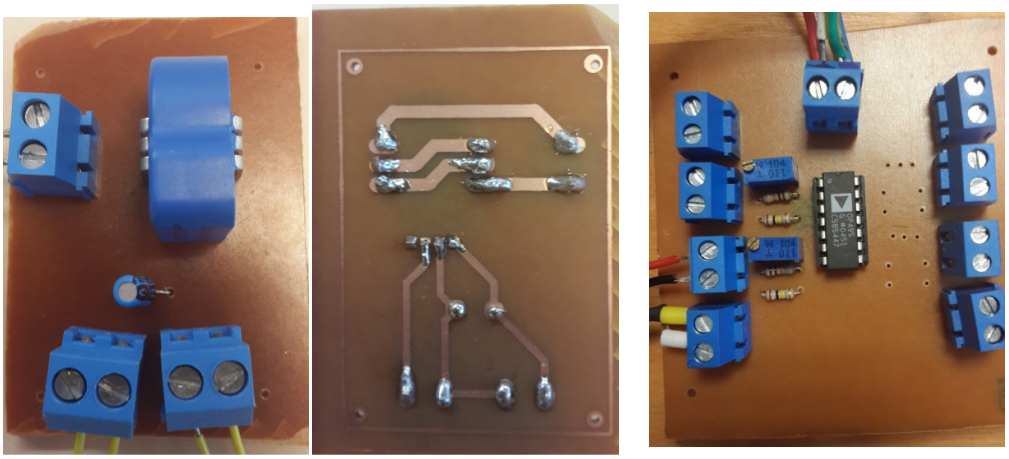

(a) (b)

Figure 6-3 Implementation of current sensor (a) and voltage sensor (b)

Boost converter implementation schematic is shown in Figure 6-4. Careful examination of the schematic reveals the topological similarity between buck and boost

converters. For the experimental purposes same power topology from Fig. 6.2. is used to implement boost converter. In fact boost converter is obtained by simple source/load inversion of buck converter and different place of the voltage sensor. Implementation details of the DC-DC converter experimental setup are given in Table.6.1.

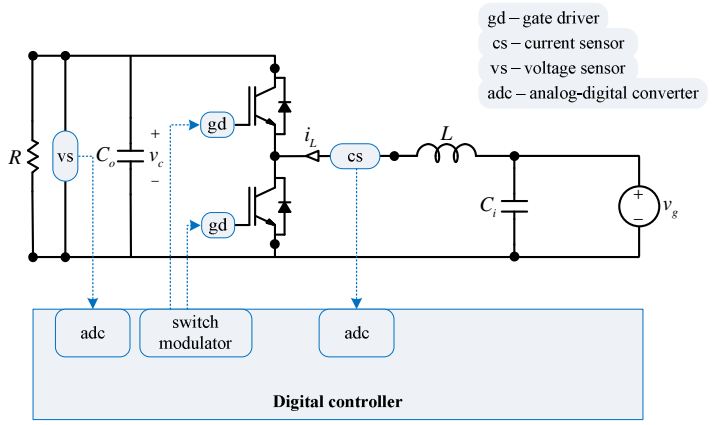

Figure 6-4 Boost converter implementation schematic

Implementation details of DC-DC converter	
MOSFET	IRF530
Schottky diode	MBR10100ct
Gate driver	IR2104
Current sensor	LEM LTSR15np
Voltage sensor	Resistor divider + conditioning circuit (OP495)
Inductor (L)	330 µH
Capacitor (C)	220 µC
Digital controller	dSpace DS1103

Table 6-1 Implementation details of DC-DC converter

6.1.2 Control of DC-DC Converters

Buck converter dynamics are given by (4.46) with s_{11} as the control input and measured i_L inductor current and v_c capacitor voltage. Current in inductor is controlled using expressions from (4.70), (4.72) and (4.73). Current controller achieves $i_L^{ref} = i_L$. Voltage is then controlled using linear, proportional integral (PI), controller in the form of $i_L^{ref} = K_i \int \left(v_c^{ref} - v_c \right) dt + K_p \left(v_c^{ref} - v_c \right)$; $K_p, K_i > 0$. Obtained i_L^{ref} is reference inductor current necessary to achieve desired voltage level. This cascaded control structure is depicted in the Figure 6-5.

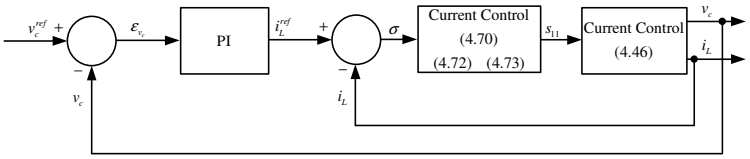

Figure 6-5 Buck converter control block diagram

Dynamics of DC-DC boost converter are given in (4.51) with $1-s_{12}$ as control input and measured i_L inductor current and v_c capacitor voltage. Inductor current is controlled using (4.74) and (4.76). Current controller achieves $i_L^{ref} = i_L$. Voltage is then controlled using linear, proportional integral (PI) controller in the form $i_L^{ref} = K_i \int \left(v_c^{ref} - v_c \right) dt + K_p \left(v_c^{ref} - v_c \right);\ K_p, K_i > 0$. Obtained i_L^{ref} is reference inductor current providing desired voltage level. This control structure is depicted in Figure 6-6.

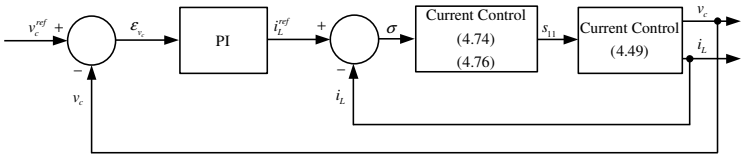

Figure 6-6 Boost converter control block diagram

6.1.3 DC-DC Buck Converter Experimental Results

Voltage control of buck converter is implemented using setup presented in the previous subsection. Current control results are shown here to verify the control capabilities of the proposed controllers. In the first case, shown in the Figure 6-7 the buck inductor current is controlled to the constant reference value of 0.5A. Controller shows satisfactory performance with fast settling time, no overshoot and negligible steady state error in response. In the second experiment inductor current is controlled to the constant reference value of 1A and results are shown in the Figure 6-8. Similar results are achieved as in previous experiment.

In the next experiment buck capacitor voltage is controlled to the desired reference value. In the first experiment output voltage reference is set to 10V and controller performance is evaluated. Controller response is satisfactory with fast settling time, no overshoot and minimum steady state error. Controller response is shown in the Figure 6-9. In the second experiment, voltage reference of 20V is supplied to the

controller and response is given in the Figure 6-10. The controller shows the same performance. For further testing purposes voltage reference is changed in the form of staircase signal and voltage response is shown in the Figure 6-11. Additional experimental parameters are given in Table 6-2.

DC-DC buck converter experiment parameters	
Load resistance R	22Ω
Control loop sampling frequency	10 kHz
Input voltage v_g	32V
PI controller parameters K_p, K_i	75, 1000

Table 6-2 DC-DC buck converter experiment parameters

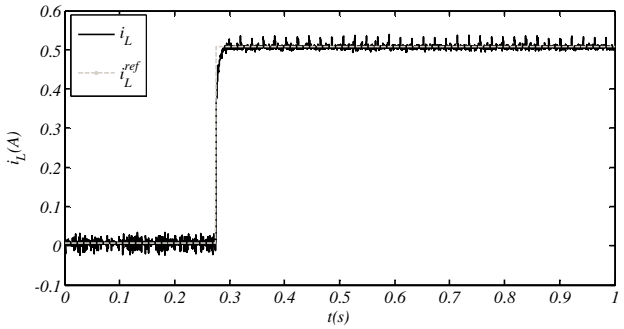

Figure 6-7 Buck converter inductor current control (0.5A reference)

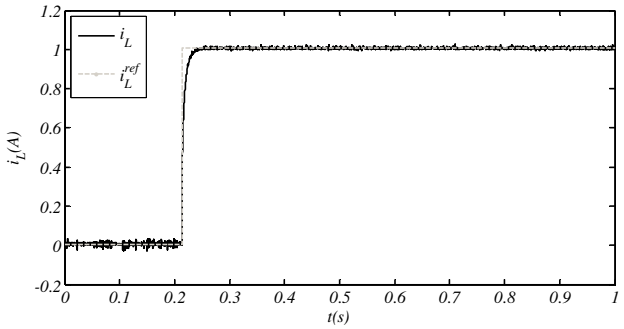

Figure 6-8 Buck converter inductor current control (1A reference)

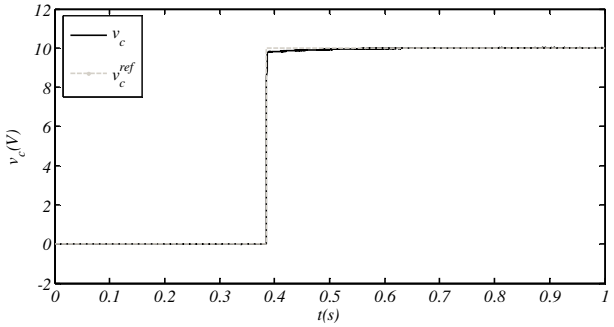

Figure 6-9 Buck converter capacitor voltage control (10V reference)

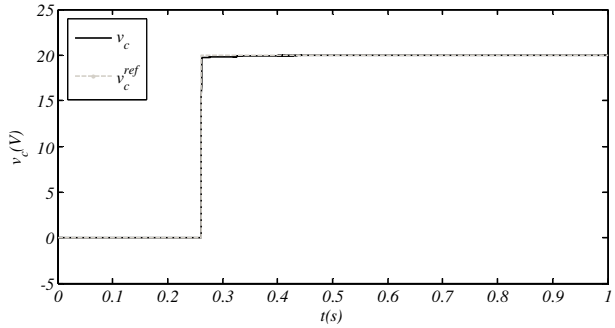

Figure 6-10 Buck converter capacitor voltage control (20V reference)

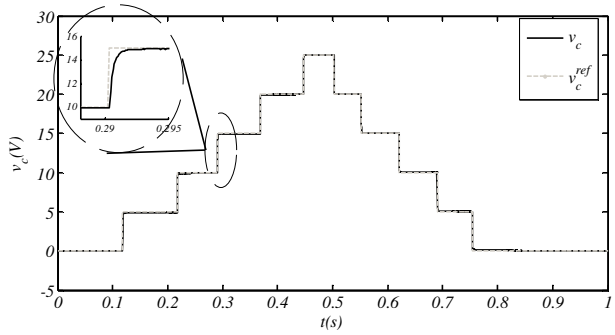

Figure 6-11 Buck converter capacitor voltage control (staircase reference)

6.1.4 DC-DC Boost Converter Experimental Results

Experiments with boost converter are done for the inductor current control. In the first experiment inductor current reference is controlled to the value of 1.7A. Controller exhibits good performance with fast settling time, minimum steady state error and minimum overshoot. Current response is shown in Figure 6-12. with magnified transient period for better view. Boost converter is initially controlled to 0.35A current value; open loop initial current is 0.31A due to the nature of boost topology.

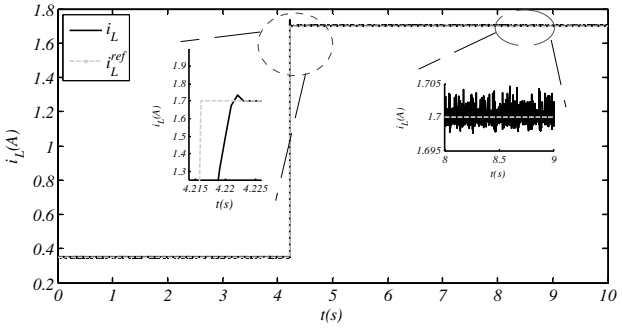

Figure 6-12 Boost converter inductor current control (1.7A reference)

Second experiment show boost current control performance against a slow time varying reference current. Reference current is supplied in the form of ramp signal with both positive and negative slopes. Controller shows excellent tracking performance. Current response for this case is shown in Figure 6-13. Current error is shown in Figure 6-14. Additional experiment parameters are shown in Table 6-3.

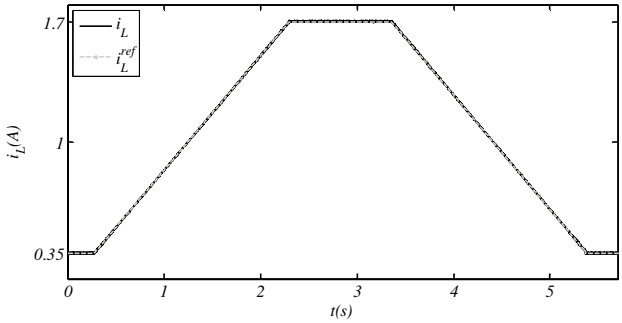

Figure 6-13 Boost converter inductor current control (ramp reference)

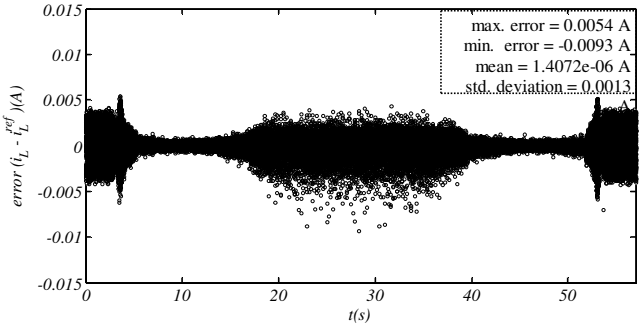

Figure 6-14 Current tracking error (ramp reference)

DC-DC boost converter experiment parameters	
Sampling frequency	10kHz
Load resistance R	106Ω
Input voltage v_g	21V

Table 6-3 DC-DC boost converter experiment parameters

6.2 PV System Experimental Results

6.2.1 PV System Experimental Setup

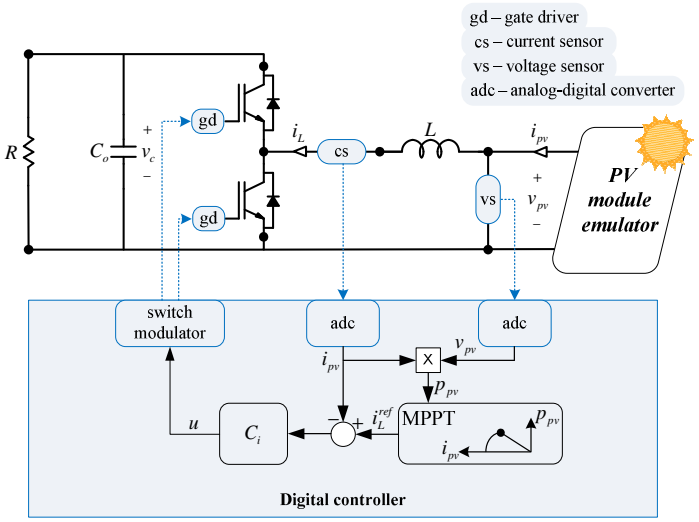

Figure 6-15 PV System experimental system

Experimental setup for PV system is shown in the Figure 6-15. Setup consists of PV module emulator with DC-DC boost converter attached at its output terminals and resistive load at the output of boost converter for power dissipation purposes.

Implementation of boost converter used in this experiment is explained in the previous section. Boost converter inductor current control is implemented as depicted in

Figure 6-6 with inductor current reference i_L^{ref} supplied by MPPT algorithm described in Chapter 5. In Figure 6-15, C_i block represents current controller.

For experimental purposes PV module emulator is implemented using buck converter as the power stage as shown in Figure 6-16. Output capacitor voltage of buck converter is controlled using controller from

Figure 6-5. Buck converter output current is measured, based on that information and PV module I-V characteristics information, the reference output voltage of buck converter is generated. Set output voltage is obtained using PV model (Chapter 3),

$$\underbrace{i_{ph} - i_{pv}}_{g} = \underbrace{\frac{V_d}{R_{sh}} + i_0\left(e^{\frac{V_d}{V_t}} - 1\right)}_{h}; \tag{6.1}$$

$$v_{pv} + R_s i_{pv} - V_d = 0. \tag{6.2}$$

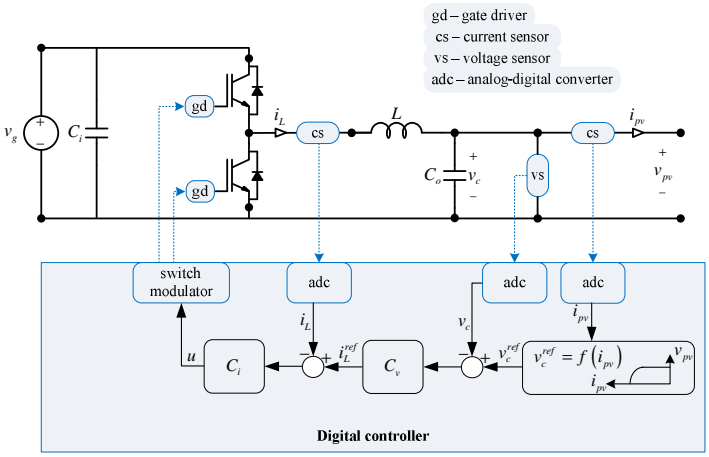

Figure 6-16 PV module emulator

In the equation (6.1) and (6.2), i_{ph} is known photo-generated current proportional to the given irradiance, i_{pv} is the measured buck converter output current and R_{sh}, V_t, i_0, R_s parameters are known for the PV module under consideration. In order to obtain the $v_{pv}\left(=v_c^{ref}\right)$ for a measured i_{pv}, diode voltage V_d needs to be calculated from (6.1) and inserted into (6.2). However, explicit solution of (6.1) doesn't exist, so this equation has to be solved in some other manner.

In the available literature, the value of diode voltage is most commonly found by iterative root finding methods such as Newton-Raphson. However, when such algorithms are run in real-time, convergence is hard to be guaranteed, hence, such solution may fail. Instead, different solution is proposed including offline curve parameterization. Namely, all possible V_d values for a given PV module are plotted against the right hand side of (6.1) denoted by *h*. Obtained curve is parameterized to get solution in the form of $V_d = f(h)$, where $f(h)$ is polynomial of some known degree. Now for any given *h* within the permitted range V_d value can be obtained by calculating the value of the polynomial. Since $h = g$ (the right hand side of (6.1)) it can be calculated in each sampling period as the difference of photo-generated current and buck converter output current.

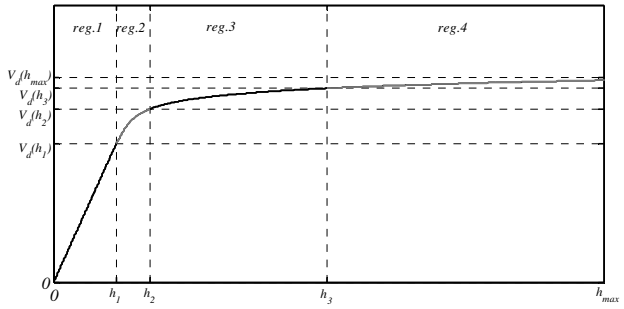

Figure 6-17 Parameterization of diode voltage curve

The plot of V_d vs. h is shown in Figure 6-17. Practically polynomial of very high degree is necessary to obtain the parametric description of this curve. For the implementation purposes the curve has been divided into four regions and each region is estimated by a 6^{th} order polynomial. This degree of polynomial for each region is not the optimal but for our purposes it is satisfactory considering the estimation error. Obtaining optimal degree of polynomial for each region is the matter of future work.

6.2.2 PV Module Emulator - Simulation and Experimental Results

PV module emulator depicted in Figure 6-16 has been simulated using Matlab/Simulink 2012b and experimentally verified using buck converter presented in the previous section. Simulation model of PV module emulator is shown in Fig.6.18. Simulation and experimental results are compared for the sake of verification and satisfactory results are obtained.

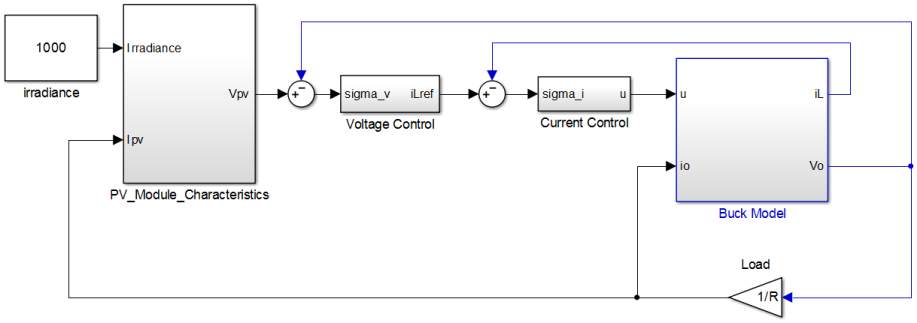

Figure 6-18 PV module emulation simulation model

In the first experiment, PV module emulator performance is examined when the resistive load is attached to it. When the load is attached current starts to flow at the output of the emulator which in return causes the change of the output voltage in accordance to the I-V characteristics of the emulated PV module. Results of this experiment are shown in Figure 6-19. Without load, emulator output voltage is at its maximum (open circuit voltage) for given irradiance, when the load is attached, the actual drop on the output voltage is determined by the loading condition.

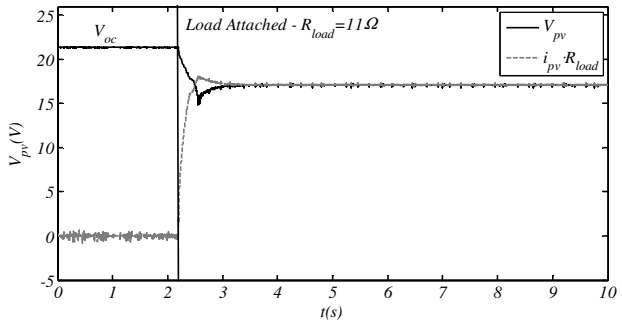

Figure 6-19 PV module emulator – load connection experiment

Power extracted from the PV module emulator is determined by the current flowing at its output, in other words, power is determined by the load impedance. For the attachment of the given load in the first experiment power graph is shown in Figure 6-20. At the beginning of the experiment there is no power flow to the output, once the load is attached, power starts to flow to the output as seen in the figure. For the given loading condition, power extracted from the emulator is 26.58W.

Second experiment with PV module emulator is done for the sudden load change at the output. In the beginning of the experiment there is 11Ω load attached to the output of the emulator. At some arbitrary point in time output load is changed to 22Ω and

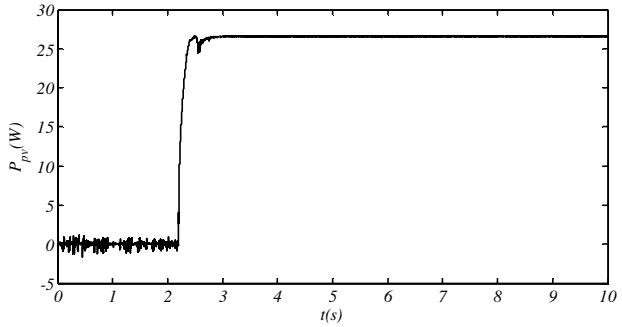

Figure 6-20 PV module emulator – power flow

emulator output current and voltage are observed. For this change, output current decreases while output voltage increases as shown in Figure 6-21. It is important to notice that the value of current is given with an offset of 20A for better display purposes. Fast settling time of the PV emulator is observed.

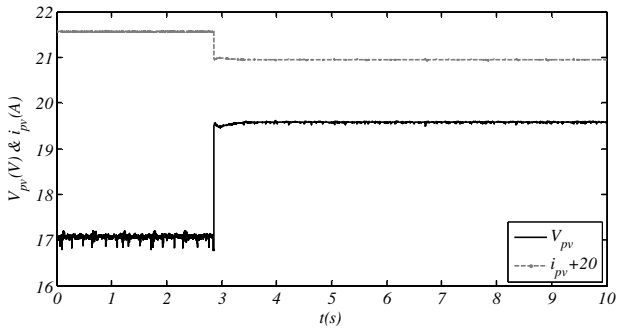

Figure 6-21 PV module emulator – output load change response

For better interpretation of the results and comparison of the experimental and simulation results, the I-V characteristics of the emulator are simulated using model from Figure 6-18. The output current value is varied between its minimum and maximum values and emulator output voltage is recorded. The I-V characteristic curve is plotted in Figure 6-22. Additional to that the two load lines are plotted on the same graph; first load line is plotted for 11Ω and second load line is plotted for the load of 22Ω. In ideal conditions, for a given load at its output, it is expected that emulator output voltage and output current have values that that are equal to the values of operating point where load line intersects the I-V curve. Operating points for two values of load (11Ω and 22Ω) are obtained from simulations and experiments and compared as depicted in the Figure 6-22. Simulation and experimental results are very close to the expected operating point as it can be seen from the graph.

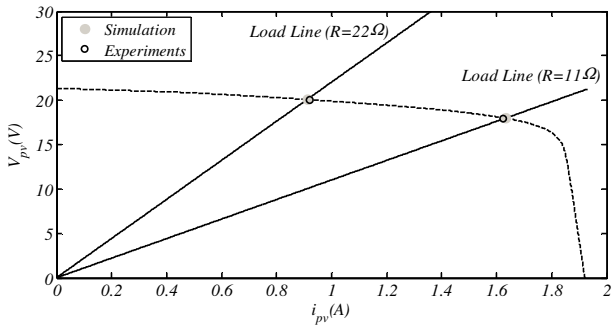

Figure 6-22 PV module emulator – comparison against load lines

Experimental setup from Figure 6-15 was used to perform third experiment. For the purposes of this experiment, boost inductor current reference was changed from its minimum value to its maximum value as shown in Figure 6-23, and emulator output voltage and output power is observed. In addition, experimentally obtained results are compared to the simulation results for the performance evaluation. The comparison of simulated and experimentally obtained I-V curve is shown in the Figure 6-24. Power curve results are given in the Figure 6-25. It is important to notice that these all of these experiments are done for the maximum irradiance of 1000 W/m^2. All of the necessary simulation and experimental data is given in the Table 6-4.

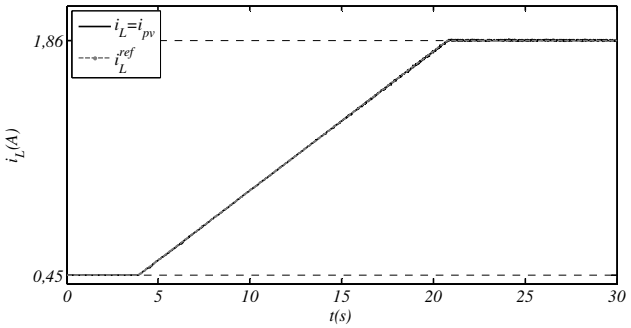

Figure 6-23 PV module emulator – change of output current

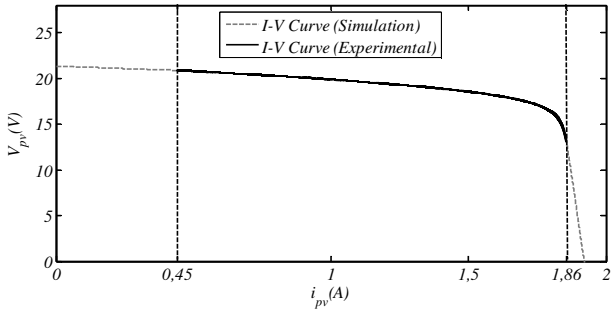

Figure 6-24 PV module emulator – I-V curve (simulation vs. experiments)

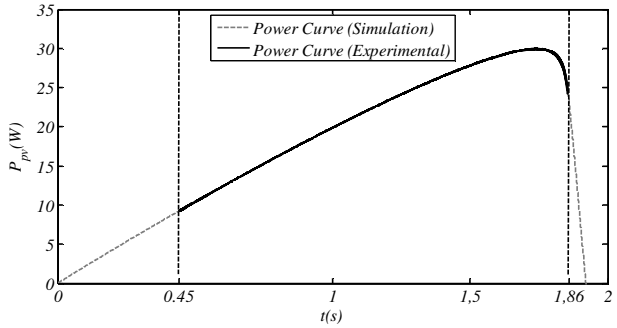

Figure 6-25 PV module emulator – power curve (simulation vs. experiments)

PV Module Emulator Simulation and Experiment Parameters	
PV module	
Open circuit voltage Voc	21.6 V
Short circuit current Isc	1.93 A
Rated voltage (@ MPP)	17.2 V
Rated current (@ MPP)	1.74 A
Rated power (@ MPP)	30 W
Experimental parameters	
Sampling frequency	10 kHz
Input voltage v_g	32V

Table 6-4 PV Module Emulator Simulation and Experiment Parameters

6.2.3 MPPT – Simulation Results

In this section simulations of PV module with DC-DC boost converter at its output are described. Boost converter is feeding a resistive load. Modeling and simulation of electrical characteristics of PV module is covered in Chapter 3 and technical data of simulated module and other simulation parameters are given in the Table 3.1. MPPT algorithm based on sliding mode optimization from Chapter 5 was implemented using smooth sigmoid functions. As an output of MPPT algorithm boost converter inductor current references are generated.

In first simulation case, sun irradiance was set to its maximum value of 1000 W/m^2. For this value of irradiance it is expected that PV module can produce 300W at its output. Current and voltage values of PV module at maximum power are specified in Table 3-1. as 5.49A and 54.7V respectively. Figure 6-26 shows the performance of MPPT algorithm in maximum power point search. PV modules output power is compared to the optimization reference denoted as g . Power tracks the optimization reference that, as a result of MPPT, reaches the PV module maximum power value of 300W. There are few important facts that can be seen on the Figure 6-26. First; boost converter output voltage has some initial value so there exist some initial value of current at the input. This input current manifests itself through power at the time 0s. After the simulation is started, output power picks up MPPT optimization reference quickly and optimization reference increases until it reaches the maximum power point and stays there with certain amount of oscillations around the maximum power point. Maximum power point reaching time is relatively fast, however it is a result of selected MPPT design parameters. For the same test case of 1000 W/m^2 irradiance reference

inductor current and inductor current response are shown in the Figure 6-27. Inductor current settles at 5.49A as specified by PV module datasheet. PV module output voltage change is shown in Figure 6-28. Voltage falls from open circuit value to 54.7V at MPP.

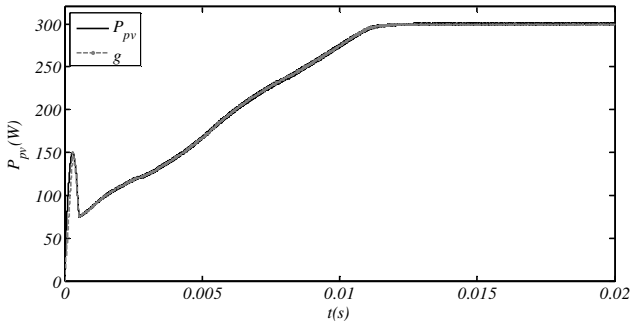

Figure 6-26 Maximum power point tracking for PV system

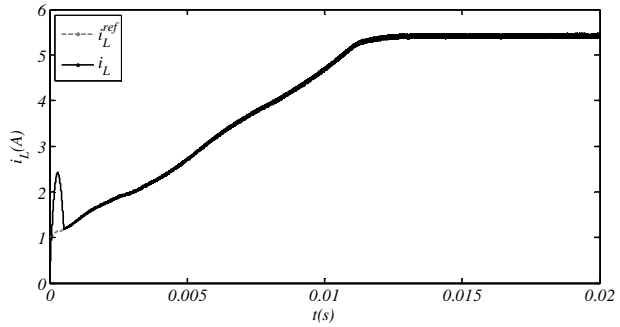

Figure 6-27 PV module current response

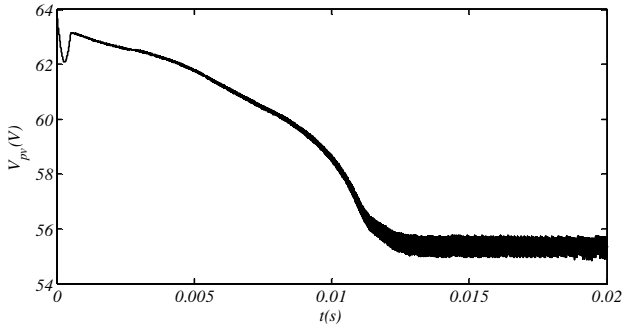

Figure 6-28 PV module voltage response during MPPT

MPPT was simulated for changing irradiance values to test the tracking performance of the algorithm. Irradiance was changed as a sine value of 500W/m^2 peak to peak value starting at 750 W/m^2, rising to 1000W/m^2 and falling down to 500W/m^2 the frequency of sine irradiance value is 20Hz. Simulation results of MPPT are shown in Figure 6-29 At the peak value of irradiance PV module power reaches its maximum

value of 300W and for 500W/m^2 irradiance module power is at half of that value. Corresponding boost converter inductor current tracking is shown in Figure 6-30.

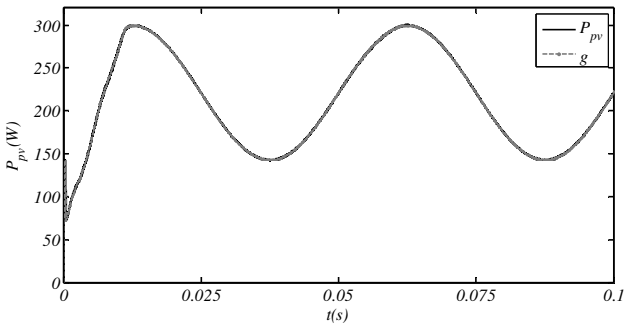

Figure 6-29 MPPT for varying irradiance

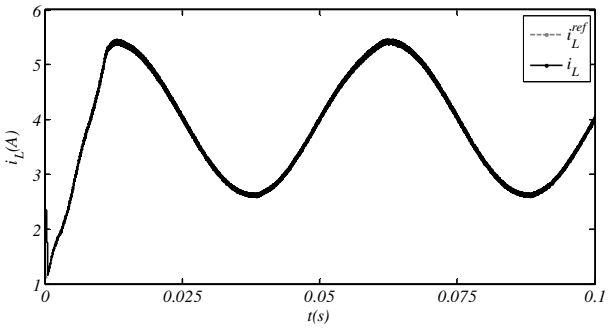

Figure 6-30 PV output current response for varying irradiance

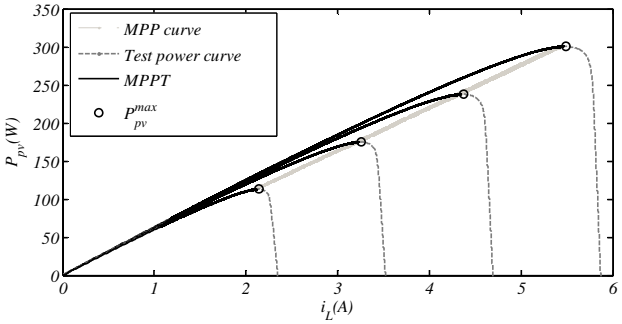

Figure 6-31 MPPT performance shown on power curve

Final simulation scenario shows the performance of MPPT against the test power curve for irradiances of 1000W/m^2, 800W/m^2, 600W/m^2, 400W/m^2. MPPT tracking is achieved and demonstrated along those curves in Figure 6-31. It is observed that power reaches the maximum point and stays in that point. MPPT for varying irradiance is shown on the same curve. It appears as the curve crossing the test maximum power points. Certain linearity is observed among current at MPPs and power values. In some offline MPPT algorithms this linearity is explored and used to set reference current

values for a given irradiance. MPPT algorithm parameters and the rest of simulation parameters are shown in Table 6-5 MPPT simulation parameters.

MPPT Simulation Parameters	
u_0	500
δ	0.5
ρ	1000
M	50000
k	1000

Table 6-5 MPPT simulation parameters

6.2.4 MPPT – Experimental Results

MPPT was implemented using setup shown in Figure 6-15. First experiment was done for the maximum irradiance (1000W/m^2). According to the emulated PV module specifications it is expected that MPPT settles at about 30W power. Results shown in Figure 6-32 verify this expectation. At the beginning of the experiment certain amount of power is drawn from the PV module emulator due to the boost converter initial current (0.45A). For that current value of PV module voltage is 20.91V so resulting power drawn from emulator is 9.4W. After some arbitrary point in time MPPT is started (using commands in software). MPPT algorithm starts to drive the system to the maximum power point and this process can be clearly seen in the graph. When maximum power point is reached MPPT algorithm keeps system in that point until MPP changes. The boost inductor current reference commanded by MPPT is shown in Figure 6-33. Boost inductor current tracks the reference current during MPP reaching. Figure 6-34 shows the PV module output voltage change. Voltage settles at 17.2V, rated voltage at MPP.

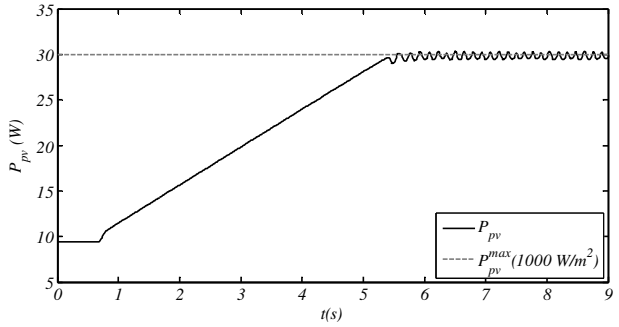

Figure 6-32 PV module power during MPPT

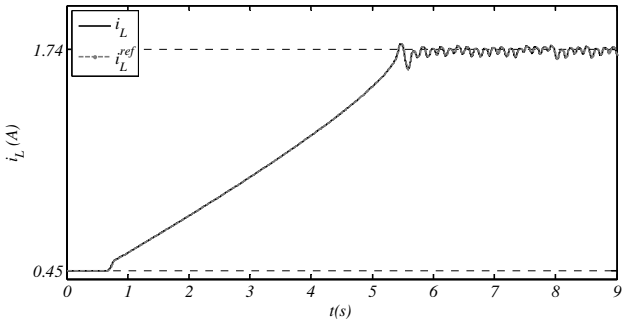

Figure 6-33 PV module current during MPPT

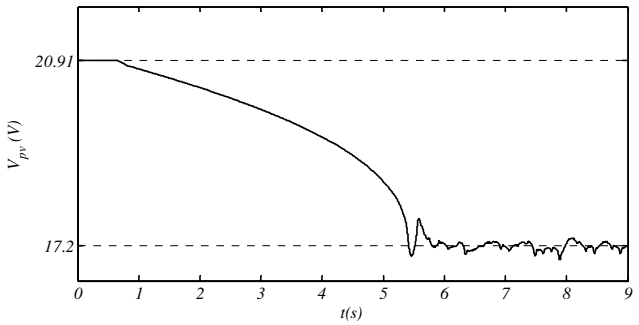

Figure 6-34 PV module voltage during MPPT

Reaching of the maximum power point for the first experiment is shown on the simulated power curve in Figure 6-35. It can be seen that experimentally obtained power values match the power curve and MPPT forces the system to settle at its maximum power of 30W.

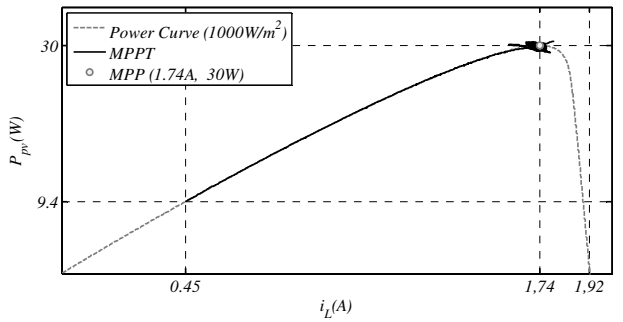

Figure 6-35 PV module power during MPPT compared to the simulation case

In second experiment MPPT was tested for variance change. The following scenario was experimentally tested, at the beginning of the experiment irradiance was set to 750W/m^2, and MPPT was started, after enough time for MPPT settling was allowed irradiance was gradually changed from 750W/m2 up to 1000W/m2. Results of

the MPPT were recorded and compared against the simulated power curves as shown in Figure 6-36. It can be seen that at the beginning of the experiment the module outputs about 10.7W of power. After MPPT is enabled the power of the module rises to the value of 22.5W which is the maximum power point at given irradiance of 750W/m^2. With the change of irradiance to 1000W/m^2, the module output power raises to the value of 30W. Boost inductor current response is shown in the Figure 6-37. From this figure the MPP reaching (0s-3s), settling (3s-5s), irradiance change(5s-8s) and settling to new value (8s-9s) can be clearly seen.

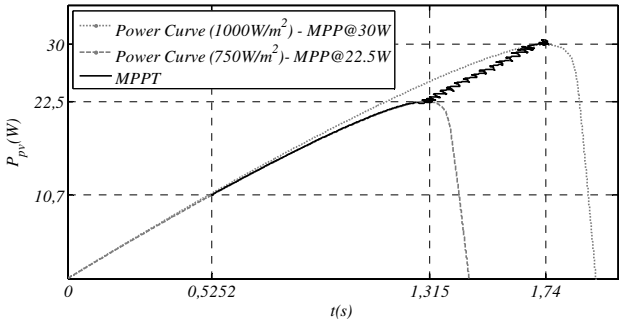

Figure 6-36 PV module power during MPPT for irradiance change

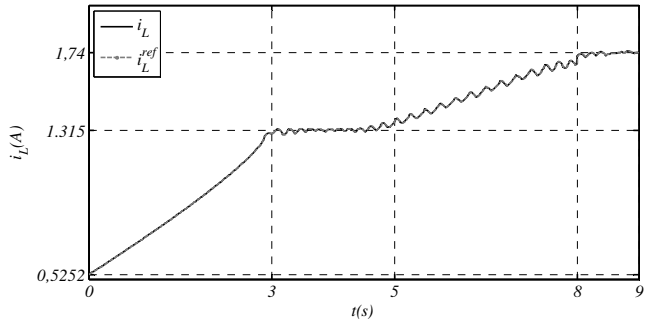

Figure 6-37 PV module current during MPPT for irradiance change

6.3 Three Phase Switching Converter Experimental and Simulation Results

6.3.1 Experimental setup - three phase switching converter

The three phase switching converter was design for testing purposes of three phase converters for various applications (Figure 6-38). The central component of the

designed three phase switching inverter is intelligent power module (IPM) that consists of three IGBT based half bridge components and their gate drivers (gd). The board was designed to properly interface IPM with necessary components. Board additionally includes the current sensors (cm) at the AC power side for the measurement of phase currents. Board also features optical isolators for IGBT gate signals, auxiliary power supply to power the gate drivers and optical isolators (not shown in Figure 6-38). All of the analog and digital signals are collected at the single interface for easier connection of the board and digital controller. The overall design of the electronics is characterized with modularity which offers ease of the troubleshooting.

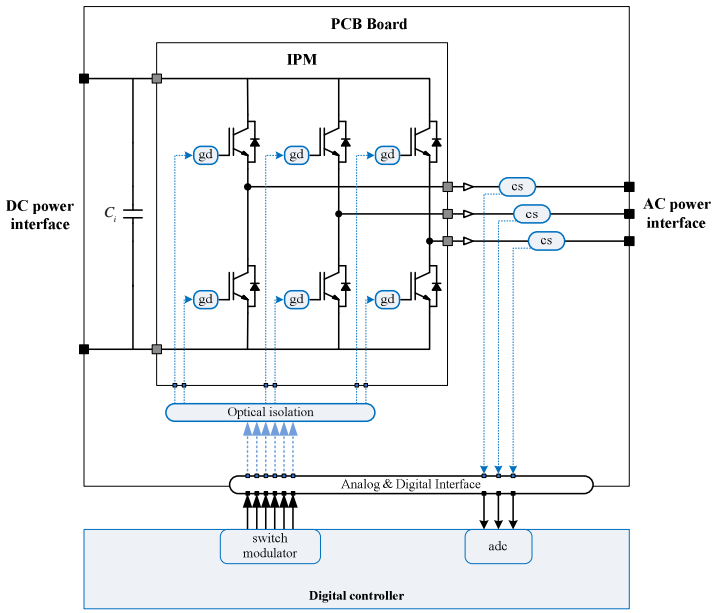

Figure 6-38 Three phase switching converter design schematic

Intelligent power module on the board is Fairchild Semiconductor's FNB41060-B2, 10A, 600V IGBT module. This module consists of three half bridges and corresponding gate drivers. Internally, module has implemented safety procedures for over-current fault, under-voltage lockout and excess temperature protections using a thermistor. This is a low cost, small footprint module and requires very few additional components to be fully interfaced.

In order to separate digital and high power grounds and in that way guaranty the safety of the controller equipment the switch control signals are optically isolated through direct current drive opto-coupler. Outputs of the opto-couplers are connected to the IPM IGBT gate driver inputs.

The half bridge currents measurement is done using fully integrated, Hall-effect based, low offset, high precision linear current sensors. The sensor is capable of measuring RMS currents up to 25A value. Terminals of the conductive current path are magnetically isolated from the conditioning circuit. This sensor integrates the output voltage conditioning circuit, so the measurement signals can be interfaced directly to the digital controller without further conditioning or isolation.

The implementation of the hardware requires the availability of supply voltages of different values. Basically the conditioning circuits require 5V, gate drivers require 15V and DC bus voltage is a matter of preference with limit of 600V. Board is designed such that it requires auxiliary 24V supply to power on-board 15V and 5V regulators.

Collection of the all relevant analog and digital signals is done into a single breakout connector for easy interface. Special attention was paid to the routing and layouting of the circuit due to the accommodation of different types of signals; analog, digital and high power.

The hardware module can be used in combination with many different digital controllers, for the purposes of this work, dSpace DS1103 is used because it provides rapid prototyping capability, high processing I/O speed and accuracy.

Figure 6-39 and Figure 6-40 show the implementation of three phase switching converter explained above. All of the components are clearly identified on the figures.

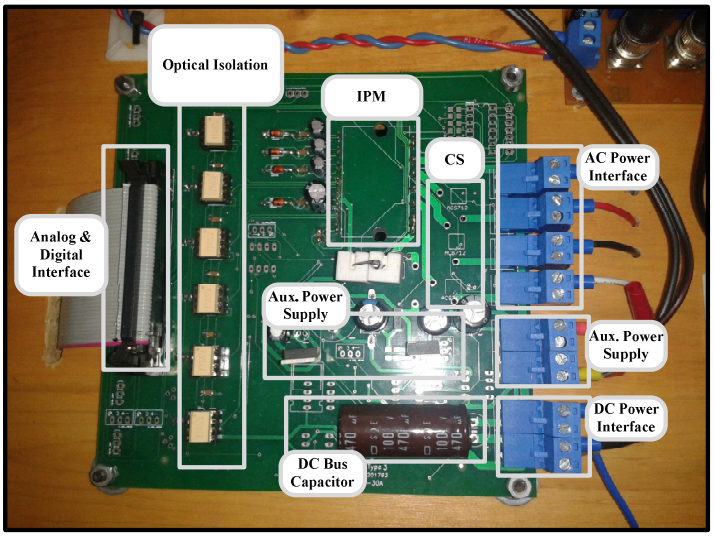

Figure 6-39 Implementation of three phase converter

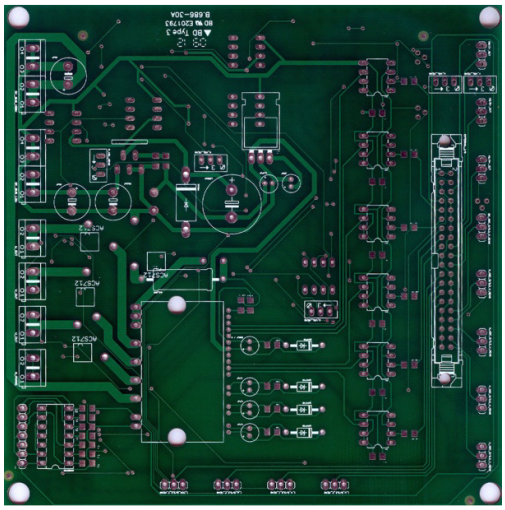

(a)

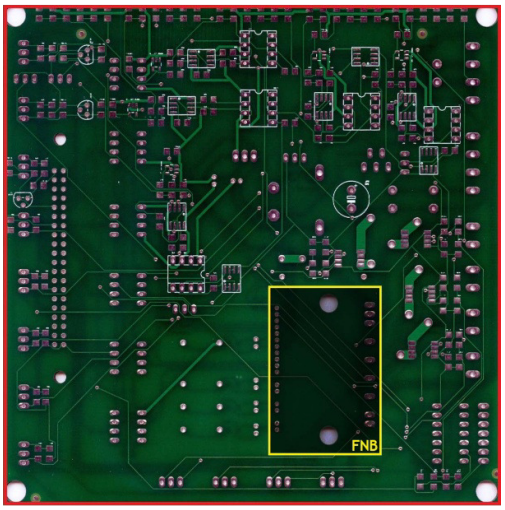

(b)

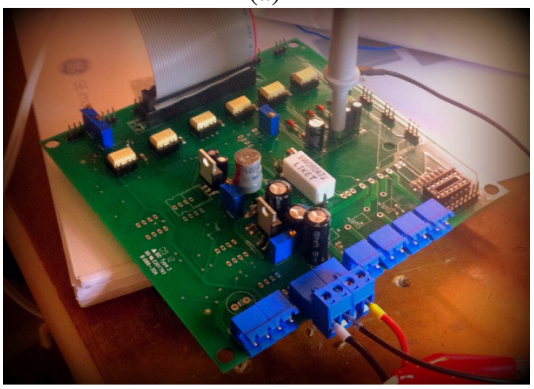

(c)

(d)

Figure 6-40 Converters PCB design (a) and (b), test period of converter (c), IPM outlook (d)

Designed three phase switching converter can be used both as the inverter and rectifier as it permits the bidirectional power flow. For the purposes of this thesis the converter was tested as inverter driving the rotor circuit of doubly fed induction generator (DFIG). For the implementation of full setup necessary to drive and control the DFIG some additional equipment is used together with the converter. The schematic of the experimental setup for interface of DFIG is shown in Figure 6-41. Laboratory setup consists of the doubly fed induction generator and another asynchronous motor. The shafts of both machines are coupled mechanically. Asynchronous motor is used as wind turbine emulator and it is driven from a regular commercial speed controller. Outputs of the three phase inverter interfacing a DFIG are connected to the rotor terminals of the DFIG, and stator terminals of DFIG are connected to the three phase electrical load or utility grid. Additionally current and voltage measurement circuits are

added to the stator side of generator and voltage measurements for the grid voltage. DC bus voltage for the inverter is supplied from a separate DC power supply. Setup is controlled using dSpace DS1103 controller system. DFIG is shown in Figure 6-42.

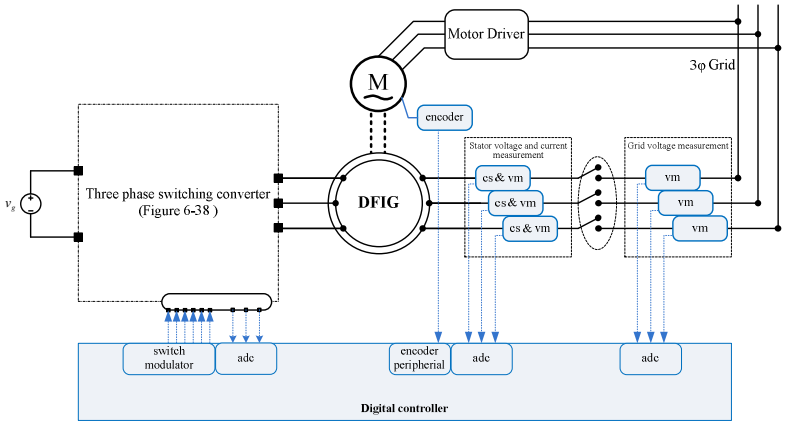

Figure 6-41 Three phase inverter driving a DFIG rotor circuit

Figure 6-42 DFIG (on the right) coupled to wind turbine emulator (on the left)

6.3.2 Three Phase Inverter Simulation and Experimental Results

Three phase buck inverter was simulated using following expressions for inductor current and capacitor voltages (see Figure 4-15),

$$
\begin{aligned}
L\frac{di_{L1}}{dt} &= -\frac{2}{3}v_{C1}+\frac{1}{3}v_{C2}+\frac{1}{3}v_{C3}+\frac{2}{3}v_{g1}s_{11}-\frac{1}{3}v_{g2}s_{12}-\frac{1}{3}v_{g3}s_{13};\\
L\frac{di_{L2}}{dt} &= \frac{1}{3}v_{C1}-\frac{2}{3}v_{C2}+\frac{1}{3}v_{C3}-\frac{1}{3}v_{g1}s_{11}+\frac{2}{3}v_{g2}s_{12}-\frac{1}{3}v_{g3}s_{13};\\
L\frac{di_{L3}}{dt} &= \frac{1}{3}v_{C1}+\frac{1}{3}v_{C2}-\frac{2}{3}v_{C3}-\frac{1}{3}v_{g1}s_{11}-\frac{1}{3}v_{g2}s_{12}+\frac{2}{3}v_{g3}s_{13};
\end{aligned}
\tag{6.3}
$$

$$C_1 \frac{dv_{C1}}{dt} = i_{L1} - R_1 v_{C1};$$
$$C_2 \frac{dv_{C2}}{dt} = i_{L2} - R_2 v_{C2}; \tag{6.4}$$
$$C_3 \frac{dv_{C3}}{dt} = i_{L3} - R_3 v_{C3};$$

$$s_{1j}(t) = \begin{cases} 1 & \text{for} \quad S_{1j} = ON \quad \& \quad S_{2j} = OFF \\ 0 & \text{for} \quad S_{1j} = OFF \quad \& \quad S_{2j} = ON \end{cases} \quad j = 1,2,3. \tag{6.5}$$

This dynamical model is given in (*a,b,c*) frame of references. For the control purposes this model is transformed into (*d,q*) frame of references as follows,

$$\frac{di_{Ld}}{dt} = -\frac{v_{cd}}{L} + \omega_r i_{Lq} + \frac{v_g}{L} u_d(S_i);$$
$$\frac{di_{Lq}}{dt} = -\frac{v_{cq}}{L} - \omega_r i_{Ld} + \frac{v_g}{L} u_q(S_i); \tag{6.6}$$

$$\frac{dv_{cd}}{dt} = -\frac{v_{cd}}{RC} + \omega_r v_{cq} + \frac{i_{Ld}}{C};$$
$$\frac{dv_{cq}}{dt} = -\frac{v_{cq}}{RC} - \omega_r v_{cd} + \frac{i_{Lq}}{C}; \tag{6.7}$$

$$\frac{d\theta_r}{dt} = \omega_r;$$
$$\mathbf{u_{dq}} = \mathbf{F}(\theta_r)\mathbf{u}, \tag{6.8}$$

where ω_r is the angular velocity of the desired output voltage, control vector $\mathbf{u}$ is defined in stationary (*a,b,c*) frame as,

$$u_j(t) = \begin{cases} 1 & \text{with switch} \quad S_{1j} = \text{ON} \quad \text{and} \quad \text{S}_{2\text{j}} = \text{OFF} \\ 0 & \text{with switch} \quad S_{1j} = \text{OFF} \quad \text{and} \quad \text{S}_{2\text{j}} = \text{ON} \end{cases}; \quad j = 1,2,3, \tag{6.9}$$

and $u_d(S_i)$ and $u_q(S_i)$, $i = 1,...,8$ correspond to control inputs based on the permissible switch combinations as shown in the Figure 6-43 .

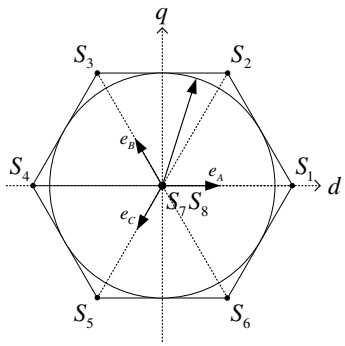

Figure 6-43 Permissible switch configurations for three phase inverter

Control of the three phase inverter is done by controlling the inductor currents to their reference values. As a result of voltage control these current references are calculated. For inductor current control, errors are constructed as $\sigma_d = i_{Ld}^{ref}(t) - i_{Ld}$ and $\sigma_q = i_{Lq}^{ref}(t) - i_{Lq}$. Taking the time derivative of the current errors following expressions are obtained,

$$\begin{aligned} \frac{d\sigma_d}{dt} &= \frac{di_{Ld}^{ref}}{dt} - \frac{di_{Ld}}{dt}; \\ \frac{d\sigma_q}{dt} &= \frac{di_{Lq}^{ref}}{dt} - \frac{di_{Lq}}{dt}. \end{aligned} \tag{6.10}$$

Now by substituting the current dynamics from (6.6) into (6.10) and equating the error derivatives to zero expressions for equivalent control are obtained as in (6.12) .

$$\begin{aligned} \frac{d\sigma_d}{dt} &= \frac{di_{Ld}^{ref}}{dt} + \frac{v_{cd}}{L} - \omega_r i_{Lq} - \frac{v_g}{L} u_d(S_i) = 0; \\ \frac{d\sigma_q}{dt} &= \frac{di_{Lq}^{ref}}{dt} + \frac{v_{cq}}{L} + \omega_r i_{Ld} - \frac{v_g}{L} u_q(S_i) = 0; \end{aligned} \tag{6.11}$$

$$\begin{aligned} u_d^{eq} &= \frac{L}{v_g}\left(\frac{di_{Ld}^{ref}}{dt} + \frac{v_{cd}}{L} - \omega_r i_{Lq} \right); \\ u_q^{eq} &= \frac{L}{v_g}\left(\frac{di_{Lq}^{ref}}{dt} + \frac{v_{cq}}{L} + \omega_r i_{Ld} \right). \end{aligned} \tag{6.12}$$

As discussed earlier equivalent control is the component of the control that, once applied to the plant, guaranties that change of error is zero. Substituting (6.12) back into (6.11) following expressions are obtained,

$$\begin{aligned} \frac{d\sigma_d}{dt} &= \frac{v_g}{L}\left(u_d^{eq} - u_d(S_i) \right); \\ \frac{d\sigma_q}{dt} &= \frac{v_g}{L}\left(u_q^{eq} - u_q(S_i) \right). \end{aligned} \tag{6.13}$$

Control selection is done using sliding mode control design principle based on Lyapunov stability criteria, namely, $\dot{\sigma}_d \sigma_d < 0$ and $\dot{\sigma}_q \sigma_q < 0$. This condition can be expressed in somewhat different form as,

$$\begin{aligned} sign\left(u_d^{eq} - u_d(S_i) \right) &= -sign(\sigma_d) \\ sign\left(u_q^{eq} - u_q(S_i) \right) &= -sign(\sigma_q) \end{aligned} \tag{6.14}$$

Control problem is now narrowed down to the selection of one of the permissible switch configuration that will in turn guaranty sliding mode existence and $\sigma_d, \sigma_q = 0$.

Figure 6-44 depicts the all of the possible switch combinations and resulting values of $\left(L/v_g\right)\dot{\boldsymbol{\sigma}}_{\mathbf{dq}}$ vector. Since there are often more than one switch combinations satisfying the constraints from (6.14) an additional constraint can be added such that switch is selected according to the minimum change of error. Switching algorithm is summarized in (6.15).

$$S_i = \left\{ \begin{array}{c} \min \left\| \mathbf{u}_{eq}(t) - \mathbf{u}\ \left(S_i\right) \right\| \\ \& \\ sign\left\{ \left[u_{eqd} - u_d\left(S_i\right) \right] \cdot \sigma_d(t) \right\} = -1 \\ \& \\ sign\left\{ \left[u_{eqq} - u_q\left(S_i\right) \right] \cdot \sigma_q(t) \right\} = -1 \end{array} \right\}; \quad i = \left(1,2, \ldots\ldots\ldots ,8,9\right). \tag{6.15}$$

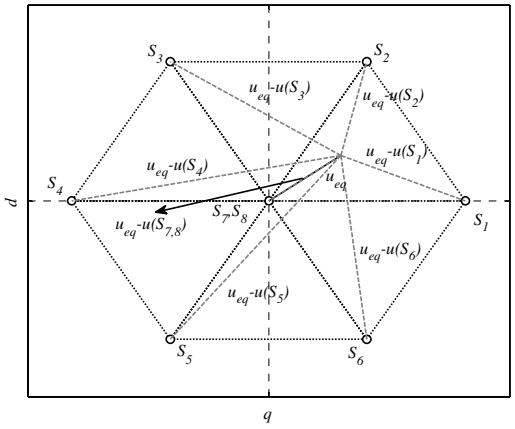

Figure 6-44 Selection of control for given vector of equivalent control

Inductor current control achieves that $i_{Ld}^{ref} = i_{Ld}$ and $i_{Lq}^{ref} = i_{Lq}$. Now i_{Ld}^{ref} and i_{Lq}^{ref} can be selected according to the desired output behavior. For this simulation case output capacitor voltage control is targeted. For capacitor voltage control errors are selected as $\sigma_d = v_{cd}^{ref} - v_{cd}$ and $\sigma_q = v_{cq}^{ref} - v_{cq}$ and resulting reference inductor current is obtained using following expressions,

$$\begin{aligned} i_{Ld}^{ref} &= \frac{C}{\tau} \cdot v_{Cd}^{ref} - (\frac{C}{\tau} - \frac{1}{R}) \cdot v_{Cd} - C \cdot \omega_r \cdot v_{Cq}; \\ i_{Lq}^{ref} &= \frac{C}{\tau} \cdot v_{Cq}^{ref} - (\frac{C}{\tau} - \frac{1}{R}) \cdot v_{Cq} + C \cdot \omega_r \cdot v_{Cd}, \end{aligned} \tag{6.16}$$

where τ can be seen as the response time constant. Control block diagram of three phase buck inverter is shown in Figure 6-45.

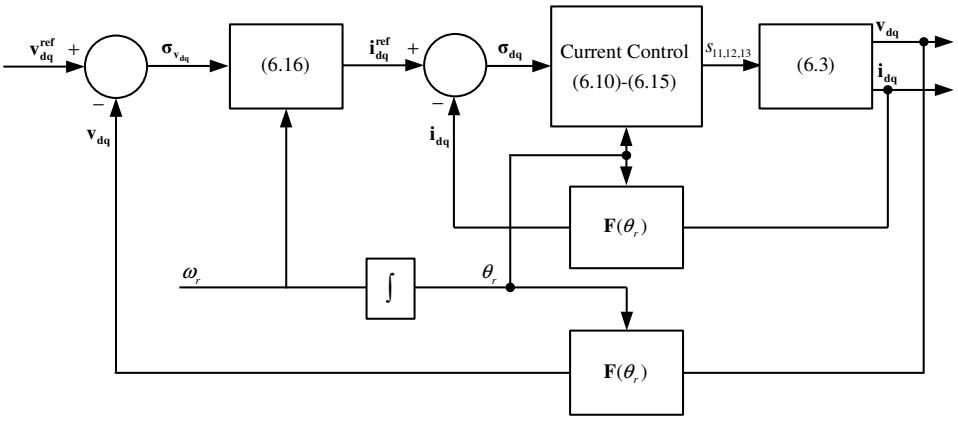

Figure 6-45 Three phase inverter control block diagram

Model was simulated using Matlab/Simulink 2012 and desired variables are plotted for the simulation scenario. Results of the voltage control are shown in Figure 6-46 and Figure 6-47. For the controller test purposes the *d* component of the voltage is changed from initial 220V to 310V and lowered down to 220V after some time. The responses are shown in Figure 6-46. Settling time is dictated by the τ parameter in (6.16). Similarly response for *q* component of the voltage is given in Figure 6-47, where the reference is changed from 0V to 120V and back to 0V. Controller shows excellent performance with desired settling time, no overshoot and minimum steady state error.

Resulting capacitor voltages in *(a,b,c)* frame of references are shown in Figure 6-48. Capacitor voltages are sinusoidal in shape, their amplitude is determined by *d* and *q* component magnitudes and have desired angular frequency value (for the simulation purposes 60Hz).

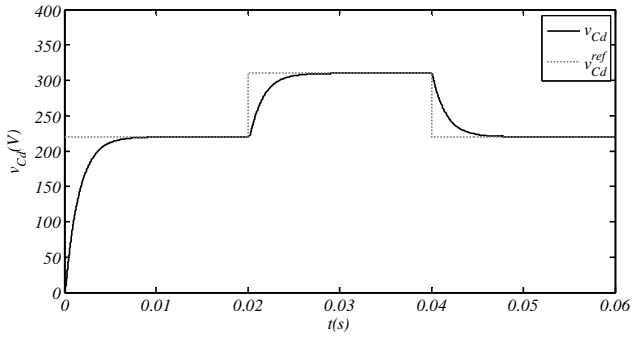

Figure 6-46 Voltage control response – *d* component

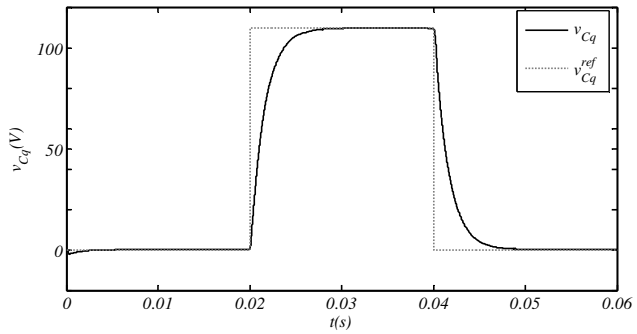

Figure 6-47 Voltage control response – q component

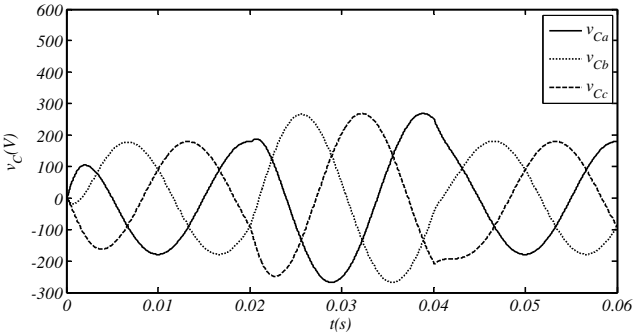

Figure 6-48 Capacitor voltage response – (a,b,c) frame of references

As mentioned earlier for given voltage control, inductor current references are generated and inductor current controller performs control based on those references. The inductor current responses for voltage control in this simulation scenario are given in Figure 6-49 (d component) and Figure 6-50 (q component). Switching consequences can be seen in current ripples. The magnitude of these current ripples is dictated by the width of hysteresis used in current controller. Hysteresis is used for implementation of sign function as relay to avoid high switching frequencies. Switch selection is shown in Figure 6-51 in (α,β) frame of references. Simulation parameters are given in Table 6-6.

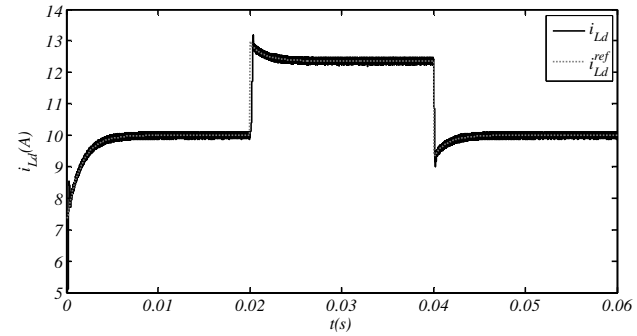

Figure 6-49 Inductor current response – d component

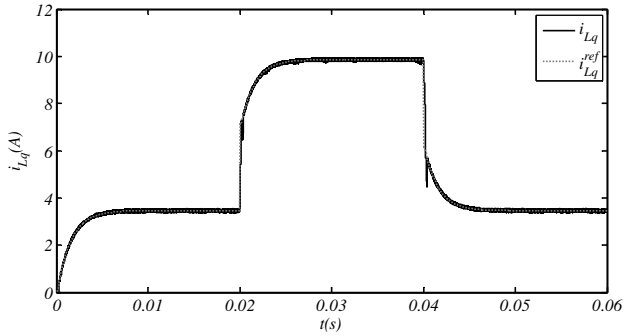

Figure 6-50 Inductor current response – q component

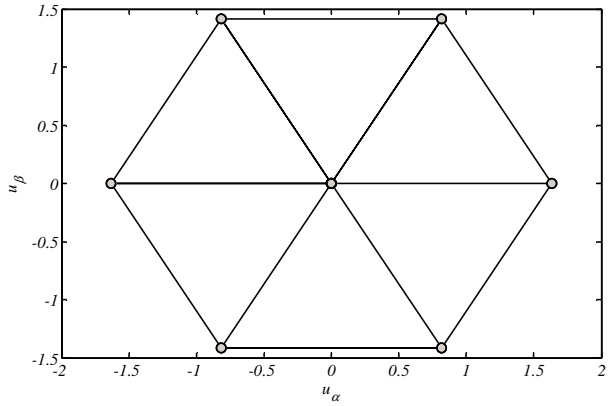

Figure 6-51 Switches state selection according to the switching algorithm

DC-AC buck inverter simulation parameters	
Inductor value L	15mH
Capacitor value C	50μF
Load resistance R	22Ω
Input voltage v_g	538V
Synchronous speed ω_r	2π50 rad/s
Time constant τ	1.5 ms
ODE solver and step size	Ode1 (euler), 1e-6s

Table 6-6 Three phase inverter simulation parameters

For the purposes of experimental verification of the designed controller experimental setup depicted in Figure 6-41 is used. Current control of three phase inverter with rotor circuit attached at its output is realized. DFIG rotor circuit can be seen as the load of the inverter. Experiment scenario is depicted in Figure 6-52.

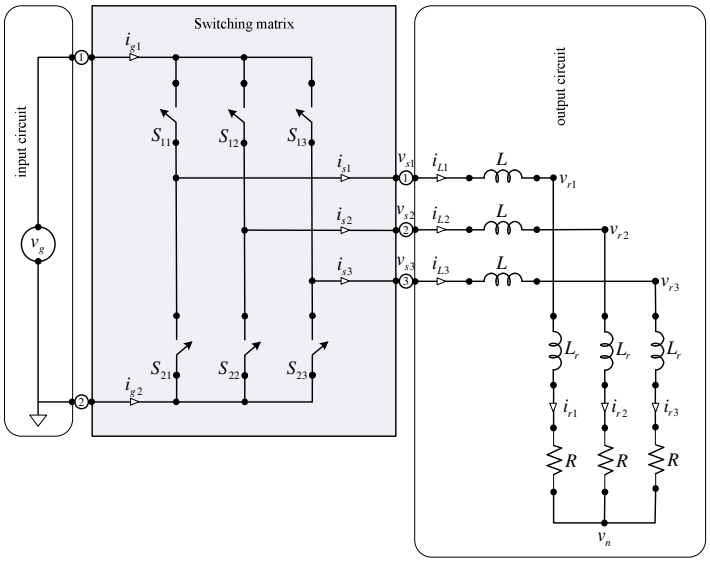

Figure 6-52 Three phase inverter with DFIG rotor circuit as the load

For the circuit in Figure 6-52 inductor currents dynamics in the synchronous frame of references can be rewritten as follows,

$$\begin{aligned} L\frac{di_{Ld}}{dt} &= -v_{rd} + L\omega_r i_{Lq} + v_g u_d\left(S_i\right); \\ L\frac{di_{Lq}}{dt} &= -v_{rq} - L\omega_r i_{Ld} + v_g u_q\left(S_i\right); \end{aligned} \tag{6.17}$$

$$\begin{aligned} \frac{d\theta_r}{dt} &= \omega_r; \\ \mathbf{u_{dq}} &= \mathbf{F}(\theta_r)\mathbf{u}, \end{aligned} \tag{6.18}$$

where ω_r is the angular velocity of the desired DFIG rotor voltage. Rotor current dynamics can be rewritten from (3.13) and (3.14) as,

$$\begin{aligned} L_r\frac{di_{rd}}{dt} &= v_{rd} - R_r i_{rd} + \omega_r\left(L_r i_{rq} + L_m i_{sq}\right) - L_m\frac{di_{sd}}{dt}; \\ L_r\frac{di_{rq}}{dt} &= v_{rq} - R_r i_{rq} - \omega_r\left(L_r i_{rd} + L_m i_{sd}\right) - L_m\frac{di_{sq}}{dt}. \end{aligned} \tag{6.19}$$

with desired angular velocity $\omega_r = \omega_s - \omega$. All the variables of DFIG rotor current dynamics are explained in Chapter 3. By expressing (6.19) in terms of rotor voltages, substituting them into (6.17) and noting that $i_{rq} = i_{Lq} = i_{Lq}^*$ and $i_{rd} = i_{Ld} = i_{Ld}^*$ following current dynamics can be obtained,

$$\frac{di_{Ld}^{*}}{dt}=\underbrace{\frac{1}{(L+L_r)}\left(-R_r i_{Ld}^{*}+(L+L_r)\omega_r i_{Lq}^{*}+L_m\omega_r i_{sq}-L_m\frac{di_{sd}}{dt}\right)}_{f_{sd}}+\underbrace{\left(\frac{v_g}{(L+L_r)}\right)}_{B_{sd}}u_d(S_i);$$
$$\frac{di_{Lq}^{*}}{dt}=\underbrace{\frac{1}{(L+L_r)}\left(-R_r i_{Lq}^{*}-(L+L_r)\omega_r i_{Ld}^{*}+L_m\omega_r i_{sd}-L_m\frac{di_{sq}}{dt}\right)}_{f_{sq}}+\underbrace{\left(\frac{v_g}{(L+L_r)}\right)}_{B_{sq}}u_q(S_i); \quad (6.20)$$

Current controller can now be designed as described earlier. For the implementation purposes equivalent control is estimated with equivalent control observer from [129].

When doubly fed induction generator is integrated in HES, its power references are generated by the MPPT algorithm. Active and reactive powers are controlled by controlling stator currents. Control of stator currents can be implemented considering the stator current dynamics from (3.11) and (3.12), where corresponding rotor currents are considered as the control input. In other words $i_{Ld}^{*ref}(t)$ and $i_{Lq}^{*ref}(t)$ are obtained from the stator current control loop.

In general DFIG can act as either voltage or current source. When DFIG is used in grid connected mode, stator voltage is defined by grid voltage and DFIG acts as the current source. On the other hand, when DFIG is used in island mode, stator voltage is defined by the currents flowing in stator circuit and given loading so DFIG can act as the voltage source. In the following sections, behavior of the designed controller for both cases is examined and proposed current controller is tested for robustness in multiple scenarios.

In order to verify the performance of the rotor current controller, set of three basic experiments has been performed. DFIG rotor shaft is driven by an induction motor attached to it. Such setup is used to simulate the behavior of real wind turbine. In the first experiment rotor current controller performance was tested while no load was attached to the stator side of DFIG. Second experiment was performed when combination of resistive and inductive loads are suddenly connected and disconnected from the stator. For both of these experiments, rotor mechanical speed was kept constant. Third experiment was performed when the DFIG is subjected to the mechanical speed changes. All of the relevant results are shown below.

Rotor is supplied from a voltage source of 24V and speed change of wind turbine simulating asynchronous machine is changed manually. Three phase electrical load is connected to or disconnected from stator terminals by means of manual mechanical

switch. In all of the experiments current responses are looked at individually, in other words, when $i_{Ld}^{*ref}(t)$ is supplied, $i_{Lq}^{*ref}(t)$ is kept at zero and vice versa.

In the first experiment stator circuit is left open (no load) and rotor mechanical speed is kept constant. Current reposes for d and q component are shown in Figure 6-53 and Figure 6-54. The controller shows satisfactory performance in both transient and steady state regions, with minimum steady state error and fast rise time. Rotational speed was kept constant at 125rad/s during the experiment.

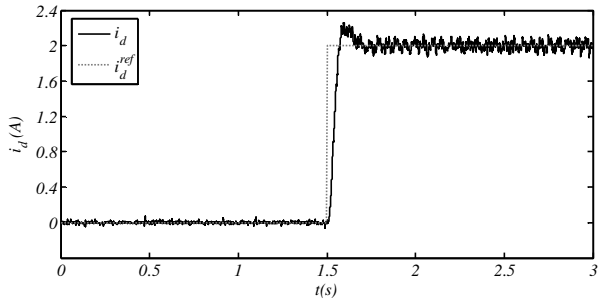

Figure 6-53 Current Controller Response, *d*-component, no load

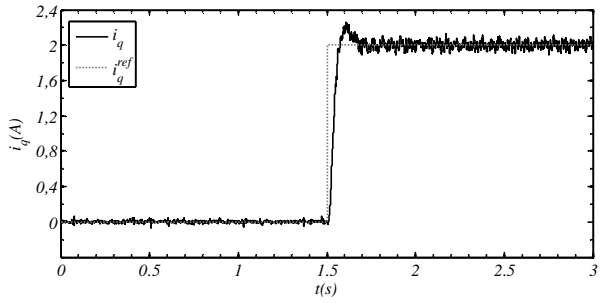

Figure 6-54 Current Controller Response, *q*-component, no load

In the second experiment current controller was tested against the stator load variation. Responses for the rotor *d* and *q* components of the current are shown in the Figure 6-55. and Figure 6-56 respectively. These responses resemble the responses from previous experiment. At some arbitrary point in time after 1.5s stator is connected to three phase resistive-inductive load and disconnected after an arbitrary time by operating manual switch. Clearly marked points on the figures as ”Load ON” and ”Load OFF” represent the load connection and disconnection. Presence of load causes stator currents to change, creating disturbance to the rotor side of DFIG. Nevertheless, current

controller shows robustness and it is able to quickly compensate for the occurring changes. Resistance and inductance of the load have values of 200Ω and 19mH respectively. Rotational speed was kept constant at 125rad/s in this experiment as well.

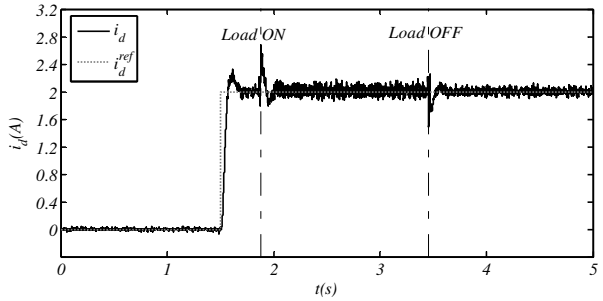

Figure 6-55 Current Controller Response, *d*-component, resistive-inductive load

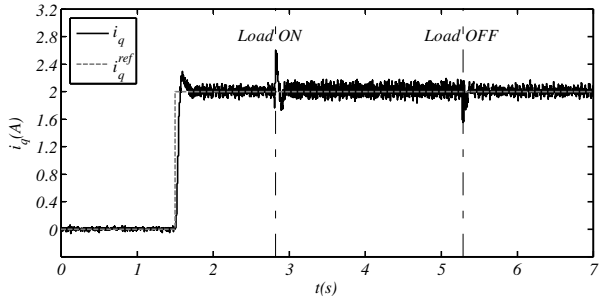

Figure 6-56 Current Controller Response, *q*-component, resistive-inductive load

In third experiment *d* and *q* current references are kept at the same value as for previous experiments. Resistive-inductive load is connected to the stator terminals and controller response is examined for significant speed changes. Speed was changed manually throughout the experiment, the speed is at 125*rad/s* at the beginning of the experiment, then it drops to 80*rad/s* in less than 5.5*s* and rises back to 110*rad/s* by the end of 9*s* of experiment. Figure 6-57 shows the *q* component of output current response for mechanical speed changes. The *d* component has similar response and is not explicitly shown because of that. From the dynamics of rotor current it is obvious that the speed change influences the system response. Despite the changes in speed, current controller is capable of maintaining the desired value with slight increase in error.

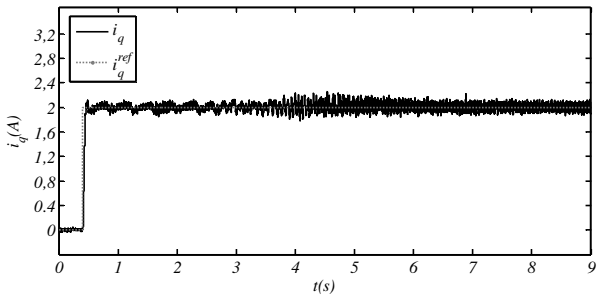

Figure 6-57 Current Controller Response, *q*-component, speed change case

For the sake of further experimentation and controller verification grid stator is connected to the utility grid and set of experiments was performed. Experiments are performed in the following manner. Firstly, controlled amount of *d* component of rotor current has been supplied to the rotor circuit. As a result voltage has been formed at the stator circuit. Magnitude of this current determines the amplitude of voltage formed at the stator. For these experiments current magnitude has been determined to be 4A. After the desired stator voltage is reached and synchronization between grid and stator is achieved, stator is tied to the grid and desired current step references are supplied.

In this experiment, *q* component of rotor current response and its contribution to the power flow from stator circuit has been clearly shown. Current controller performance is observed with step reference current response as shown in Figure 6-58.

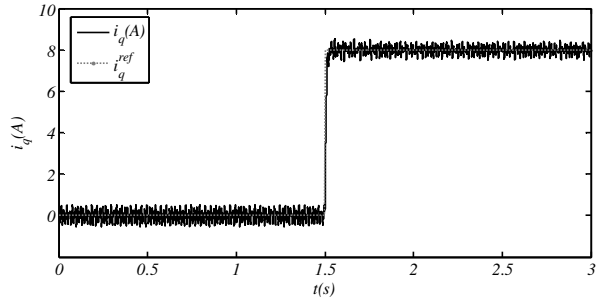

Figure 6-58 Current controller response, *q*-component

As it can be seen from the stator current dynamics, *q* component of rotor current affects the *d* component of stator current which in turn changes the active power flowing from stator. Step change of converter *q* current component causes step change in *d* component stator current and consequently step change of active power that flow from stator to the grid. For a rotor current *q* component reference of 8A we can observe

the change in stator *d* component current of $i_{ds} = 1.46A$ as shown in the Figure 6-59. Utility grid is connected to DFIG through step down transformer so that grid voltage seen by stator is 100V peak. Stator voltage is oriented with *d* component of grid voltage so $v_{ds} = 100V$. With $i_{ds} = 1.46A$ and $v_{ds} = 100V$, stator active power is $P_s = 219W$, this result is verified in Figure 6-60.

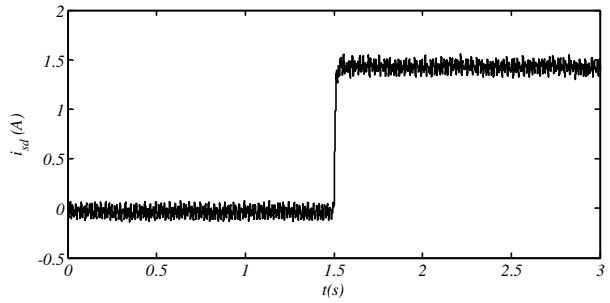

Figure 6-59 d-component stator current change for q- component rotor current step change

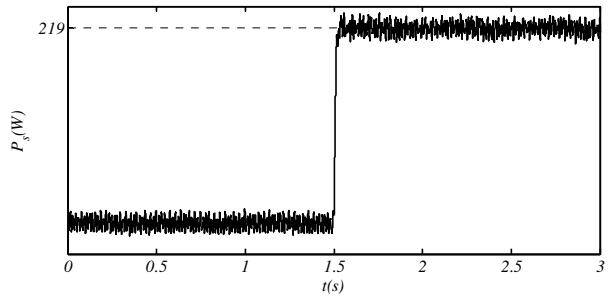

Figure 6-60 Active stator power change for current step change

7 CONCLUSION AND FUTURE WORK

Microgrid is relatively new concept and research on this topic is still in its infant stage. As literature review, done in the second chapter of this thesis, suggests, the research topics in this area are diverse and wide. Microgrids are substantially different than the classical electrical distribution network because they are dominated by the sources that are integrated through power electronic devices. In addition to that, in microgrid, usually all of the sources act together to form a stable and reliable electrical network. Due to these facts, majority of the research challenges in this field are found in the area of power conversion, power control and power management.

Sources, storage units and loads are interfaced to the microgrid through power electronics. In this way their controllability is increased but in the same time this makes the control problem more complex. For the sake of easier implementation of microgrids and reducing the control problem complexity, hybrid energy source is introduced to microgrid. In hybrid energy source all power conversion, control and management is done locally and microgrid acts as a supervisor to such a system. Hybrid energy source integrates renewable energy sources that are characterized with stochastic power delivery dependent on the environmental conditions. It additionally includes storage units and sometimes other dispatchable sources to smooth out power profile and be able to deliver power on demand. As such hybrid energy source from microgrid perspective can be seen as a dispatchable (intelligent) source.

7.1 Summary

In this thesis we discuss a control framework that, up to a large extent, standardizes the way the hybrid energy source, as a part of microgrid, is controlled and analyzed. In that light, modeling and analysis of selected renewable energy sources (wind, PV, fuel cell) and storage units (battery) is done. Such analysis is done with the

sole purpose of understanding the electrical characteristics and power behavior of those sources and storage units. Result of this analysis gave an insight in the operational requirements for power electronics interface in hybrid energy source.

Following the modeling and electrical analysis of the sources and storage units, their power electronics interfaces and control system requirements are defined. Power electronics interfaces and their control systems showed many structural and functional similarities. Resulting from that fact, generalized power electronics interface and control system is derived and presented at the end of the third chapter.

Analysis and control of converter topologies is presented in fourth chapter. This chapter is the main technical core of the thesis. Firstly, power electronics converters are analyzed as switching matrix to generally describe their functionality. Further the switching matrix characteristics are applied to the analysis of DC-DC, single phase AC (rectifier and inverter) and three phase AC (rectifier and inverter). The structural and functional similarities between all of the converters become obvious once the analysis is done in this way. After obtaining the dynamics of the mentioned converters the control system design is discussed. Most important results are obtained for the current controller of three phase converters, where it is shown that the same algorithm can be applied to all three phase converters (buck inverter/rectifier, boost inverter/rectifier). Switching algorithm used to produce switching signals for the converters is realized as the direct consequence of sliding mode control, which in turn brings all of the advantages of this control into attention.

Last topic that is discussed in this thesis is the interconnection of hybrid source to microgrid. In the scope of discussion three main points are covered, namely, power control and management, control of converter interfacing DC bus of hybrid source and microgrid and maximum power point tracking method for renewable energy sources. Control and management of power inside the hybrid energy source and microgrid in general is indeed hot research topic. Use of dispatching algorithms and linear programming is one of the possible solutions; another solution is based on the rule based strategies possibly including some intelligent control methods (fuzzy, neural network). In this thesis we don't go into details of implementation of those methods nor do we propose specific solution since this topic is out of the scope of the thesis. Information given is solely for to have completeness of the text. On the other hand power control of the so called output side converter is discussed in detail and mathematical formulation of the problem is given. Since this converter acts both as the

current source converter and voltage source converter depending on the microgrid requirements (modes of operation), a control strategy is developed for both cases. Finally maximum power point tracking for the power control of renewable energy sources is discussed.

Verification of control algorithms is done both experimentally and by simulation. All of the relevant experimental and simulation results are discussed in sixth chapter. Experimental results include the current control of DC-DC buck and boost converters and voltage control of DC-DC buck converter. PV emulator is implemented using buck converter with output voltage control where voltage reference is generated according to the i-v characteristics of PV module. Experimental results verifying the proposed MPPT algorithm are done using boost converter attached to the output of PV emulator. Boost is current controlled where reference current is generated by the MPPT algorithm. Finally simulation and experimental results for control of three phase switching inverter is presented. Simulation is done for inverter feeding a balanced resistive three phase load and experimental results are obtained by considering control of inverter feeding a rotor circuit of doubly fed induction generator (in literature referred to as rotor side converter - RSC). Three phase current controller is tested for robustness against different disturbances and shows satisfactory results.

7.2 Contributions of the Thesis

Throughout the thesis much information is presented to achieve the completeness of the text however the main contributions of this thesis can be narrowed down to the following;

- Generalization of control problem for power electronics interfaces in hybrid energy source;
- Development of switching algorithm for three phase switching converters based on the closed loop behavior of the converters;
- Development of a maximum power point tracking algorithm for the renewable energy sources.

7.2.1 Generalization of Control Problem for Power Electronics Interfaces in HES

The hybrid energy source control system can be divided into three different layers as discussed in the Chapter 5. Top layer is responsible for power management such that power sharing is guaranteed among the available sources and storage units according to some predefined strategy and power references obtained from the microgrid controller. Middle layer is responsible for power control based on the references generated by the top layer; and bottom layer of the control system achieves the current control in each individual converter. In this thesis generalization of the control approach is done for the bottom and middle layer of the HES control system.

Main power electronic converter topologies used for interface of hybrid energy source are DC-DC converters for DC sources, AC-DC rectifiers for AC sources and DC-AC inverters for the hybrid energy source interface to microgrid electrical network which is usually AC type. Using the analysis procedure developed in Chapter 4 the mathematical description for the dynamics of the converter is given. It has been shown that dynamics description can be put into certain mathematical form to describe a class of systems for which the control approach is then developed. The control approach is based on sliding mode control principles and it has been shown that the same design can be done for all of the converters. This result is particularly interesting from the standardization point of view. Control of the converters is done as the two step approach; first the control input is found that realizes the inductor current control (bottom layer); and then inductor current reference is found as the result of control of some other relevant variable – in the case of HES it is power (middle layer). Such cascaded control approach allows for the control design as for systems with reduced order dynamics.

7.2.2 Switching Algorithm for Three Phase Switching Converters

In Chapter 4 switching algorithm for the three phase converters is developed. Switching pattern for three phase converters is determined based on the desired closed loop behavior of converter. Control design is performed such that sliding mode exists in a manifold resulting in reference current tracking. Reference current generation is done taking into consideration the desired closed loop behavior of the converter. Switching

algorithm combines the closed loop behavior and selection of switching pattern into one problem which is usually not the case for majority of the control methods found in literature. Current control is performed in (d,q) frame of references resulting in two values of control, however, since the control vector has three components for three phase converter the selection of switching pattern may not have unique solution. In the presented algorithm an additional constraint is added so switching pattern is selected to guaranty the minimum rate of change of error. In this way number of switch transitions is minimized leading to the minimization of switching losses. The switching algorithm is summarized in (4.112) and with minimum modifications can be applied to all three phase switching converters.

7.2.3 MPPT Algorithm for the Renewable Energy Sources

MPPT algorithm details are given in Chapter 5. This algorithm is based on the sliding mode control optimization proposed in [128]. Original optimization algorithm was used in anti-lock breaking system implementation for slip minimization. In this thesis we present modified version of that algorithm with applications as the MPPT for PV module, wind turbine and fuel cell. Following modifications to the algorithm are done; optimization is treated as the maximization problem and discontinuous control function and relay elements are replaced with their smooth counterparts. By the second implementation strictly speaking the sliding mode is lost however the algorithm exhibits less oscillation around the maximum point. MPPT algorithm is formulated for applications in control of PV module, wind turbine and fuel cell. The control follows earlier described procedure where converters attached to the sources are current compensated and MPPT has sole function of power maximization.

7.3 Future Work

Future work will mostly be based on the improvement of switching algorithm for three phase converters. Since the calculation of control vector from values of control obtained in (d,q) or (α,β) frame of references doesn't have unique solution additional requirements can be added to the control system. These requirements can be related to

the minimization of total harmonic distortion, for example.

Another future development will be the construction of the complete hybrid system emulator. The development of this emulator is started through this thesis by constructing the 30W PV module emulator and 1.1kW DFIG based wind turbine emulator. Future work will focus on the implementation of emulator for fuel cell and addition of battery storage system. This kind of experimental setup would allow realization of more heavy duty experiments with the complete HES system. It could further be used for testing of power management and power sharing strategies.

REFERENCES

[1] Lasseter, Robert H. "Microgrids and distributed generation." *Journal of Energy Engineering* 133.3 (2007): 144-149.

[2] Ackermann, Thomas, Göran Andersson, and Lennart Söder. "Distributed generation: a definition." *Electric power systems research* 57.3 (2001): 195-204.

[3] Basu, Ashoke Kumar, et al. "Microgrids: Energy management by strategic deployment of DERs—A comprehensive survey." *Renewable and Sustainable Energy Reviews* 15.9 (2011): 4348-4356.

[4] Lasseter, Robert, et al. "Integration of distributed energy resources. The CERTS Microgrid Concept." (2002). [5] Lasseter, Robert H., and Paolo Paigi. "Microgrid: a conceptual solution." *Power Electronics Specialists Conference, 2004. PESC 04. 2004 IEEE 35th Annual*. Vol. 6. IEEE, 2004.

[6] Lasseter, Robert H. "Smart distribution: Coupled microgrids." *Proceedings of the IEEE* 99.6 (2011): 1074-1082.

[7] Varaiya, Pravin P., Felix F. Wu, and Janusz W. Bialek. "Smart operation of smart grid: Risk-limiting dispatch." *Proceedings of the IEEE* 99.1 (2011): 40-57.

[8] Majumder, Ritwik, et al. "Power management and power flow control with back-to-back converters in a utility connected microgrid." *Power Systems, IEEE Transactions on* 25.2 (2010): 821-834.

[9] Hatziargyriou, Nikos, et al. "Microgrids." *Power and Energy Magazine, IEEE* 5.4 (2007): 78-94.

[10] Farhangi, Hassan. "The path of the smart grid." *Power and Energy Magazine, IEEE* 8.1 (2010): 18-28.

[11] Jenkins, Nicholas. "Embedded generation. Part 1." *Power engineering journal*9.3 (1995): 145-150.

[12] Chowdhury, Sunetra, and Peter Crossley. *Microgrids and active distribution networks*. The Institution of Engineering and Technology, 2009.

[13] Sels, Tom, Catalin Dragu, Thierry Van Craenenbroeck, and Ronnie Belmans. "Electrical energy storage systems: Existing systems versus newest systems-an overview." In *International Conference Power Generation and Sustainable Development (AIM), Liège, Belgium, Oct*, pp. 8-9. 2001.

[14] Tan, Xingguo, Qingmin Li, and Hui Wang. "Advances and trends of energy storage technology in Microgrid." *International Journal of Electrical Power & Energy Systems* 44.1 (2013): 179-191.

[15] Katiraei, Farid, et al. "Microgrids management." *Power and Energy Magazine, IEEE* 6.3 (2008): 54-65.

[16] Driesen, Johan, and Farid Katiraei. "Design for distributed energy resources."*Power and Energy Magazine, IEEE* 6.3 (2008): 30-40.

[17] Lund, Henrik, et al. "From electricity smart grids to smart energy systems–a market operation based approach and understanding." *Energy* 42.1 (2012): 96-102.

[18] Kurohane, Kyohei, et al. "A hybrid smart AC/DC power system." *Industrial Electronics and Applications (ICIEA), 2010 the 5th IEEE Conference on*. IEEE, 2010.

[19] Molderink, Albert, et al. "Management and control of domestic smart grid technology." *Smart Grid, IEEE Transactions on* 1.2 (2010): 109-119.

[20] Mizuguchi, K., et al. "A new decentralized DC power system for telecommunications systems." *Telecommunications Energy Conference, 1990. INTELEC'90., 12th International*. IEEE, 1990.

[21] Ciezki, John G., and Robert W. Ashton. "Selection and stability issues associated with a navy shipboard DC zonal electric distribution system." *Power Delivery, IEEE Transactions on* 15.2 (2000): 665-669.

[22} Chan, C. C. "The state of the art of electric and hybrid vehicles." *Proceedings of the IEEE* 90.2 (2002): 247-275.

[23] Xu, Lie, and Dong Chen. "Control and operation of a DC microgrid with variable generation and energy storage." *Power Delivery, IEEE Transactions on* 26.4 (2011): 2513-2522.

[24] Lago, Jackson, and Marcelo Lobo Heldwein. "Operation and control-oriented modeling of a power converter for current balancing and stability improvement of DC active distribution networks." *Power Electronics, IEEE Transactions on* 26.3 (2011): 877-885.

[25] Baran, Mesut E., and Nikhil R. Mahajan. "DC distribution for industrial systems: opportunities and challenges." *Industry Applications, IEEE Transactions on*39.6 (2003): 1596-1601.

[26] Sannino, Ambra, Giovanna Postiglione, and Math HJ Bollen. "Feasibility of a DC network for commercial facilities." *Industry Applications, IEEE Transactions on* 39.5 (2003): 1499-1507.

[27] Chakraborty, Arindam. "Advancements in power electronics and drives in interface with growing renewable energy resources." *Renewable and Sustainable Energy Reviews* 15.4 (2011): 1816-1827.

[28] Baroudi, Jamal A., Venkata Dinavahi, and Andrew M. Knight. "A review of power

converter topologies for wind generators." *Renewable Energy* 32.14 (2007): 2369-2385.

[29] Biczel, Piotr. "Power electronic converters in DC microgrid." *Compatibility in Power Electronics, 2007. CPE'07*. IEEE, 2007.

[30] Justo, Jackson John, et al. "AC-microgrids versus DC-microgrids with distributed energy resources: A review." *Renewable and Sustainable Energy Reviews* 24 (2013): 387-405.

[31] Chakraborty, Sudipta, Manoja D. Weiss, and Marcelo Godoy Simoes. "Distributed intelligent energy management system for a single-phase high-frequency AC microgrid." *Industrial Electronics, IEEE Transactions on* 54.1 (2007): 97-109.

[32] Strzelecki, Ryszard, and Grzegorz Benysek. *Power electronics in smart electrical energy networks*. London: Springer, 2008.

[33] Wang, Xiongfei, et al. "A review of power electronics based microgrids." *Journal of Power Electron* 12.1 (2012): 181-192.

[34] Jiang, Zhenhua, and Xunwei Yu. "Hybrid DC-and AC-linked microgrids: towards integration of distributed energy resources." *Energy 2030 Conference, 2008. ENERGY 2008. IEEE*. IEEE, 2008.

[35] Barave, Sushant P., and Badrul H. Chowdhury. "Hybrid AC/DC power distribution solution for future space applications." *Power Engineering Society General Meeting, 2007. IEEE*. IEEE, 2007.

[36] Wang, Peng, et al. "Harmonizing AC and DC: A Hybrid AC/DC Future Grid Solution." *Power and Energy Magazine, IEEE* 11.3 (2013): 76-83.

[37] Hatti, M., A. Meharrar, and M. Tioursi. "Power management strategy in the alternative energy photovoltaic/PEM Fuel Cell hybrid system." *Renewable and Sustainable Energy Reviews* 15.9 (2011): 5104-5110.

[38] Peas Lopes, J. A., C. L. Moreira, and A. G. Madureira. "Defining control strategies for microgrids islanded operation." *Power Systems, IEEE Transactions on* 21.2 (2006): 916-924.

[39] Serban, Emanuel, and Helmine Serban. "A control strategy for a distributed power generation microgrid application with voltage-and current-controlled source converter." *Power Electronics, IEEE Transactions on* 25.12 (2010): 2981-2992.

[40] Shahabi, M., et al. "Microgrid dynamic performance improvement using a doubly fed induction wind generator." *Energy Conversion, IEEE Transactions on*24.1 (2009): 137-145.

[41] Kasem Alaboudy, A. H., H. H. Zeineldin, and James L. Kirtley. "Microgrid stability characterization subsequent to fault-triggered islanding incidents."*Power Delivery, IEEE Transactions on* 27.2 (2012): 658-669.

[42] Lidula, N. W. A., and A. D. Rajapakse. "Microgrids research: A review of experimental microgrids and test systems." *Renewable and Sustainable Energy*

Reviews 15.1 (2011): 186-202.

[43] Karki, Shankar, et al. "Efficiency improvements through combined heat and power for on-site distributed generation technologies." *Cogeneration and Distributed Generation Journal* 22.3 (2007): 19-34.

[44] Majumder, Ritwik, et al. "Power management and power flow control with back-to-back converters in a utility connected microgrid." *Power Systems, IEEE Transactions on* 25.2 (2010): 821-834.

[45] IEEE Standards Association. "IEEE std 1547.4-2011, IEEE guide for design, operation, and integration of distributed resource island systems with electric power systems [S]." *New York: IEEE* (2011).

[46] Østergaard, Poul Alberg. "Comparing electricity, heat and biogas storages' impacts on renewable energy integration." *Energy* 37.1 (2012): 255-262.

[47] Madureira, A. G., and JA Pecas Lopes. "Coordinated voltage support in distribution networks with distributed generation and microgrids." *IET Renewable Power Generation* 3.4 (2009): 439-454.

[48] Dobakhshari, AMRA Salehi, Sadegh Azizi, and Ali Mohammad Ranjbar. "Control of microgrids: Aspects and prospects." *Networking, Sensing and Control (ICNSC), 2011 IEEE International Conference on*. IEEE, 2011.

[49] Lago, Jackson, and Marcelo Lobo Heldwein. "Operation and control-oriented modeling of a power converter for current balancing and stability improvement of DC active distribution networks." *Power Electronics, IEEE Transactions on* 26.3 (2011): 877-885.

[50] Katiraei, Faridaddin, Mohammad Reza Iravani, and P. W. Lehn. "Micro-grid autonomous operation during and subsequent to islanding process." *Power Delivery, IEEE Transactions on* 20.1 (2005): 248-257.

[51] Majumder, Ritwik, et al. "Load sharing and power quality enhanced operation of a distributed microgrid." *Renewable Power Generation, IET* 3.2 (2009): 109-119.

[52] Noroozian, R., et al. "Combined operation of DC isolated distribution and PV systems for supplying unbalanced AC loads." *Renewable Energy* 34.3 (2009): 899-908.

[53] Zamora, Ramon, and Anurag K. Srivastava. "Controls for microgrids with storage: Review, challenges, and research needs." *Renewable and Sustainable Energy Reviews* 14.7 (2010): 2009-2018.

[54] Ross, M., et al. "Energy storage system scheduling for an isolated microgrid."*IET renewable power generation* 5.2 (2011): 117-123.

[55] Erdinc, O., and M. Uzunoglu. "Optimum design of hybrid renewable energy systems: Overview of different approaches." *Renewable and Sustainable Energy Reviews* 16.3 (2012): 1412-1425.

[56] Madureira, A. G., and JA Pecas Lopes. "Coordinated voltage support in

distribution networks with distributed generation and microgrids." *IET Renewable Power Generation* 3.4 (2009): 439-454.

[57] Guerrero, Josep M., et al. "Control strategy for flexible microgrid based on parallel line-interactive UPS systems." *Industrial Electronics, IEEE Transactions on* 56.3 (2009): 726-736.

[58] Lasseter, R. H., et al. "The CERTS microgrid concept." *White paper for Transmission Reliability Program, Office of Power Technologies, US Department of Energy* (2002).

[59] Soultanis, N. L., and N. D. Hatziargyriou. "Dynamic simulation of power electronics dominated micro-grids." *Power Engineering Society General Meeting, 2006. IEEE*. IEEE, 2006.

[60] Engler, Alfred. "Applicability of droops in low voltage grids." *International Journal of Distributed Energy Resources* 1.1 (2005): 3-15.

[61] Hatziargyriou, Nikos, Aris Dimeas, and Antonis Tsikalakis. "Centralized and decentralized control of microgrids." *International Journal of Distributed Energy Resources* 1.3 (2005): 197-212.

[62] Gil, Nuno José, and JA Peças Lopes. "Hierarchical frequency control scheme for islanded multi-microgrids operation." In *Power Tech*, pp. 473-478. 2007.

[63] Su, Wencong, and Jianhui Wang. "Energy management systems in microgrid operations." *The Electricity Journal* 25, no. 8 (2012): 45-60.

[64] Nguyen, Minh Y., Yong T. Yoon, and Nack H. Choi. "Dynamic programming formulation of micro-grid operation with heat and electricity constraints." In*Transmission & Distribution Conference & Exposition: Asia and Pacific, 2009*, pp. 1-4. IEEE, 2009.

[65] Alvarez, Eduardo, Antonio Campos Lopez, J. Gómez-Aleixandre, and N. de Abajo. "On-line minimization of running costs, greenhouse gas emissions and the impact of distributed generation using microgrids on the electrical system." In*Sustainable Alternative Energy (SAE), 2009 IEEE PES/IAS Conference on*, pp. 1-10. IEEE, 2009.

[66] Colson, C. M., M. H. Nehrir, and S. A. Pourmousavi. "Towards real-time microgrid power management using computational intelligence methods." In *Power and Energy Society General Meeting, 2010 IEEE*, pp. 1-8. IEEE, 2010. [67] Olivares, Daniel E., Claudio A. Cañizares, and Mehrdad Kazerani. "A centralized optimal energy management system for microgrids." In *Power and Energy Society General Meeting, 2011 IEEE*, pp. 1-6. IEEE, 2011.

[68] Hatziargyriou, N., Georges Contaxis, M. Matos, JA Pecas Lopes, Georges Kariniotakis, Didier Mayer, J. Halliday et al. "Energy management and control of island power systems with increased penetration from renewable sources." In*Power Engineering Society Winter Meeting, 2002. IEEE*, vol. 1, pp. 335-339. IEEE, 2002.

[69] Korpas, Magnus, and Arne T. Holen. "Operation planning of hydrogen storage connected to wind power operating in a power market." *Energy Conversion, IEEE*

Transactions on 21.3 (2006): 742-749.

[70] Chakraborty, Sudipta, and M. Godoy Simoes. "PV-microgrid operational cost minimization by neural forecasting and heuristic optimization." In *Industry Applications Society Annual Meeting, 2008. IAS'08. IEEE*, pp. 1-8. IEEE, 2008.

[71] Noroozian, R., and H. Vahedi. "Optimal management of MicroGrid using bacterial foraging algorithm." In *Electrical Engineering (ICEE), 2010 18th Iranian Conference on*, pp. 895-900. IEEE, 2010.

[72] Vahedi, H., R. Noroozian, and S. H. Hosseini. "Optimal management of microgrid using differential evolution approach." In *Energy Market (EEM), 2010 7th International Conference on the European*, pp. 1-6. IEEE, 2010.

[73] Hatziargyriou, N. D., A. Dimeas, A. G. Tsikalakis, JA Pecas Lopes, G. Karniotakis, and J. Oyarzabal. "Management of microgrids in market environment." In *Future Power Systems, 2005 International Conference on*, pp. 7-pp. IEEE, 2005.

[74] Logenthiran, T., Dipti Srinivasan, and David Wong. "Multi-agent coordination for DER in MicroGrid." In *Sustainable Energy Technologies, 2008. ICSET 2008. IEEE International Conference on*, pp. 77-82. IEEE, 2008.

[75] Oyarzabal, J. R. A. E. J., J. Jimeno, J. Ruela, A. Engler, and C. Hardt. "Agent based micro grid management system." In *Future Power Systems, 2005 International Conference on*, pp. 6-pp. IEEE, 2005.

[76] Gungor, Vehbi C., Dilan Sahin, Taskin Kocak, Salih Ergut, Concettina Buccella, Carlo Cecati, and Gerhard P. Hancke. "Smart grid technologies: communication technologies and standards." *Industrial informatics, IEEE transactions on* 7, no. 4 (2011): 529-539.

[77] Gao, Jingcheng, Yang Xiao, Jing Liu, Wei Liang, and C. L. Chen. "A survey of communication/networking in Smart Grids." *Future Generation Computer Systems* 28, no. 2 (2012): 391-404.

[78] Dike, D. O., and S. M. Mahajan. "Utilization of L-index in microgrid interconnected power system network." In *Power and Energy Society General Meeting-Conversion and Delivery of Electrical Energy in the 21st Century, 2008 IEEE*, pp. 1-6. IEEE, 2008.

[79] Zayandehroodi, Hadi, Azah Mohamed, Hussain Shareef, and Marjan Mohammadjafari. "Distributed generator and their effects on distribution system protection performance." *Australian Journal of Basic and Applied Sciences* 5, no. 10 (2011): 398-405.

[80] Monfared, Mohammad, and Saeed Golestan. "Control strategies for single-phase grid integration of small-scale renewable energy sources: A review."*Renewable and Sustainable Energy Reviews* 16.7 (2012): 4982-4993.

[81] Peesapati, V., I. Cotton, T. Sorensen, T. Krogh, and N. Kokkinos. "Lightning protection of wind turbines–a comparison of measured data with required protection levels." *IET renewable power generation* 5, no. 1 (2011): 48-57.

[82] Basak, Prasenjit, S. Chowdhury, S. Halder nee Dey, and S. P. Chowdhury. "A literature review on integration of distributed energy resources in the perspective of control, protection and stability of microgrid." *Renewable and Sustainable Energy Reviews* 16, no. 8 (2012): 5545-5556.

[83] Haron, Ahmad Razani, Azah Mohamed, and Hussain Shareef. "A Review on Protection Schemes and Coordination Techniques in Microgrid System." *Journal of Applied Sciences* 12.2 (2012).

[84] Ustun, Taha Selim, Cagil Ozansoy, and Aladin Zayegh. "Modeling of a centralized microgrid protection system and distributed energy resources according to IEC 61850-7-420." *Power Systems, IEEE Transactions on* 27, no. 3 (2012): 1560-1567.

[85] Chedid, R., H. Akiki, and Saifur Rahman. "A decision support technique for the design of hybrid solar-wind power systems." *Energy conversion, ieee transactions on* 13.1 (1998): 76-83.

[86] Kellogg, W. D., et al. "Generation unit sizing and cost analysis for stand-alone wind, photovoltaic, and hybrid wind/PV systems." *Energy conversion, ieee transactions on* 13.1 (1998): 70-75.

[87] Giraud, Francois, and Zyiad M. Salameh. "Steady-state performance of a grid-connected rooftop hybrid wind-photovoltaic power system with battery storage."*Energy Conversion, IEEE Transactions on* 16.1 (2001): 1-7.

[88] Agbossou, Kodjo, et al. "Performance of a stand-alone renewable energy system based on energy storage as hydrogen." *Energy Conversion, IEEE Transactions on* 19.3 (2004): 633-640.

[89] Agbossou, K., R. Chahine, J. Hamelin, F. Laurencelle, A. Anouar, J-M. St-Arnaud, and T. K. Bose. "Renewable energy systems based on hydrogen for remote applications." *Journal of Power Sources* 96, no. 1 (2001): 168-172.

[90] Nelson, D. B., M. H. Nehrir, and C. Wang. "Unit sizing and cost analysis of stand-alone hybrid wind/PV/fuel cell power generation systems." *Renewable energy*31.10 (2006): 1641-1656.

[91] Miao, Z., M. A. Choudhry, R. L. Klein, and L. Fan. "Study of a fuel cell power plant in power distribution system. Part I. Dynamic model." In *Power Engineering Society General Meeting, 2004. IEEE*, pp. 2220-2225. IEEE, 2004.

[92] Sedghisigarchi, Kourosh, and Ali Feliachi. "Dynamic and transient analysis of power distribution systems with fuel Cells-part II: control and stability enhancement." *Energy Conversion, IEEE Transactions on* 19, no. 2 (2004): 429-434.

[93] Sharma, Hari, Syed Islam, and Trevor Pryor. "Dynamic Modelling and Simulation of a Hybrid Wind Diesel Remote Area Power System." *International Journal of Renewable Energy Engineering* 2, no. 1 (2000): 123-128.

[94] Bonanno, F., A. Consoli, A. Raciti, B. Morgana, and U. Nocera. "Transient analysis of integrated diesel-wind-photovoltaic generation systems." *Energy Conversion, IEEE Transactions on* 14, no. 2 (1999): 232-238.

[95] Wang, Caisheng. "Modeling and control of hybrid wind/photovoltaic/fuel cell distributed generation systems." PhD diss., MONTANA STATE UNIVERSITY Bozeman, 2006.

[96] Moutawakkil, Karim, and Steffen Elster. "RE hybrid systems: Coupling of Renewable Energy Sources on the AC and DC Side of the Inverter." *Refocus* 7, no. 5 (2006): 46-48.

[97] Siraki, Arbi Ghrakhani, Nathan Curry, Pragasen Pillay, and Sheldon S. Williamson. "Power electronics intensive solutions for integrated urban building renewable energy systems." In *Industrial Electronics, 2009. IECON'09. 35th Annual Conference of IEEE*, pp. 3998-4006. IEEE, 2009.

[98] Sera, Dezso, Remus Teodorescu, and Pedro Rodriguez. "PV panel model based on datasheet values." In *Industrial Electronics, 2007. ISIE 2007. IEEE International Symposium on*, pp. 2392-2396. IEEE, 2007.

[99] Amirat, Yassine, Mohamed Benbouzid, Bachir Bensaker, and René Wamkeue. "The state of the art of generators for wind energy conversion systems."*Electromotion* 14, no. 4 (2007): 163-172.

[100] Chen, Zhe, Josep M. Guerrero, and Frede Blaabjerg. "A review of the state of the art of power electronics for wind turbines." *Power Electronics, IEEE Transactions on* 24, no. 8 (2009): 1859-1875.

[101] Pena, R., J. C. Clare, and G. M. Asher. "Doubly fed induction generator using back-to-back PWM converters and its application to variable-speed wind-energy generation." *IEE Proceedings-Electric Power Applications* 143, no. 3 (1996): 231-241.

[102] Datta, Rajib, and V. T. Ranganathan. "Direct power control of grid-connected wound rotor induction machine without rotor position sensors." *Power Electronics, IEEE Transactions on* 16, no. 3 (2001): 390-399.

[103] Muyeen, S. M., Junji Tamura, and Toshiaki Murata. *Stability augmentation of a grid-connected wind farm*. Berlin: Springer, 2009.

[104] Isermann, Rolf. *Mechatronic systems: fundamentals*. Springer, 2005.

[105 Demirok, Erhan. "Grid-connected variable speed generator application with doubly-fed induction machine." MsC Thesis (2007).

[106] Tolbert, Leon M., and Fang Z. Peng. "Multilevel converters as a utility interface for renewable energy systems." In *Power Engineering Society Summer Meeting, 2000. IEEE*, vol. 2, pp. 1271-1274. IEEE, 2000.

[107] San Martín, Jose Ignacio, Inmaculada Zamora, Jose Javier San Martín, Victor Aperribay, and Pablo Eguia. "Hybrid fuel cells technologies for electrical microgrids." *Electric Power Systems Research* 80, no. 9 (2010): 993-1005.

[108] Kirubakaran, A., Shailendra Jain, and R. K. Nema. "A review on fuel cell technologies and power electronic interface." *Renewable and Sustainable Energy Reviews* 13, no. 9 (2009): 2430-2440.

[109] del Real, Alejandro J., Alicia Arce, and Carlos Bordons. "Development and experimental validation of a PEM fuel cell dynamic model." *Journal of power sources* 173, no. 1 (2007): 310-324.

[110] Chen, Haisheng, Thang Ngoc Cong, Wei Yang, Chunqing Tan, Yongliang Li, and Yulong Ding. "Progress in electrical energy storage system: A critical review." *Progress in Natural Science* 19, no. 3 (2009): 291-312.

[111] Dunn, Bruce, Haresh Kamath, and Jean-Marie Tarascon. "Electrical energy storage for the grid: A battery of choices." *Science* 334, no. 6058 (2011): 928-935.

[112] Ribeiro, Paulo F., Brian K. Johnson, Mariesa L. Crow, Aysen Arsoy, and Yilu Liu. "Energy storage systems for advanced power applications." *Proceedings of the IEEE* 89, no. 12 (2001): 1744-1756.

[113] Tan, Xingguo, Qingmin Li, and Hui Wang. "Advances and trends of energy storage technology in Microgrid." *International Journal of Electrical Power & Energy Systems* 44, no. 1 (2013): 179-191.

[114] Carrasco, Juan Manuel, Leopoldo Garcia Franquelo, Jan T. Bialasiewicz, Eduardo Galván, RC Portillo Guisado, Ma AM Prats, José Ignacio León, and Narciso Moreno-Alfonso. "Power-electronic systems for the grid integration of renewable energy sources: A survey." *Industrial Electronics, IEEE Transactions on* 53, no. 4 (2006): 1002-1016.

[115] Ribeiro, Paulo F., Brian K. Johnson, Mariesa L. Crow, Aysen Arsoy, and Yilu Liu. "Energy storage systems for advanced power applications." *Proceedings of the IEEE* 89, no. 12 (2001): 1744-1756.

[116] Goswami, D. Yogi, and Frank Kreith, eds. *Energy conversion*. CRC press, 200

[117] Bolund, Björn, Hans Bernhoff, and Mats Leijon. "Flywheel energy and power storage systems." *Renewable and Sustainable Energy Reviews* 11, no. 2 (2007): 235-258.

[118] Jiancheng, Zhang, Lipei Huang, Chen Zhiye, and Wu Su. "Research on flywheel energy storage system for power quality." In *Power System Technology, 2002. Proceedings. PowerCon 2002. International Conference on*, vol. 1, pp. 496-499. IEEE, 2002.

[119] Li, Peiwen. "Energy storage is the core of renewable technologies."*Nanotechnology Magazine, IEEE* 2, no. 4 (2008): 13-18.

[120] Tremblay, Olivier, and Louis-A. Dessaint. "Experimental validation of a battery dynamic model for EV applications." *World Electric Vehicle Journal* 3, no. 1 (2009): 1-10.

[121] Alesina, Alberto, and M. Venturini. "Analysis and design of optimum-amplitude nine-switch direct AC-AC converters." *Power Electronics, IEEE Transactions on* 4, no. 1 (1989): 101-112.

[122] Alesina, Alberto, and M. Venturini. "Solid-state power conversion: A Fourier

analysis approach to generalized transformer synthesis." *Circuits and Systems, IEEE Transactions on* 28, no. 4 (1981): 319-330.

[123] Filippov, Aleksei Fedorovich. "Differential equations with discontinuous right-hand side." *Matematicheskii sbornik* 93, no. 1 (1960): 99-128.

[124] Utkin, Vadim Ivanovich. *Sliding modes and their application in variable structure systems*. Mir Publishers, 1978.

[125] Utkin, Vadim, Jürgen Guldner, and Ma Shijun. *Sliding mode control in electro-mechanical systems*. Vol. 34. CRC press, 1999.

[126] Van Der Broeck, Heinz Willi, H-C. Skudelny, and Georg Viktor Stanke. "Analysis and realization of a pulsewidth modulator based on voltage space vectors."*Industry Applications, IEEE Transactions on* 24, no. 1 (1988): 142-150.

[127] Mocci, F., and M. Tosi. "Comparison of power converter technologies in photovoltaic applications." In *Electrotechnical Conference, 1989. Proceedings.'Integrating Research, Industry and Education in Energy and Communication Engineering', MELECON'89., Mediterranean*, pp. 11-15. IEEE, 1989.

[128] Utkin, Vadim I. *Sliding modes in control and optimization*. Vol. 116. Berlin: Springer-Verlag, 1992

[129] Sabanovic, Asif, and Kouhei Ohnishi. *Motion control systems*. John Wiley & Sons, 2011.

[130] Yan, Wenguang. "Multilevel sliding mode control in hybrid power systems." PhD diss., The Ohio State University, 2007.